Automated Control Beyond the Limits of Friction

A nonlinear model predictive control approach with production vehicle experimental verification

Master of Science Vehicle Engineering

S. Meijer

Delft University of Technology | BMW AG

TU Delft

BMW GROUP

Automated Control Beyond the Limits of Friction

A nonlinear model predictive control approach with production vehicle experimental verification

by

S. Meijer

This thesis is confidential and cannot be made public until July 11, 2025.

Thesis Committee Chair:	R. Happee
Supervisor:	B. Shyrokau
University Instructor:	A. Bertipaglia
Company Manager :	P. Ludwig
Company Support :	P. Bader
Institution:	Delft University of Technology
	Faculty of Mechanical, Maritime and Materials Engineering, Delft
Company:	BMW AG
	BMW Group Forschungs- und Innovationszentrum, Munich

Cover Image: BMW M3 Performing Drifting Maneuver, Source: BMW AG

TU Delft

Preface

I want to thank all individuals that contributed to this challenging project through support on both an academic, as well as on a personal level. First of all, as the thesis supervisor, Barys Shyrokau has been a great support and motivation during the project. He has been a great source of both academic knowledge on both vehicle dynamics and control systems, which he was able to bring up immediately. Barys was the best in both theoretical and practical support, which was available at all times.

Furthermore, I would like to thank Alberto Bertipaglia as a daily consultant during the writing process of the thesis and academic paper. His contribution has made significant improvements to the academic level of writing with helpful comments to the thesis, as well as the graduation process in general.

I would like to extend a sincere acknowledgement to the project manager at BMW, Philipp Ludwig, who initiated the project and has always expressed his confidence in my abilities.

During the project, Peter Bader has been a great support on the implementation on the experimental test bench, his experience in the field of measurement technology has brought enormous benefits, and has certainly contributed to the fact that the experiment has been secured.

Furthermore, I would like to thank all other colleagues at BMW, that have contributed to successful performing of the project, both on a technical- as well as on a personal level. From colleagues that supported subjects like simulation, tyre development, control systems and measurement technology, to colleagues that are just pleasant to talk with during numerous coffee breaks.

Many thanks to the BMW AG, for internally rewarding this project with a Thesis Award. This allows me to pursue a career within the BMW Group, starting at function development in brake control systems.

To my friends and family all over the world, many thanks for the support and understanding, no matter the time and distance.

S. Meijer
Munich, July 2023

Summary

Drifting can be described as intentionally bringing a vehicle to a state of high sideslip and the rear wheels are saturated due to high proportions of longitudinal- and lateral slip, while the front wheels align with the direction of travel. As the tire behavior for high quantities of slip reaches a nonlinear behavior, drifting can be described as vehicle motion beyond the limits. As the vehicle states beyond the tire friction limits extends the possible motion primitives, future automated safety systems are likely to be deployed with applications that enable safe control while in high sidelip state. This can be in the form of an integrated vehicle system, with the aim of promoting the safety of the driver or the environment, but also as an eye-catcher with regard to attracting customers for high performance vehicles with automated or auxiliary drifting capabilities.

The key component to successful automated drifting lies with the reference drifting state that finds its origin in an equilibrium analysis. Equilibrium locations of of a set of differential equations that describe the dynamical system of a drifting vehicle, show that the drifting state of a vehicle equals an unstable equilibrium, that can be stabilized using control inputs. As experimentally verified, equilibrium locations of a single-track model show great correspondence with an experimental setup, which therefore proves that equilibrium locations can be used as references for the proposed control strategy.

In this research, a control strategy is proposed using a nonlinear model predictive controller to stabilize the vehicle into a high sideslip state, while dynamic referencing is used to to adjust references such that path curvature becomes variable. As solely referencing the path curvature would not ensure converging towards a desired path, an additional PID controller is applied to adjust the path curvature by means of the lateral path deviation.
Simulation of the proposed control strategy shows the ability of the controller to track a desired reference drifting state, while converging towards a desired path. Experimental verification has shown that the use of a standard production vehicle without significant hardware and- or software modifications is not able to convert desired control inputs into the applied control inputs, due to unsuccessful processing of the desired steering angle. However, a semi-automatic verification of the controller has proven that the NMPC sideslip stabilization controller proposed control inputs are very likely to stabilize the drifting motion, as the desired steering input is corresponding in behavior of a manual driver.

The approached control strategy shows that in case parametric knowledge is known, or at least approximated within certain limits, the NMPC is able to bring the vehicle into a desired high-slip state. However, this implies that if the control approach would be proposed for safety purposes, knowledge of that particular situation should be estimated before being used in the controller. In a simulation environment, this is relatively easy to be deployed, however a real road situation could become quite critical. The latency that would exist due to filtering, estimation and data transfer could be too significant to account for a critical evasive maneuver, not to mention the computational performance the NMPC desires. In similar fashion, knowledge of model parameters could be highly differing between variations of wheels, e.g. μ-split situations. Allowing adjustment to a multi-purpose controller would imply a significant amount of logic that would allow such system.

Contents

Nomenclature

Abbreviations

Abbreviation	Definition
ABS	Anti-lock braking system
ACADO	Automatic Control and Dynamic Optimization
ADAS	Advanced driver assistance systems
ADS	Automated driving systems
AWD	All-wheel drive
DME	Digital motor electronics
EPS	Electronic power steering
FAS	Fahrer assistent systeme (Driver assistance systems)
FuSi	Funktionale Sicherheit (Functional safety)
FWD	Front-wheel drive
LSD	Limited-slip differential
LQR	Linear quadratic regulator
NMPC	Nonlinear model predictive control
OCP	Optimal control problem
ODD	Operational driving domain
RWD	Rear-wheel drive
SAE	Society of Automotive Engineers

Symbols

V	Absolute velocity	[m/s]
V_i	Directional velocity	[m/s]
r	Vehicle yaw rate	[rad/s]
β	Vehicle side-slip angle	[rad]
F_{yi}	Lateral tire force	[N]
F_{xi}	Longitudinal tire force	[N]
α_i	Tire lateral slip angle	[rad]
κ_i	Tire longitudinal slip coefficient	[-]
δ	Steering angle	[rad]
μ_i	Friction coefficient	[-]
δ	Steering angle	[rad]
$\dot{\delta}$	Steering angle rate	[rad/s]
T_i	Drive torque	[Nm]

List of Figures

List of Tables

1 Introduction

All racing fans are known with the term drifting, where drivers operate their rear tires on the limits of friction deliberately, with impressive vehicle behavior observed. Opposed to conventional straight-forward driving, a drifting vehicle performs movement under an angled pose with respect to the driving direction i.e. the rear of the vehicle ´breaks out´and remains in that state, as depicted in Figure 1.1.

The angled pose of the vehicle can be described by an angle commonly known as the vehicle sideslip angle β. The sideslip angle describes the angle between the longitudinal axis of the vehicle and the direction of the absolute velocity vector V, measured at the vehicles centre of gravity (CoG). The sideslip angle can be geometrically obtained through the mathematical relation expressed in equation 1.1, where V_y and V_x denote the lateral- and longitudinal velocity components of the vehicle velocity, respectively. At the front wheels counter-steering is perceived, where the wheels align in the direction of travel, where the front wheel behavior resembles rolling movement.

$$\beta = \arctan\left(\frac{V_y}{V_x}\right) \tag{1.1}$$

As for most vehicles, the rear wheels align with the vehicle from a top view perspective. This implies that during conventional driving, minor rear lateral tire slip angles α_r are found due to the wheel constraints. Similarly, while drifting, the lateral tire slip angles are significantly large and can be found in the same order of magnitude as the vehicle sideslip angle. As the front tires usually align with the direction of travel, front lateral tire slip angles α_r are commonly minor. The lateral tire slip angles are in fact mathematically common to the vehicle sideslip angle, as the angle describes the angle between the longitudinal- and lateral velocity components of the center of the tire contact patch. In this case, the local tire frame velocity components [34]are required to determine the slip angles .
Similarly, due to relatively large rear-drive torques the rear wheels undergo significant longitudinal wheel slip s_{ij}, with notable high tire temperatures in case of high friction surfaces. Figure 1.2 shows the schematics of a transition between conventional driving and drifting, with indications of tire saturation. Where a saturated tire implies that the tire finds itself beyond the peak friction force of tire characteristics, as a result of a large absolute rear tire slip.

Counter intuitively, driving at large angles of sideslip does not necessarily imply terminal loss of control, as it actually forms the foundation of the sport of drifting. Drifting challenges skilled drivers to travel along a track while sustaining a large sideslip angle by exploiting coupled nonlinearities in the tire force response [1]. The lateral tire force response on the rear are considered saturated during a sustained drift [36].

In the sport of rally racing, drivers are often exposed to low friction surfaces such as gravel, mud, or even snow and ice. Achieving the fastest lap under such circumstances is often achieved by operating the vehicle while the rear tires are saturated, utilizing the drifting maneuver to remain a high pace while remaining on track. The maneuver allows to decrease cornering time due to larger allowable velocities, as well as its inverse, increasing the cornering angle at larger velocities (1.3).

Figure 1.1: BMW M4 Drifting Team performing a drifting maneuver [4]

In general, controlling the vehicle in a stable drift requires a significant amount of practice, where most average drivers would not be able to perform such maneuver without practice. Similarly, the powertrain layout as well as configuration of the vehicle can significantly influence the ability for a vehicle to drift. The transition between driving and drifting can be determined as highly in-stable, where achieving a steady-state operation point with rear tire saturation is very limited. This can also be mathematically supported by the steady-state drifting equilibria being an unstable saddle-point in terms of phase portraits.

1.1. Motivation

Complex driving maneuvers from racing origins have initially formed the basis for several well known safety systems. A safety system incorporating control on the limits of friction would have similar origin as for example ABS. ABS mainly copies the earlier technique of skilled drivers that performed cadence braking to avoid the permanent lockup of a braked wheel on emergency stops [26], which allows to steer while brake, but also to improve both acceleration and deceleration. In similar fashion, both drifting as well as cadence braking are driver actions that only high skilled drivers are capable of doing. Corresponding to ABS, incorporating control on the limits of handling, or drifting, also has potential to contribute to vehicle safety and performance in the future. As drifting maneuvers have already show their contribution to driving performance in rally racing, these performance enhancing maneuvers can also be deployed with the purpose of increasing general vehicle safety. Larger cornering angles and velocities, extends the amount of possible vehicle states and therefore its trajectories. This contributes to the possibilities of behalf of obstacle evasion, where a high sideslip vehicle state is able to perform certain action that a conventionally driven vehicle has reached its handling limit. These limits can be directed to the tire behavior of the the vehicle, where conventional driving is said to be driving in the linear region of the tire response, where a drifting state reaches the nonlinear state of the tire response. The transition point between the linear- and nonlinear tire behavior is named the friction limit.

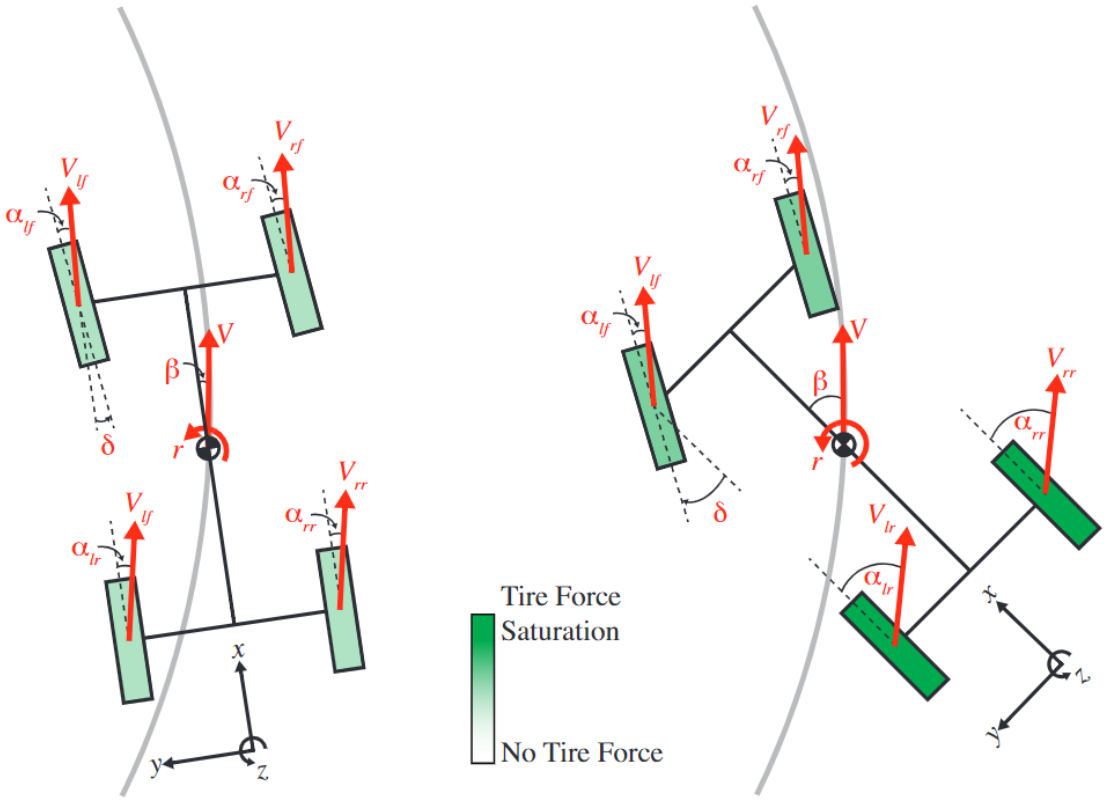

Figure 1.2: A schematic representation of a drifting maneuver. Note rear tire saturation, high sideslip and counter-steer [36]

1.2. Performance Enhancement

As briefly introduced, drifting on itself is considered a sport where where drivers operate their rear tires on the limits of friction deliberately, with entertaining vehicle behavior as a result. Drifting competitions became popular in the 1970s in Japan, which globally popularized by the 1995 manga series Initial D. In modern day, drifting competitions are held worldwide and are judged according to the speed, angle, distance to objects, driven lines and showmanship [1]. Besides the impressive looks of it, vehicle control beyond the limits of handling is widely applicable in motor sports since it has positive effects on driving performance in particular cases. Especially in low friction environments, such as rally, professional drivers have applied drifting techniques for decades to handle corners at a larger cornering velocities compared to traditional driving. As a result, the corners can be negotiated much quicker, with a larger exit velocity.

Compared to existing research on vehicle dynamics control, the drifting maneuver and its control has not been as extensively explored. However, several works have shown significant research on behalf of control beyond the limits of handling. Several works on optimisation-based research studies have shown that determining optimal vehicle cornering in high dynamic situations, resulting trajectories propose drifting behavior in particular driving conditions. Velenis and Tsiotras [30] investigated the objective of a maximum exit velocities during cornering, which shows that the determined optimal trajectories in low friction conditions show obvious signs of drifting behavior. Whereas in another research [33], real-time data of rally drivers is collected performing a so called trail-braking' maneuver, and converted into a minimum-time cornering problem which is solved through nonlinear optimisation. Figure 1.3 shows the result of simulating a maneuver while incorporating optimal properties of the trail-braking maneuver. The resulted minimum time cornering solutions showed and excellent agreement between the determined parameterization and guidelines provided by expert rally drivers. In similar fashion, Gustaffsson [13] applied optimal control techniques on minimizing lap times for various racing conditions. The research has shown that for rally racing conditions, applied optimisation techniques indeed show drifting behavior for negotiating to turn hairpin corners. However, for each optimisation-

based method, a sustained drift has not been seen as part of an optimally determined trajectory. The vehicle seems to be in a transient state between turning and drifting for most cases.
Achieving the fastest lap under low friction circumstances is often achieved by operating the vehicle while the rear tires are saturated, utilizing the drifting maneuver to remain a high pace while remaining on track. The maneuver allows to decrease cornering time due to larger allowable velocities, as well as its inverse, increasing the cornering angle at larger velocities.

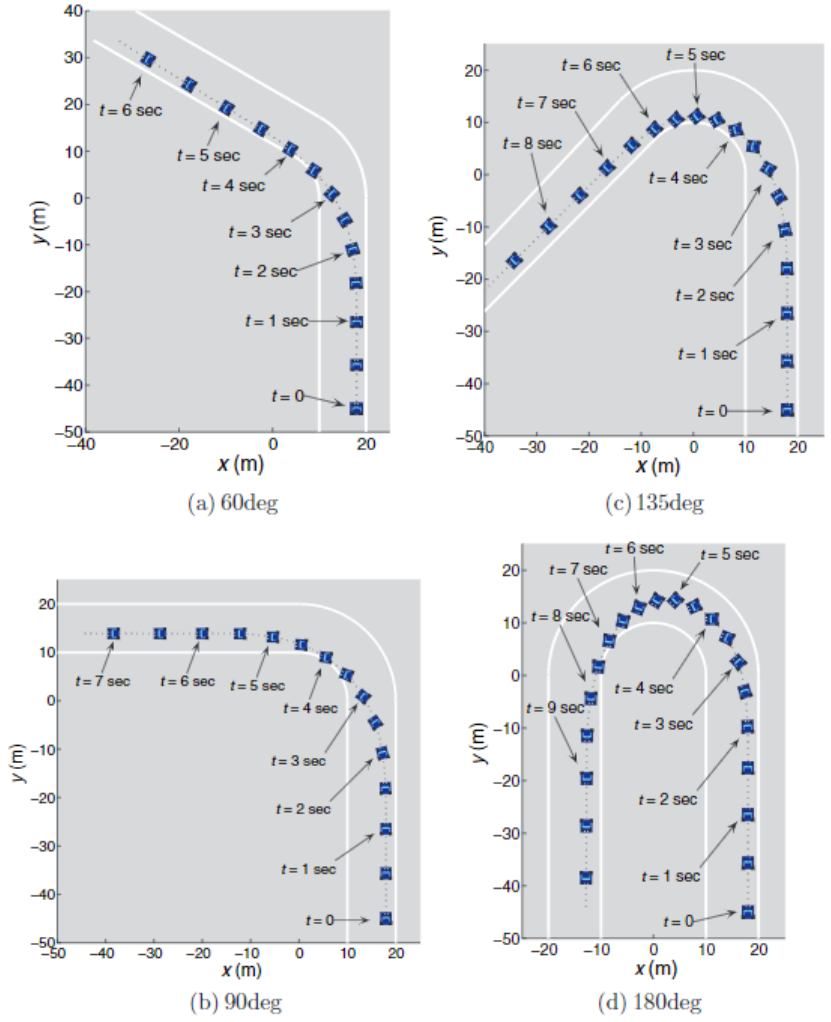

Figure 1.3: Optimally determined cornering trajectories, where narrow corners are handled best with large side-slip angles [33]

The 2004 DARPA Urban Challenge [29] initiated an increasing interest in autonomous robot competitions, with significant increase in autonomous technologies. Where none of the participants in 2004 Darpa managed to conquer the defined trajectory, participants of the Indy Autonmous Challenge reach velocities of 270km/h while driving fully autonomous [28]. Since drifting on itself is considered a popular part of motor-sports, future autonomous drifting competitions could initiate existence in junction current autonomous racing competitions. As drifting maneuvers have shown optimality for several racing conditions, the application of automated drifting control in future autonomous racing competitions is a good method to improve performance.

1.3. Safety

All modern day vehicles are equipped with a variety of automated vehicle safety features that contribute to safe and efficient vehicle utilization, which can be named under the collective names of advanced

driver-assistance system (ADAS) and automated driving systems (ADS). Each automated technology can be be scaled according to the level of automation with respect to the amount of driver interference, as well as the vehicle's operational design domain (ODD).

These levels of automation are mostly scaled by means of the Society of Automotive Engineers level scale, denoted SAE. SAE describes 6 seperate levels, where the scale progresses from level 0 to 5. Where safety features of level 0 mostly consist of warning and momentary assistance, where one can think of AEB and LDW. More consistent control is applied from level 1, where accelerating- or steering commands are constantly determined and controlled by automated systems such as ACC or lane centering. Level 2 describes a combination of both accelerating- and steering commands at the same time, where the initiation of both ACC and lane centering would immediately imply an SAE level 2 system.

Up until the point of level 2, the driver should be in constant supervision of vehicle control, which changes from SAE level 3. An automated vehicle system of level 3 has the possibility to perform automated driving tasks, but may request to takeover from the driver in a specific ODD. This means that the vehicle is able to control the vehicle in specific traffic situations, for example deployment of traffic jam chauffeurs.

From level 4, the automated vehicle will not request to take over anymore, which therefore is the first level at which the vehicle can be named autonomous. As autonomous implies that all decision making is done by the system, this term will be avoided throughout this report. Reason for this is that the driver will in any case choose a start and en goal of a possible automated vehicle. The significant difference between SAE level 4 and 5 lies in the aspect of the ODD. Where a level 4 vehicle is designed to drive for specific a ODD, a SAE level 5 should be able to automatically drive in any ODD.

As an example, an SAE level 4 could be designed to drive highly structured highway roads, but is not capable of driving in unknown rural areas, where an SAE level 5 vehicle should be able to drive both highway as well as unknown rural areas. As an example, local driver-less buses, which are designed for a specific part of a city centre.

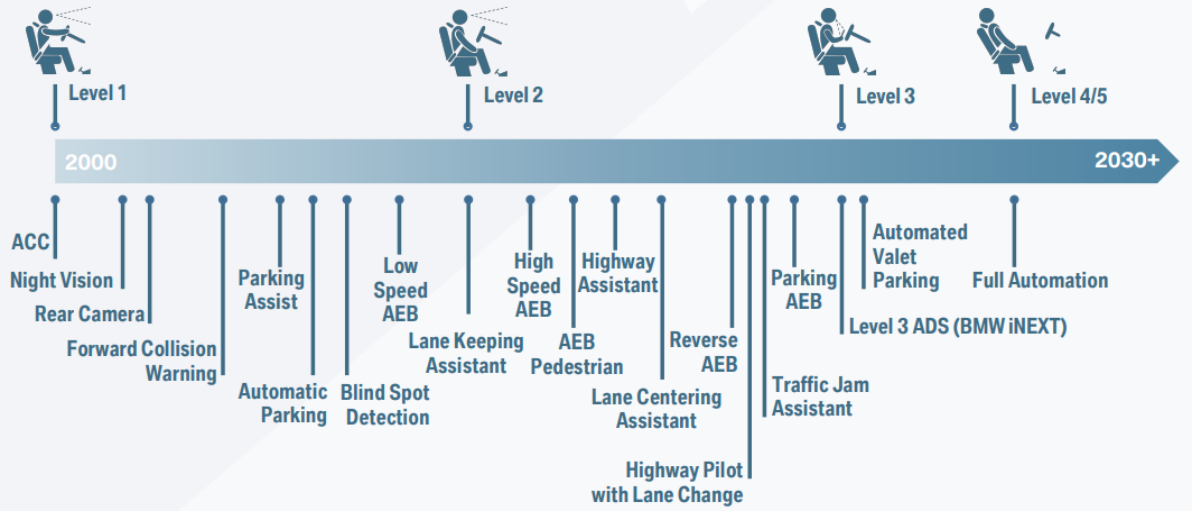

Figure 1.4: Development of ADAS and ADS at the BMW Group [5]

1.4. Automating vehicle testing at the limits of friction

An application that also builds upon the safety for general vehicle utilisation as well as performance enhancement, is vehicle testing of development vehicles. At BMW, experienced factory test drivers are required to reproducible perform a variety of maneuvers, at high performance and consistence, in order to obtain testing data which is of certain quality. These maneuvers vary broadly among longitudinal and lateral positioning, velocity and acceleration, where both low- and high dynamic maneuvers may cause negative influence the physical and psychological state of the driver.

For vehicle testing on very low dynamics, the monotonous execution of similar maneuvers can decrease the alertness and therefore performance of the test driver, which may result deviations in the execution of maneuvers. In similar fashion, highly dynamical vehicle tests on the limits of friction, such as the ISO 3888-2 [17] moose test demand high performing human drivers, as the maneuver also takes place at $160km/h$. As each tests requires a significant amount of precision under pressure, energy levels of the driver decreases significant. As a result of the energy demand, performance of the human driver will decrease rather quickly. Therefore test drivers are obliged to have a have a significant amount of rest in between sets of repetitions, which leaves the vehicle not collecting testing data. These mentioned negative aspects that come along with vehicle testing contribute to an important factor, namely costs. Extra costs contribute to lower profit for the listed company of BMW, which should therefore be avoided, preferably in advance.

As an automated system does not face compulsive moments of rest, more repetitions of a testing maneuver can be executed as compared to a human driver, which means that more data can be retrieved on a similar working day. Automated vehicles at verified settings, would drive the maneuvers in a much more reproducible manner as compared to a human test driver, which is prone to deviations in driving behavior. Since this method of vehicle testing implies driver-less vehicles, the operator controlling the vehicle, can take control of multiple vehicles at once. As a result, a significant amount of extra testing data can be gathered at much higher consistency.

When it comes to automating vehicle maneuvers on the limits of friction also implies that each repetition would be much closer to each other in the scope of performance, as human drivers are prone to differences in precise execution on each run. A proposed drifting controller will be an excellent application for a controlled drifting maneuver, such as the ISO Lane Change at 160 km/h, where it is a requirement that the driver remains a steady-state drift for a given trajectory.

1.5. Customer satisfaction

Besides possibilities to improve general vehicle safety in traffic situations, automated drifting control can also function as a form of user satisfaction. As customers of the high-performance segment often want to perform high skilled maneuvers, while they are not able to do so properly due to lack of experience or underestimating the power of the vehicle. If an inexperienced driver decides to perform a drifting maneuver after all, consequences can be catastrophic.

A programmed drifting maneuver which can be initiated by the driver, might answer the need for such system. Integration of an automated drifting maneuver for entertainment purposes may seem a bit far-fetched, but there are actually quite some high-performance vehicles with integrated systems with the purpose of performing highly experienced driving actions which are not intended for public road use. Among these systems include integrated lap timers in through GPS data (BMW Track Timer), tire warming programs for drag racing purposes (Dodge Challenger Demon), as well as a drift analyzer. The latter is a feature that is currently installed in both G80 and G81 BMW models, which grades a drift performed by a driver through estimation of the performed sideslip angle, path distance and -curvature.

As many modern sport vehicles currently have a launch control function installed, which systematically remains the drive torque of an engine at optimal value at standstill, in order to allow take off as fast as possible. In general, mentioned types of driving actions and advisory- or assisting supporting systems are not intended for public road use, but rather on premises for motor-sport purposes. As certain types of production vehicles are already equipped with active drifting support system, there will be most likely be a market for high performing vehicles having integrated drifting controllers that could both initiate or maintain a steady-state drift. Where currently deployed systems found many sports vehicles controls the stability of the drift, by means of a maximum allowable sideslip angle for performance purposes, BMW could propose a system that performs a drift fully automatically, without any driver inputs. Therefore an automated drifting maneuver could be a unique selling point for purchasers of high performance vehicles.

1.6. Objective

This research aims on a pre-development control strategy that functions as a foundation for an evasive drift maneuver for actual production vehicles. This implies that the research describes the design of a model predictive control strategy, enabling three main functionalities required for a an evasive drifting maneuver. Where the first functionality is the establishment of bringing the vehicle into a desired high sideslip state, which extends the available motion primitives of the vehicle. Similarly, for a successful evasive maneuver, the vehicle should follow a desired trajectory in order to enable the vehicle to move around undesired obstacles. At last, in correspondence to the current state of automated vehicle control, the control system should be able to incorporate a future state reference in order to 'look ahead' into the vehicle position and state, in order to anticipate on movements of the environment. As a potential drifting control system should be deployed on a production vehicle, feasible powertrain architectures are also researched, as a purely FWD vehicle is capable of reaching high sideslip angles through locking the rear axle by deploying the handbrake [31], but remaining a continuous drift is infeasible.

Summarized, the objective of this research is to design a nonlinear model predictive control (NMPC) approach that is able to stabilize a vehicle in a drifting motion, while remaining on a desired course. Adding to that, the proposed control strategy should be focused on a real-time implementation with results conducted on a production vehicle In order to achieve this, several subgoals are determined.

- Equilibrium analysis: Find the optimal states of drifting vehicle.
- Powertrain setup: Research the allowable powertrain configurations for automated drifting control while considering real-time implementation.
- Steady-state stabilisation: Design of a NMPC controller approach that stabilizes a drifting motion.
- Course stabilisation with dynamical equilibrium selection: Consider additional modifications to enable a vehicle to both stabilize a drift along a path.
- Real-time implementation: What type of adjustments are required of using a production vehicle as a testbench for automated drifting

The research aims on conducting an experiment with a production vehicle in case of low-friction wet surface. Other researches, such as the experiment conducted by Hindiyeh ([15], have proven that real-time, full size implementation of a drifting controller is possible, however, the experimental platform had powertrain properties that are not seen on common road vehicles, i.e. fully locked differential. Adding to that, an evasive drifting controller should be generally designed to be adapted to a low friction surface, such as a wet surface or snow as these are the road conditions are most useful for safe evasion maneuvers. This research on drifting therefore differs from current state-of-art on non-linear model predictive control (NMPC) for path following drift approaches proposed ([2],[35]). As these researches show simulated results with controller setups that are real-time computational infeasible.

2

Related work

2.1. Equilibrium Analysis

The key to driving the vehicle into steady-state lies at a mathematical analysis of the dynamical system described by the set of nonlinear differential equations. Where steady-state equilibria are non-unique, where each solution could consist of all possible states of the vehicle, from conventional driving to drifting in both forwards and backward directions. In case of drifting, an equilibrium point can therefore function as a reference steady-state pose. An equilibrium analysis is extensively analysed as proposed in [36], where both drifting equilibrium locations of a rear wheel driven single-track model as well as its phase portrait analysis is proposed. The phase portrait analysis shows that the drift equilibria are saddle-points, which are considered unstable equilibrium points. This implies that a drifting controller should actively control the vehicle such that it remains its high sideslip state. New vehicle equilibria are proposed in [20], where secondary drifting equilibria are identified for four-wheel driven vehicles. The study shows that four-wheel driven vehicles are also able to stabilize a steady-state drift, in case the powertrain layout is rear axle biased.

2.2. Sliding surface control

The approach of a sliding surface controller has been proposed, which ensures the vehicle to be controlled towards a desired equilibrium drifting state ([36], [14]). The developed controller utilizes a successive loop structure in which yaw rate dynamics is used to control outer loop sideslip dynamics, while tire forces are used to control yaw dynamics of an inner loop. The controller uses a switching mode approach in order to control front lateral force F_{yF} trough the steering angle δ in a first mode, in order to drive the vehicle into the desired drifting equilibrium. However, the approach of solely controlling the front lateral force F_{yF} can be limited by the front tire friction limit, where a second mode of rear drive force is introduced. The second mode will apply an additional rear drive force F_{xR} that contributes to bringing the vehicle into a desired steady-state drifting equilibrium. As main objective of the proposed controller is bringing the vehicle into a state of drifting equilibrium, the proposed controller will result in the vehicle moving in a circular trajectory, at the desired sideslip angle β_{des}. Where a physical implementation of a drive-by wire test vehicle has shown that the proposed drift controller achieves sustained, robust drifts while operating on a surface with considerably varying friction coefficient μ. Furthermore, the proposed stability analysis through phase portraits and a numerically-validated Lyapunov function have shown that the controller is able to stabilize a vehicle into desired drift equilibrium while creating a region of attraction that is large enough to drive a vehicle physically towards that equilibrium point.

2.3. Combined drifting and path-following approach

The more complex approach of a drifting controller has been proposed, which additionally ensures the vehicle to be following a defined trajectory, while controlling the vehicle into a desired equilibrium drifting state ([9], [10], [11]). The control approach uses the lateral error e_y with respect to a reference path, to control movement along certain trajectory, while a the sideslip error e_β with respect to a reference

sideslip β_{ref} will ensure bringing the vehicle into a state of drifting. In order to both follow certain specified path and sideslip β, the steering angle δ and rear drivetrain torque τ are functioning as control inputs of the vehicle, which are determined through a function of imposed error dynamics, a nonlinear model inversion, followed by wheelspeed control. The imposed error dynamics converts the lateral- and sideslip error into a desired course rate $\dot{\phi}_{des}$ and a desired yaw acceleration $\dot{r}_{des}$. As these values describe the state derivatives of the bicycle model (3.1), a numerical approach of nonlinear model inversion is applied to determine the desired steering angle δ and thrust angle γ_{des}. The steering angle δ can then directly be injected as an input to the system, where the desired thrust angle γ_{des} first has to be mapped to a desired wheelspeed ω_{des}, of which the latter also has its own control loop with respect to the actual wheelspeed ω.
Experimental verification of the proposed controller, has shown that the control approach is able to both track a reference path as well as sideslip reasonably well. A comparison to a control approach without the wheelspeed control loop, shows that outcomes of the nonlinear model inversion can also be injected into the system through the relation of $\tau = RF_{xR}^{des}$. However, the latter shows larger amplitudes in the control inputs, and therefore also in the tracking errors.
Both real-time continuous control strategies mentioned ([36], [14],[9], [10], [11]), experimentally show that a vehicle is able to sustain a steady-state drift, even along a defined path. However, having a closer look at the powertrain setup of the test vehicle, shows that independent electric engines simulate the behavior of a fully locked differential. This will not answer the request to design an evasive drift controller for production vehicles, as these have significantly differing powertrain layouts as described in 3.3.

2.4. Linear Quadratic Regulator

Velenis et al. [34] proposes an LQR drifting controller based on the four-wheel model, in combination with the Pacejka tire model, while optimizing for the steering angle δ and rear wheel-speed ω_i as the control inputs. The rear wheel-speed is converted from the required rear longitudinal force component F_{xR}. Park et al. [24] similarly applies the rear wheel-speed ω_i as the control input for an LQR controller, but in this case by means of the bicycle model, and the Fiala brush-tire model. Other than the work by Velenis et al., the LQR only controls the vehicle into drifting operation point, as the path following control is executed by an external feed-forward feed-backward path tracking controller. Lastly, the paper of Huang et al. [16] proposes a controller based on the four wheel model, which is required in their study or rear wheel independent control. Other than in previous papers, the input matrix contains a column with partial derivatives with respect to the front lateral force F_{yF}. In vehicles, there is no actuator that applied that force immediately, however, it can be used as an input for the system after being passed through an inverse vehicle model, that outputs the steering angle δ.

2.5. Model Predictive Control

An approach of a model predictive controller, to bring a vehicle into steady-state drifting has been proposed [7]. When it comes to the applied dynamical models, and defined dynamical systems used in the controller, significant correspondence with the LQR approaches can be observed. As in this case, system matrices are obtained through linearization of a nonlinear- bicycle and Fiala tyre model around defined state- and input variables. As a steady-state drift requires a reference equilibrium state, the systems matrices will change according to the values of equilibria, as demonstrated through equilibrium varying simulation. The approach shows that the choice of dynamical system states can be chosen relatively arbitrary, as the sidelip angle is not chosen as a state, while it is still possible to track the reference drifting state. A model predictive controller can then be designed using state- or output feedback, of which state feedback often has better performance.

The results of a benchmark between a steady-state drifting controller, using the approach of LQR and MPC [18], has shown a good substantiation of applying MPC. Where both controllers have the ability to bring a vehicle into steady-state. Results of the MPC controller are more promising as compared to LQR, as MPC reaches steady-state much faster, with mostly less amplitude in over- and undershoot. However, since these are only numerical simulations, a physical implementation of such MPC controller could face a lack of computational feasibility as compared to LQR.

An MPC approach that brings down the issues on computational effort, is a proposed controller on the limits of handling[3]. Other than previous model predictive control approaches, a simplified linear

model is used to successfully implement an model predictive controller, that modifies a human driver input such that a vehicle is stabilized on the limits of handling. The controller is not designed to fully bring a vehicle into a steady-state drift, but the applied methodology can be considered helpful in designing a real-time feasible MPC controller. As a modified linear vehicle- and tire model is used for the MPC controller, the optimization becomes convex, which reduces the computational effort, thus increasing real-time feasibility.

Another approach proposes a tire modelling concept which also allows a convex optimization with the purpose of bringing automated vehicles from standstill to the limits of handling [37], which arises questions regarding real-time feasibility to an optimization based control approach which is non-convex. The information gathered regarding MPC and LQR drifting control, shows that applying LQR and MPC can be done in relatively flexible fashion, as a variety of controller designs can function the same purpose. Varieties in the applied vehicle-, and tire models, as well as different definitions of the control inputs, allow multiple roads to a a successive drifting controller.

3

Vehicle Dynamics

In general, vehicle dynamics can be described by a variety of mathematical descriptions on different levels of complexity. With regards to automating drifting maneuvers, a modelling approach is desired which captures the most relevant aspect of the total vehicle dynamics, while maintaining simplicity for computational performance of a control system. This chapter describes the applied dynamical system used in the controller design, followed by a more extensive description of the drifting vehicle.

Figure 3.1: From a four wheeled vehicle to two wheels [6]

3.1. Single-track model

The bicycle model is also known as the single-track or lumped-tire model, of which the latter appellation gives a good hint on its representation. The bicycle model is characterized by simplifying the vehicle kinematics and dynamics of a four-wheel vehicle model by lumping the tires on the left- and right side together in the center-line of the vehicle, resulting in a two-wheeled representation as shown in figure 3.1. This conversion functions the purpose of decreasing complexity through decrease of parameters, as well as degrees of freedom. Since the Ackermann steering geometry will in practice have slight deviation [21], the lumped steering angle δ of the bicycle model is considered a good approximation

for many applications. In similar fashion, force- and moment leverage points are decreased from four to two lumped wheels by vector addition of left and right quantities. Rotational velocities as of the wheels are averaged between the left- and right wheels, whereas vertical loads are added, indicating that lateral load transfer between left- and right is not captured using the single-track model.

The dynamic bicycle model is graphically shown in figure 3.2, where the centered bicycle model is fitted over the actual vehicle. As can be derived from the schematics, there are a variety mathematical descriptions available to describe vehicle dynamics, where several three-state differential equations suffice in finding all states of the vehicle. By obtained preliminary steps of the proposed controller design, the optimally determined states are chosen, such that the direct states serve multiple purposes, with the least recalculations required. The system of equations is described (3.1), where time derivatives of the states sideslip angle β, the yaw rate r, and the absolute vehicle velocity V represent the bicycle model dynamics. The absolute velocity describes the true velocity the vehicle in space, combining both the lateral- and longitudinal velocities with respect to the vehicle frame. The sideslip angle is the angle between the vehicle x-axis and the absolute velocity, which is therefore the main indication for a vehicle being in drift at large sideslip angles. The yaw rate describes the rotation around the z-axis of the vehicle. In many vehicle motion algorithms, the bicycle model is usually not expressed in with the time derivative of the sideslip angle $\dot{\beta}$, but as information of the sideslip angle characterizes the state of a drift, it is rather convenient to directly have that value at hand, for both reading of state, as well as defining a reference. Similarly, most approaches on behalf of vehicle motion control are performed through longitudinal- or also lateral- vehicle, where in this case the absolute velocity is used. The reasoning behind this is that the having the absolute velocity available, a path following property is ensured much easier as compared to velocities with respect to the vehicle, where a path curvature κ_{path} is defined by division of the absolute velocity by the yaw rate r.

In some cases, different symbols are used for expressing same variables. In this report one can therefore encounter r or $\dot{\psi}$, which denotes the yaw rate around the z-axis of the vehicle. Velocity vectors are often noted as v_i, V_i, U_i, where lowercase i represents the direction of its unit vector with respect to the center of gravity of the vehicle.

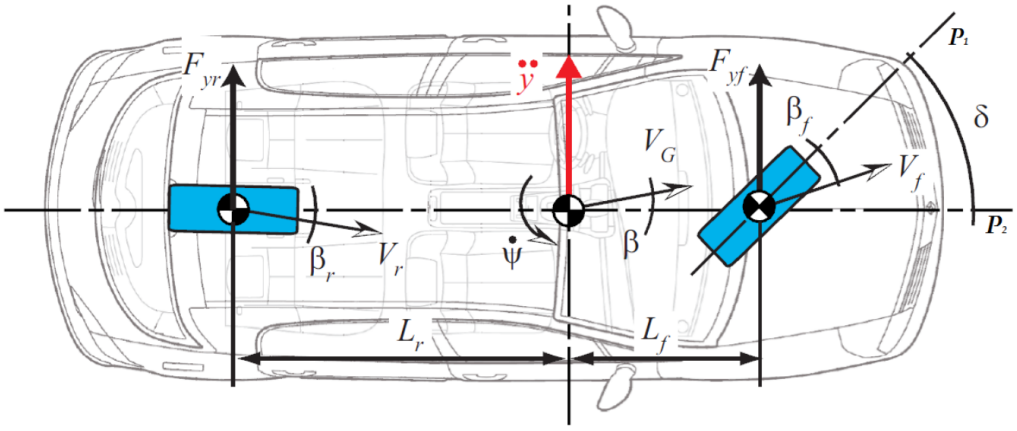

Figure 3.2: A schematic representation of the bicycle model [27]

$$\begin{aligned}
\dot{V} &= \frac{F_{xF}\cos(\delta-\beta) - F_{yF}\sin(\delta-\beta) + F_{xR}\cos\beta + F_{yR}\sin\beta}{m} \\
\dot{\beta} &= \frac{F_{yF}\cos(\delta-\beta) - F_{xF}\sin(\delta-\beta) - F_{xR}\sin\beta + F_{yR}\cos\beta}{mV} - r \\
\dot{r} &= \frac{a[F_{xF}\sin\delta + F_{yF}\cos\delta] - bF_{yR}}{I_z}
\end{aligned} \tag{3.1}$$

3.2. Tire-Road interaction

To enable a control strategy to drift automatically, the interaction between the vehicle and the road surface is of most significant importance on the drifting motion. As can be intuitively derived from the bicycle model schematics (3.1), the transition between conventional driving and drifting requires a relatively large rear lateral force to establish a state of drift, while similarly being able to maintain an optimal lateral force to remain in a steady-state drift. This implies that the knowledge of the tires should be as accurate as possible, capturing most characteristics with the least complexity. Therefore, once the drive torque exits the differential of the left and right, the torque is transmitted to the wheel, which is considered a rigid body with certain mass. As a result of the applied torque, the longitudinal component of the contact patch exerts a force in opposite longitudinal direction of travel. The dynamics of the rotating wheel are described by 3.2, where the time derivative of the rotational velocity of the wheel $\dot{\omega}$ is determined by the sum of moments around the wheel center, divided by the rotational inertia of the wheel. A schematic overview of wheel dynamics is added in case terminology requires some refreshment (3.3).

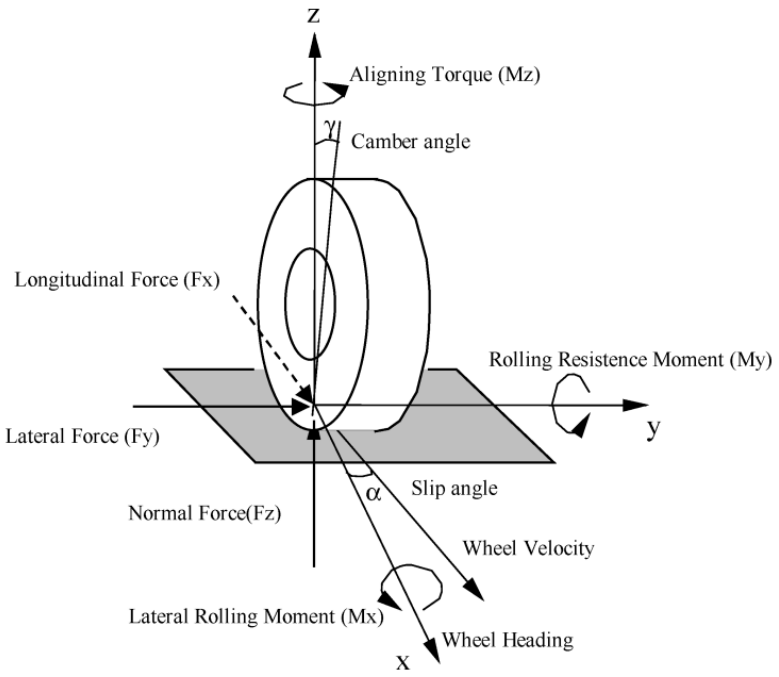

Figure 3.3: Wheel dynamics description incorporating tire-road interaction[12]

$$\dot{\omega_j} = \frac{T_j - F_{xj} r_j}{I_{\omega j}} \quad j = F, R \tag{3.2}$$

The amount movement between two surfaces describes the phenomenon of slip, where in case of wheels, the amount of sliding between contact patch between tires and road surface. In the work of [23] practical tire slip quantities are determined, for both longitudinal slip κ_i and a lateral slip angle α_i, which are mathematically described by equation 3.3. These practical tire slips preserve the view purely in lateral or longitudinal direction where in correspondence to the high sideslip angle, significant decomposition of directions occur at the rear tire slip during a drifting maneuver.

$$\kappa_i = \frac{\omega_i r_i - V_{ix}}{\omega_i r_i} \quad \alpha_i = \tan^{-1} \frac{V_{iy}}{V_{ix}} \quad i = F, R \tag{3.3}$$

Hindiyeh proposed a control strategy where only the lateral force characteristics of the tires were incorporated through the brush-tire model [15], which is a function depending on the lateral slip angle α. This has shown positive results in case of reaching a single state drifting equilibrium, however this limits the possibility of a transitional drift, as there is no information regarding the longitudinal slip components available as the longitudinal velocity of the contact path remains an unknown. This can be also seen

in the work of Goh,2020 [11] where an additional wheelspeed control has proven better performance when it comes to drifting as it contributes to stabilization of the vehicle during drift, through adding robustness to the control strategy.
The absolute slip occurring at the rear tires can be mathematically described by means of the theoretical coefficients of slip, where lateral- and longitudinal theoretical slip quantities (3.4) result in a combined slip definition (3.5) [32]. Opposed to the practical slip quantities, theoretical slip quantities take into account the effect on the directional slip component of perpendicular direction. Thus both decomposed theoretical quantities are reduced with respect to the practical slip quantities, as the slip in other directions then increase their true velocity at the contact patch. I.e. a practical lateral slip angle is determined by the longitudinal and lateral velocity component, however longitudinal slip increases the true longitudinal velocity vector at the contact patch, decreasing the true slip angle.

$$S_{xj} = \frac{V_{xj} - \omega_j r_j}{\omega_j r_j} \quad S_{yj} = \frac{V_{yj}}{\omega_j r_j} \quad j = F, R \tag{3.4}$$

$$S_j = \sqrt{S_{yj}^2 + S_{xj}^2} \quad j = F, R \tag{3.5}$$

The industry standard for tire modelling is called the Magic Formula, better known as the Pacejka Model or MF. Hans. B Pacejka proposed a series of Magic Formulas in the last couple of decades, where the model thanks its name to the fact that its origin is based on the principle of curve fitting rather than on physical substantiation, as seen for the brush-tyre model. The Magic Formula can be described by an amount of 10-20 coefficients which allows to fit a curve corresponding to experimentally obtained data, often measured in testbenches. The parameterizations allow to generate a function which tells the amount of longitudinal- and lateral tire force exerted on the tyre contact patch, as a function of a given vertical load, camber angle and slip quantity. More extensive parameterizations have the ability to include both pressure- and thermal properties of the tires, which are neglected due to the low friction surfaces, which usually come with cooling properties for the tires. However, this approach brings extra difficulty to the real-time controller performance, as wet or snowed surfaces are usually less homogeneous as dry asphalt. In case of this research, the general standardized Magic Formula 5.2 is applied (3.6), with a simplified version (3.7) being considered due to the negative computational influence on the computational performance of a proposed NMPC controller. Both equations are described with similar parameters, where B and C are stifness- and shape- factors, respectively. Magic formula parameters D and E describe the slip at peak force at rated load F_z. Figure 3.4 indicates the influence of the Magic Formula parameters to the force that will be exerted at respective slip. The amount of parameters allow to fit the Magic Formula to almost any type of measured tire, where the standardized Magic Formula is able to capture properties throughout the complete slip range quite precise. Where the simplified model lacks force estimation in the larger slip ranges, thus being a good solution for control applications within the linear range of tires. As can be derived from figure 3.4, the tire forces increase until the peak friction point is reached. Once slip becomes larger than this point, a decrease of exerted forces on the contact patch is seen. However, in case of very low friction surfaces, such as snow or ice, tire behavior often shows no peak friction forces due to the lack of available traction.

$$\mu_{ij} = D_{ij} \sin(C_{ij} \arctan B_{ij} S_j - E_{ij}(B_{ij} S_j - \arctan(B_{ij} S_j)) \quad i = x, y \quad j = F, R \tag{3.6}$$

$$\mu_{ij} = D_{ij} \sin(C_{ij} \arctan B_{ij} S_j) \quad i = x, y \quad j = F, R \tag{3.7}$$

$$F_{ij} = -\frac{S_{ij}}{S_j} F_{zj} \mu_{ij} \quad i = x, y \quad j = F, R \tag{3.8}$$

A proposed schematics 3.5 allows us to use the knowledge of the vehicle- and tire model to explain what the relation between tire forces and the practical slip. During conventional driving at the largest possible yaw rate, the tires are at the friction limits, better known as the peak friction coefficient, where the larges lateral force is exerted through the tires. From this point on, the relation with the Magic Formula is seen, where larger tire slip angles result in a decrease of tire force, which in practice means that the vehicle will reach a high sideslip state once the steering angle is increased at similar velocity. Point A in figure 3.5 shows this peak in the lateral force component of the vehicle, where the lateral tire slip is at its limit, and the longitudinal slip approached zero. Point E describes a similar driving motion,

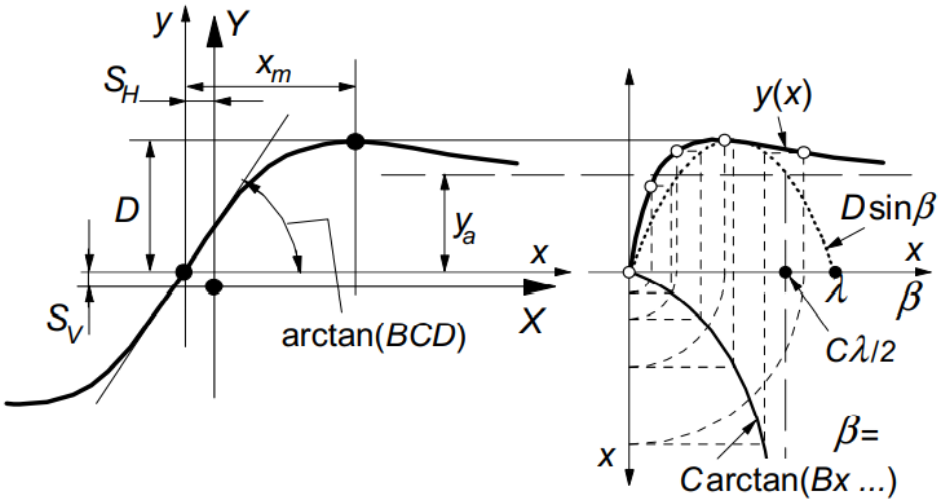

Figure 3.4: Influence of the Magic Formula coefficients on the directional force response with respect to its slip [22]

however at lower velocity or yaw rate, decreasing the lateral tire force. A drifting state is obtained at location D, where a larger rotational velocity compared to its longitudinal velocity component shows a high lateral slip state, while the wheels are spinning simultaneously. Points B and C show skidding behavior of tires at varying lateral slip angles, where the local tire velocity component in the longitudinal direction is larger than the rotational velocity of the wheel. Skidding occurs when brake torque is applied to a wheel, where tyre traction is missing such that wheels lock.

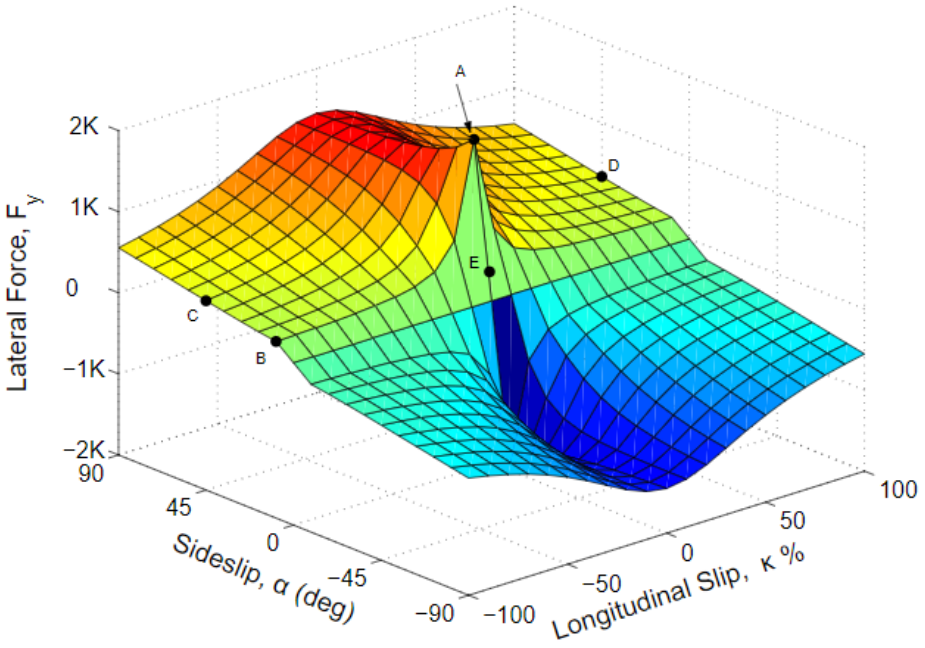

Figure 3.5: Lateral tire force variations with lateral slip angle α and longitudinal tire slip κ [1]

3.3. Differential

In general, most production vehicle have differentials installed on each driven axle, which are considered open. As the name implies, the differential enables a vehicle to have differentiated wheel rotational velocities. There is a desire for such application in case of turning during conventional driving, where the differential enables the outer wheel to have a larger angular velocity, as the this wheel has to cover a greater distance. This approach of an open differential is ideal for comfortable cornering during driving in normal road traffic, where loads and stresses on both tires and drive shafts remains minimized. The approach of an open differential does however have disadvantages and limitations when it comes to driving properties, mainly caused by too extensive differences between the left- and right wheel. For example, in case of fast cornering maneuvers, the inner wheel with respect tot the curve is relieved significantly, causing a decrease in applied torque which, limiting the torque on the outer wheel too. In combination with a driver applying aggressive throttle response might actually induce the inner wheel to start spinning, causing the outer wheel to follow that behavior accordingly. Similarly, different road-wheel interactions might also induce one wheel to start spinning, causing torque breakdown on the other wheel too. For example, one wheel being on a significantly more slippery surface such as black ice, while the other is placed on regular asphalt. But also the case where a wavy road surface causing one wheel to lose contact inducing complete loss of torque, causing the vehicle to not apply any torque at that instant.

The complete opposite to an open differential is a fully locked differential, indicating that the driveshaft on the left and right is considered rigid, causing the wheel speeds to be similar at all times. Most off-road personal vehicles enable the driver to choose between an open differential as well as a fully locked differential, in order to conquer uneven road surfaces or even tracks where there is no road contact on a wheel. However, driving with a fully locked differential induces the opposite of the advantages of the open differential, namely the overload and wear of drive-train components and tires, respectively. On top of that, the general driving response of the vehicle significantly reduces, as corresponding wheelspeed cause the vehicle to always go straight, causing understeer characteristics.

Combining both characteristics of the open differential and the fully locked rigid rear-axle is defined by a limited slip differential (LSD). For over 70 years, multi-disc locking differentials have been applied in almost all variants of motorsports, whether it is in track racing or on on off-road sports. Where on the one hand the advantages of the differential is retained, while eliminating the unacceptable disadvantages for a sporty driving style, or racing application. A properly designed limited-slip differential must therefore continue to allow for speed differences between the wheels within a certain range, but it should also be able to distribute the torque as variably and asymmetrically as possible to where it can be converted into propulsion, i.e. to the wheel with the higher grip level. In order to realise these goals, there are different types of systems for variable locking of the differential or asymmetrical distribution of torque, each of which has its specific advantages and disadvantages and should be specifically selected and used depending on the intended use and priorities. However, there are some reasons why we only find limited-slip differentials only in sporty personal vehicles, and not in all production vehicles. This is mainly due to the fact that the limited-slip differential is much more complex, as it has two functionalities, which should be selected (usually automatically) according to the driving style. This causes the development of such differential to be more complex due to the locking aspect, and therefore more expensive in both purchase and maintenance. On behalf of comfortable and efficient driving, the limited-slip differential also has two significant disadvantages, where the internal friction of the locking differential causes resistance and heat development, resulting in a minimal fuel consumption increase.

Most LSDs are based on the principle of lamella lock, where a firm connection is established through connecting inner- and outer discs, which connect due to clutch disks being pressed axially outwards on ramped differential axles. A variety of plate packages allow to vary the locking degree of the LSD. The locking degree describes the moment when the differential completely locks, as a result of the minimum locking degree and the applied preload, i.e. throttle response of the engine. The locking degree describes the point from which the differential locks as a result of a torque difference between the two drive wheels. This implies that the differential locks at torque differences smaller than the respective locking degree, whereas larger torque differences open the differential. Figure 3.6 shows

response of varying LSD setups, where the grey dotted line indicates a 0% locking 'open' differential, whereas the green plot on the right-hand plot approximates a 99% lock.

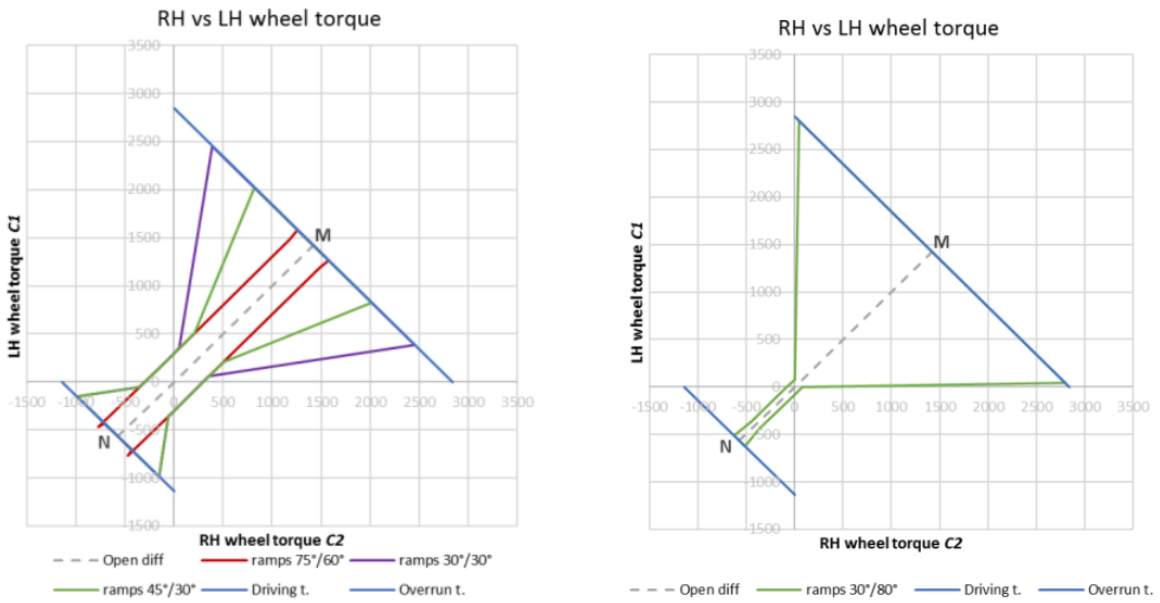

Figure 3.6: Limited slip differential, with varying ramp angles [8]

An attentive reader would have noticed that the information regarding the differential would not influence the direct characteristics of the single-track model, due to left- and right characteristics being lumped together. However, preliminary simulations of an NMPC approach show feasible results with varying degrees of locked differentials. As seen in the experiment proposed [15], a fully locked differential shows feasible drifting control. This is mainly due to the corresponding wheelspeed that occur between left and right, thus also for the single-track estimation of the vehicle state. In case of the fully locked differential the wheel torques differ amongst sides, but a resultant drive torque can still be used as a control input for an NMPC approach. In similar fashion, LSDs also lock, such that the drive torques between left and right are not larger than a respective ratio. Once a LSD locks, the wheelspeed difference also equals zero, thus the single-track relation holds. Successful controller simulations as well as experimental measurements using a driver input shows that a 30% locked differential is feasible in case a single-track vehicle modelling is feasible.

3.4. Load Transfer

A vehicle suspension system comes in many variants, as it has great influence on the driving characteristics of the vehicle. Very stiff spring coefficients are seen for racing applications, where luxury vehicles are equipped with springs that enable smooth and comfortable driving characteristics. Several proposed drifting control strategies ([14],[10],[35]) assume a static normal loads on all wheels, assuming there is no longitudinal load transfer taking place between the front- and rear axle of a vehicle. This assumption holds mainly for conventional driving in curves, where the load transfer mainly exist in lateral direction, due to the centripetal acceleration a_c (3.9) causing a load increase on the outer wheels of the vehicle. The total load on the front and rear suspension sets remain therefore almost similar, where a static load assumption for the bicycle model (3.10) usually suffices in application.

$$a_c = \frac{V^2}{R} = \frac{V}{r} \tag{3.9}$$

$$F_{zF0} = \frac{mgb}{L} \quad F_{zR0} = \frac{mga}{L} \tag{3.10}$$

3.4.1. Suspension dynamics modelling

However, in case of a drifting state of the vehicle, the velocity vector rotates significantly with respect to the the vehicles center, indicated by the large sideslip angle. The rotation of the vehicle causes the centripetal acceleration to decompose in both the lateral but also the longitudinal direction of the vehicle body. Preliminary results of an NMPC approach for drifting have shown that the static load approach (3.10) enables the vehicle to enter a state of drift, however, not reaching the desired reference states. Therefore, it is convenient to capture load transfer as much as possible, without influencing the computational capacity of the controller too much. For the bicycle model it is possible to model the suspension as depicted in figure 3.7, where one spring and one damper capture the dynamics on both the front- and rear axle, respectively. Where the pitch angle of the suspended mass θ and the vertical displacement of the CoG z and their time derivatives $\dot{\theta}$, $\dot{z}$ suffice in describing the vertical displacements Δz_i $\dot{\Delta z_i}$ for $i = F, R$ through geometrical derivation as derived in equation 3.11. Modelling the front and rear axles as spring-damper systems with coefficients K_i, C_i for $i = F, R$, respectively allow to compute the vertical loads on the front and rear axles as described in equation 3.12, where F_{zi0} is the static load distribution of the respective vehicle. The described mass-spring-damper system for the single-track vehicle model can be mathematically described by the differential equation stated 3.13.

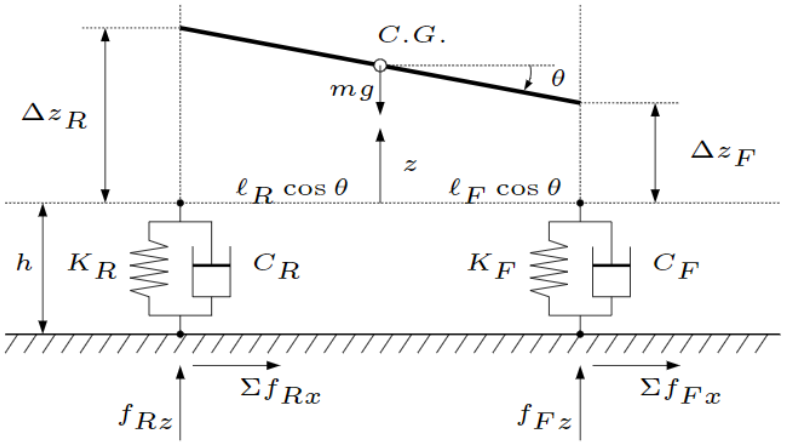

Figure 3.7: Schematics of suspension dynamics [30]

$$\begin{aligned} \Delta z_F &= z - a\sin\theta; \\ \dot{\Delta z_F} &= \dot{z} - a\cos\theta\dot{\theta} \\ \Delta z_R &= z - bsin\theta; \\ \dot{\Delta z_R} &= \dot{z} + b\cos\theta\dot{\theta} \end{aligned} \tag{3.11}$$

$$\begin{aligned} F_{zF} &= F_{zF0} - K_F\Delta z_F - C_F\dot{\Delta z_F} \\ F_{zR} &= F_{zR0} - K_R\Delta z_R - C_R\dot{\Delta z_R} \end{aligned} \tag{3.12}$$

$$\begin{aligned} \ddot{z} &= \frac{F_{zF} + F_{zR} - mg}{m} \\ \ddot{\theta} &= \frac{F_{zR}b\cos\theta - F_{zF}a\cos\theta - (F_{xF}\cos\delta - F_{yF}\sin\delta - F_{xF})(h+z)}{I_y}; \end{aligned} \tag{3.13}$$

3.4.2. Suspension dynamics estimation

Based on preliminary results of model predictive controller design, incorporating the true error dynamics of the vehicle brings an extra amount of required computational in order to optimize for the differential equation describing the suspension dynamics. Instead, an estimation of the the front and rear vertical load can be estimated through setting the sum of moments equal to zero, where incorporation of the measured longitudinal acceleration to estimate the difference in exerted vertical load between the front

and the rear axles. The difference in force can be estimated through the relation described in equation 3.14, resulting in the load estimation in equation 3.15.

$$\Delta_{F_z} = a_x \frac{mh}{L} \tag{3.14}$$

$$\begin{aligned} F_{zF} &= F_{zF0} - \Delta_{F_z} \\ F_{zR} &= F_{zR0} + \Delta_{F_z} \end{aligned} \tag{3.15}$$

3.5. Coordination of the vehicle

In order to obtain information of the state of the vehicle with respect to its environment, a path definition can be described by the relation between the absolute velocity V and path radius R and yaw rate r (3.16), where the path curvature K describes the inverse of the path radius.

$$K = \frac{r}{V} = \frac{1}{R}, \quad R = \frac{V}{r} \tag{3.16}$$

With respect to the definition of the single-track model, the path curvature and heading angle ψ allows us to describe the path by means of a curvilinear coordinate system 3.17, where the set of differential equations describe the change in heading angle ψ, travelled path s_X, and lateral deviation from the desired path s_Y.

$$\begin{aligned} \dot{\psi} &= r - K \frac{V \cos(\psi + \beta)}{1 - s_Y K} \\ \dot{s_Y} &= V \sin(\psi + \beta) \\ \dot{s_X} &= \frac{V \cos(\psi + \beta)}{1 - s_Y K}; \end{aligned} \tag{3.17}$$

4

Equilibrium analysis

As proposed mathematical analysis of vehicle states focused on drifting, shows that determining steady-state equilibria as well as a phase portrait analysis can tell us a lot about desired steady-state drift locations poses [36]. This chapter proposes a strategy of obtaining the locations of these equilibrium points (4.1), where also a comparison with experimentally obtained data is performed(4.2).

4.1. Steady-state equilibrium locations

The model description (3) and its set of nonlinear differential equations (3.1,3.2,3.13) capture most important dynamics of the vehicle states considering the single-track model. steady-states imply that the time derivatives of the system of equations is equal to zero, meaning that the state does not change with time, i.e. $\dot{V} = \dot{\beta} = \dot{r} = 0$. Based on this condition, the set differential equations can therefore be rewritten in the set of nonlinear equations (4.2). Equilibrium vehicle states are non-unique, where each solution could consist of all possible states of the vehicle, which resembles conventional driving, drifting in both forwards and backward directions. Therefore, the set of differential equations is solved using a nonlinear least-squares function of MATLAB $lsqnonlin$, as this form of optimization allows the incorporation constraints on respective states. An initial guess often allows the solver to converge to a desired state, e.g. a high sideslip drifting equilibrium, but the use of constraints on desired velocities, wheelspeeds and/or wheelslip make finding equilibria significantly faster. However, as can be mathematically derived, the proposed model contains more variables than equations, which means that certain equilibrium values therefore have to be chosen by a value that could describe a drifting motion. Therefore, the system of equations is solved using a desired sidelip angle β^{eq} while a range of experimentally confirmed feasible path radii is considered R^{eq}. As a result, the optimization variables are described by $\mathbf{x}_{eq}$ (4.1), which allows to compute all respective tire force components.

$$\mathbf{x}^{eq} = [V^{eq} \quad \beta^{eq} \quad r^{eq} \quad \omega_F^{eq} \quad \omega_R^{eq} \quad \delta^{eq} \quad T_i^{eq}]^T \tag{4.1}$$

$$\begin{aligned}
0 &= \frac{F_{xF}^{eq}\cos(\delta^{eq}-\beta^{eq}) - F_{yF}^{eq}\sin(\delta^{eq}-\beta^{eq}) + F_{xR}^{eq}\cos\beta^{eq} + F_{yR}^{eq}\sin\beta^{eq}}{m} \\
0 &= \frac{F_{yF}^{eq}\cos(\delta^{eq}-\beta^{eq}) - F_{xF}^{eq}\sin(\delta^{eq}-\beta^{eq}) - F_{xR}^{eq}\sin\beta^{eq} + F_{yR}^{eq}\cos\beta^{eq}}{mV^{eq}} - r^{eq} \\
0 &= \frac{a[F_{xF}^{eq}\sin\delta^{eq} + F_{yF}^{eq}\cos\delta^{eq}] - bF_{yR}^{eq}}{I_z} \\
0 &= \frac{T_j^{eq} - F_{xj}^{eq} r_j}{I_{\omega j}} \qquad\qquad j = F, R
\end{aligned} \tag{4.2}$$

Since the results of the equilibrium points are considered non-unique, as a drifting equilibrium is controlled through a balancing relation between the front- and rear force magnitudes. This implies that variations in rear drive torques, and its resultant longitudinal slip coefficient may vary, as the front axle

is subject to different poses, thus varying forces. The equilibrium analysis shows that the velocity of vehicle state equilibria 4.8 increases as the desired path radius at constant sideslip angle, whereas a constant radius causes a decrease in sideslip angle as a result of the force balance required between the front and rear axle. As a result, the yaw rate of the vehicle increases with the path radius through the relation 3.16.

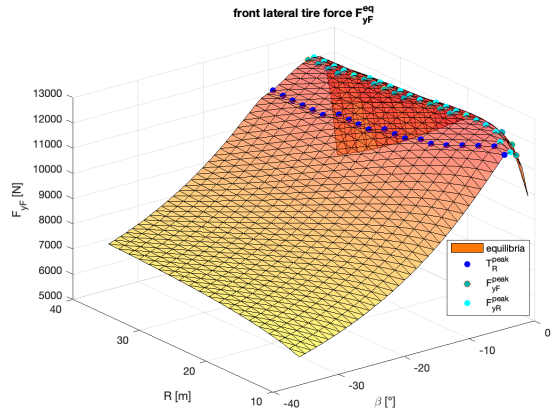

Figure 4.1: Equilibrium front lateral tire forces F_{yF}^{eq}

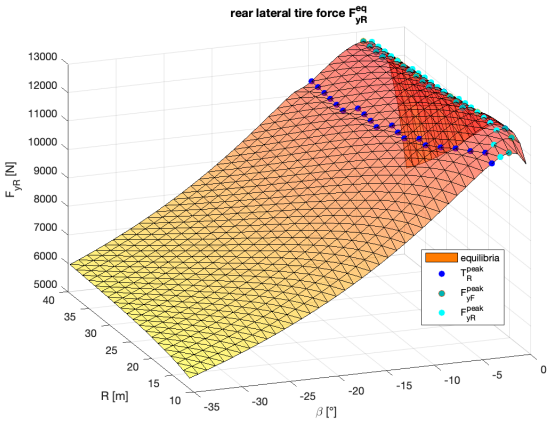

Figure 4.2: Equilibrium rear lateral tire forces F_{yR}^{eq}

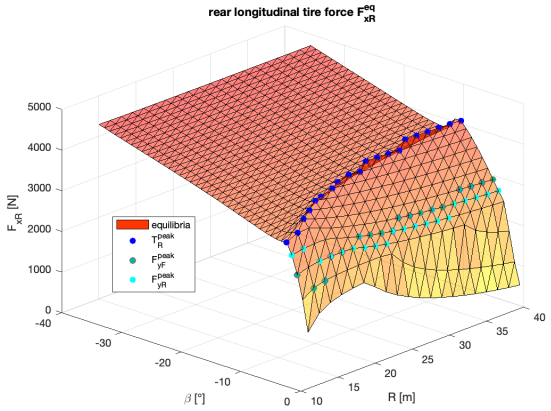

Figure 4.3: Equilibrium rear longitudinal tire forces F_{xR}^{eq}

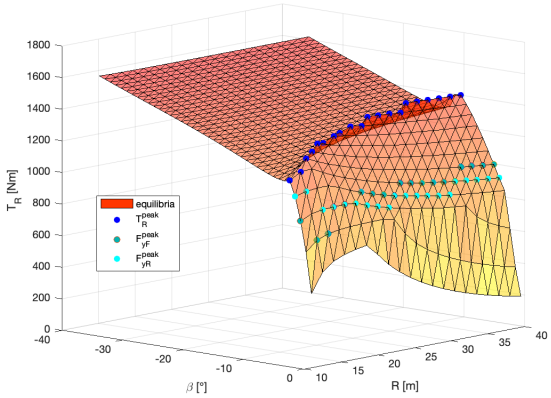

Figure 4.4: Equilibrium rear axle drive torque T_R^{eq}

In correspondence to the Magic Formula definition (3.2) figures 4.1,4.2 show that that the lateral tire forces are at its highest at relatively small sideslip angles, thus small tire slip angles. This implies that towards these peaks, the vehicle is considered conventional driving in the linear range of tires, which can also be indicated by the near corresponding wheelspeeds (4.7) and positive steering angles (4.5). At a further increasing sideslip angle, clear indications show that the front- and rear wheelspeeds start to deviate in magnitude, indicating that the vehicle state is entering a drifting state where the steering angle approaches zero, while the rear longitudinal force has not reached its peak force (4.3). This means that the applied rear torque results in a reasonable amount of slip such that the rear tires become saturated in lateral direction with a reasonable sidelip state. However, since the peak friction force in longitudinal direction is not reached, we consider the the drifting state towards this point a transient drifting state, i.e. there is a slight drift, however tires are not fully saturated nor counter steer is taking place. All equilibria plots have the locations of the peak drive torques ●, rear lateral peak forces ● and the front lateral peak forces marked ●, in order to support information.

Once the the peak longitudinal slip is reached, thus the amount of wheelspeed becomes signifcantly larger than the rear axle longitudinal velocity, we consider the tires saturated in both lateral- and longitudinal direction, where a direct change in steering angle is obtained (4.5) in order to balance the front and rear forces. Larger sideslip are considered fully drifting equilibria, where we see proportional

behavior in the steering angle, and further deviation in the wheelspeeds (4.7) which are are a result of larger required rear slip, and decreasing front wheelspeed due to decreasing yaw rate. Please note the direct relation between the longitudinal tire forces(4.3) and the applied rear torque (4.4), as a result of the equilibrium definition at the rear axle (4.2).

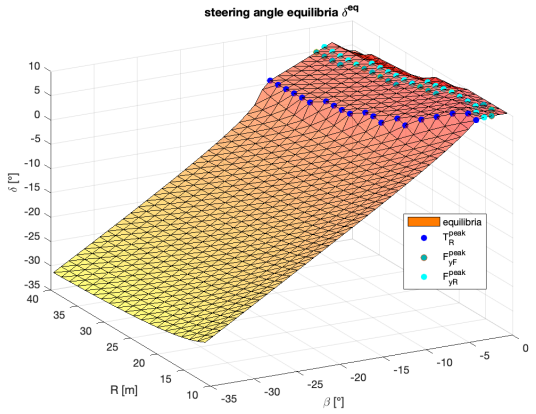

Figure 4.5: Equilibrium steering angle δ^{eq}

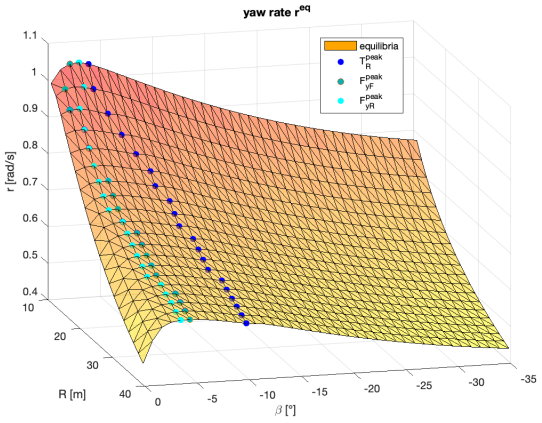

Figure 4.6: Equilibrium yaw rate r^{eq}

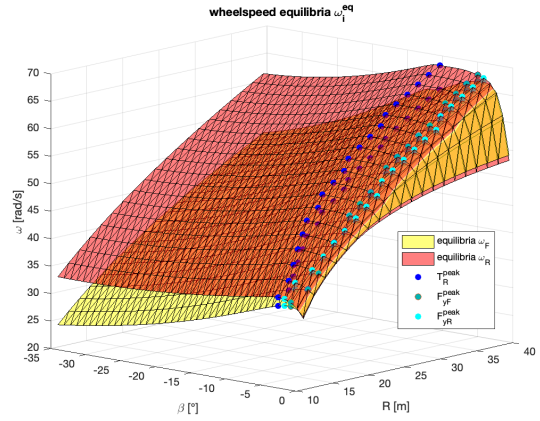

Figure 4.7: Equilibrium wheelspeeds ω_F^{eq},ω_R^{eq}

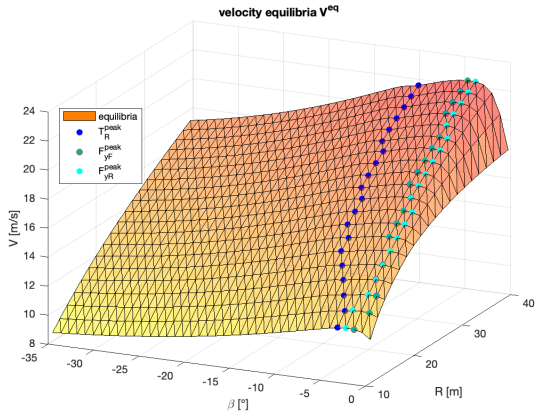

Figure 4.8: Equilibrium absolute velocity V^{eq}

4.2. Experimental verification

An experimental verification has been conducted in order to determine the correspondence between practical and theoretical equilibria, which can be deployed as a confirmation of the identified model parameters. The experimental data is obtained on the BMW proving grounds of Aschheim where a slightly conical skidpad is sprayed with constant water flow. As mentioned, the single-track model does not capture a large amount of dynamics of a production vehicle and its tire-road interaction, therefore the single-track approach should be modelled such that it corresponds to the true vehicle as best as possible. Figure 4.2 shows a comparison of theoretical equilibria with measured vehicle states, of which the latter are measured by means of the vehicle state estimation signals, which are found on the CAN bus of most production vehicles. The measured sideslip angle functions as a fixed parameter for the $lsqnonlin$ function optimizing for the equilibrium vehicle state equilibria. The measured vehicle state functions as an initial guess for the equilibrium analysis, in order to bring the equilibria as close as possible. The results show that reaching an actual equilibrium point as a manual driver is relatively hard, due to many influences on the vehicle such as road surface, and further dynamics not captured with the model definition (3). Real road surfaces are considered non-homogenous where a $5-10\%$ variation in the friction coefficient is measured for the respective proving ground, which a driver needs to compensate through changing the steering angle or throttle commands causing the steering angle

and applied drive torque never really being constant. The slightly tilted position of the vehicle due to the conical shape of the surface also remains uncaptured in the bicycle model definition, causing variations in the vertical axle loads. In addition, it should be taken into account that the driver both has to stabilize the desired drifting state, while stabilizing on a desired path. This implies that the experimental data is not considered to be in an equilibrium for all time instants, however, the comparison does show reasonable similarities in the order of magnitude.

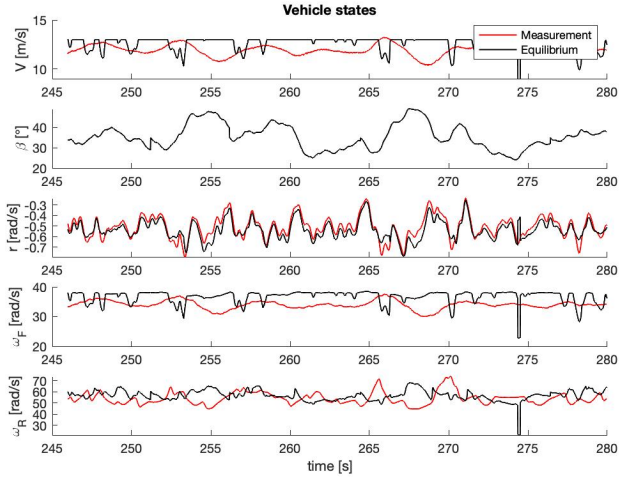

Figure 4.9: Experimental/Theoretical drifting state comparison

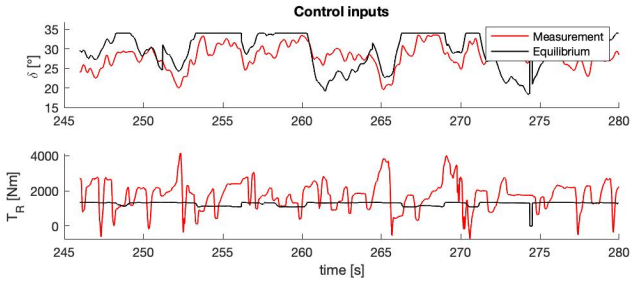

Figure 4.10: Experimental/Theoretical drifting control inputs comparison

The comparison between experimental and theorethical drifting states has shown that around an actual drift equilibria, many variations of drifting equilibria exist. Where physical constraints such as steering angle limits δ_{max} does not significantly influence the high sideslip state, as small deviations in the front lateral slip angle α_F would still converge to an equilibrium drifting state. In similar fashion, slight variations in the drive torque, thus wheelspeed show that equilibria exist for multiple wheelspeeds. As indicated by figure 4.2, the optimization algorithm converges to the maximum allowable value of steering angle δ, while the experimental data shows smaller steering angles with intervention needed reach a desired path.

5

Control system design

5.1. Controller structure

The proposed control system to both stabilize the vehicle into a high sideslip state and to maintain a desired state in space is summarized in Figure (5.1). Where a nonlinear model predictive controller (NMPC)(5.1.1) functions as the foundation of the proposed control system, which is able to compute required control inputs to reach any feasible reference state of the vehicle. This implies that the NMPC solver can be deployed to both optimize for control inputs in the high sideslip state, but also for conventional driving thus enabling an initializing drive towards a drifting motion.

Dynamic referencing allows to influence the direction of the vehicle, where the offline computed equilibria as proposed in chapter 4 can be selected dynamically by means of using positional data of the vehicle S^{veh} to alter the path curvature such that the lateral error e_y of a desired path is decreased. The combination dynamic referencing and the vehicle state controller enables to bring a vehicle in both into a desired high sideslip state, while converging towards a desired trajectory.

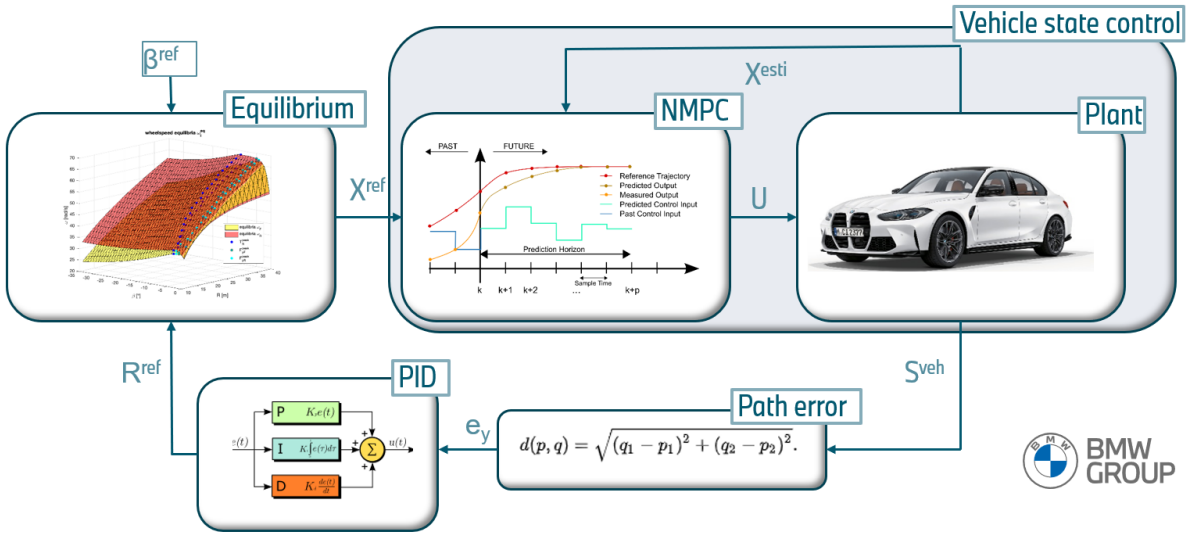

Figure 5.1: Proposed control system strategy

5.1.1. Nonlinear Model Predictive Control

Model predictive control (MPC) is one of the most popular control techniques deployed, as several variants enable a model based control strategy for both linear as well as nonlinear systems. Model-based control implies that knowledge of mathematical dynamical model is used to predict the future behavior of the system, which allows to optimize the process control over a prediction horizon. This method of

control is based on the receding horizon principle, the general purpose of which involves iterative solving of an (un-)constrained optimization problem, using predictions of future states, disturbances, and constraints over a moving time horizon to choose the optimal control action. Since constraints can be taken into account, MPC constitutes a control approach with significant increase in both performance as well as applicability with respect to other control methods. Figure 5.2 shows a schematic overview of the model predictive control strategy, to get a grasp of the functioning of MPC. At time instant k the measured state of the dynamical system is measured and compared to a desired reference state. For a defined prediction horizon, the control strategy predicts the behavior of the plant, which enables to solve an optimal control problem (OCP) at each sampling instant. The OCP tries applies optimization to find the most optimal control input that will bring the respective plant into a desired state. Once the OCP is solved, the control input at instant k functions as the required control input for that particular time instant k, whereas the future control inputs are discarded. At the next timestep Ts, the process is repeated, until.

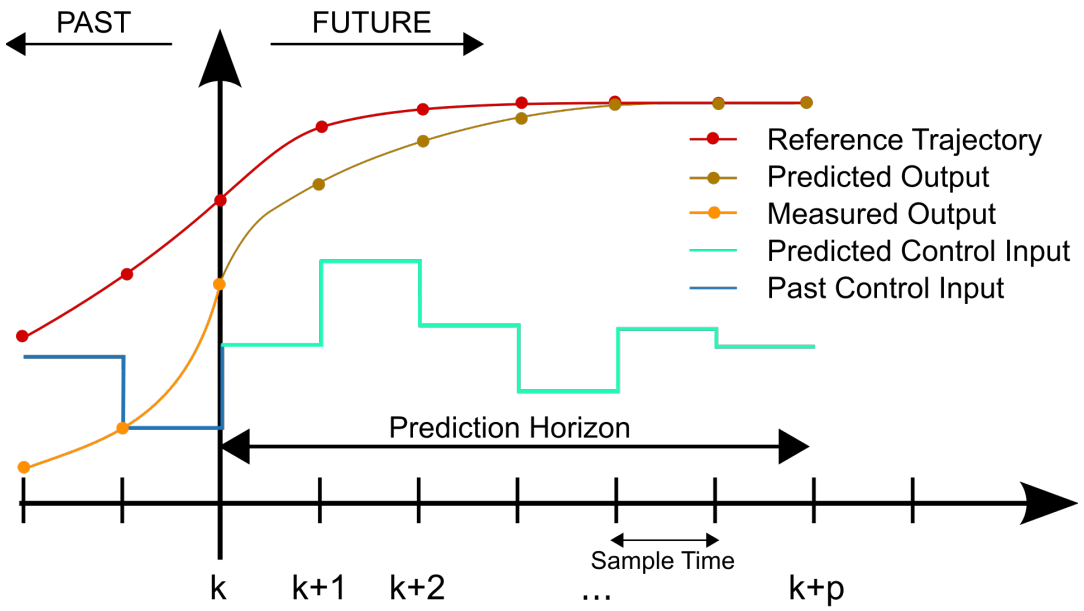

Figure 5.2: Model Predictive Control Scheme [19]

In general, the minimization of a cost function (Equation 5.2) determines the optimal control input that minimizes the error of the vehicle states with respect to a desired reference state x_{ref}. Depending on the purpose of the drifting controller, a potential reference for a steady-state drifting controller could for example be the steady-state sideslip angle or yaw rate of the vehicle, as determined by the equilibrium analysis. Similarly, a drifting pose can be expressed without explicitly referencing on the sideslip angle, as a revision on the mathematical expression of the sideslip angle (1.1) shows us that a drifting state can also be expressed by longitudinal- and lateral velocity components, as proposed [35].

$$V_N(x_0, d, y_{ref,N}) = \frac{1}{2}\sum_{k=0}^{N-1}(\ell(x(k) - x_{ref}, u(k) - u_{ref})) + V_f(x(N) - x_{ref}) \tag{5.1}$$

The cost function describes the model dynamics $x(k) = \phi(k; x_{0,k})$, while $\ell(x(k), u(k))$ and $V_f(x(N))$ are the stage cost and terminal cost, respectively. The stage cost and terminal cost are considered quadratic cost functions, with tunable positive-definite weight matrices Q, R and M, for the states x and input u alike (see Equation 5.2), while V_f is the terminal cost which is used to guarantee the steady-state is reached.

$$\begin{aligned}\ell(x(k), u(k)) &= x(k)^T Q x(k) + u(k)^T R u(k) + 2x(k)^T M u(k)\\ V_f(x(N)) &= \frac{1}{2}x(N)^T P x(N)\end{aligned} \tag{5.2}$$

The MPC optimization problem can be summarised as follows (5.3), where a minimisation of the cost function is subject to the system dynamics and constraints. The inequality constraints are represented in form where the matrices G and H contain information on the application of constraints, for both the states x as input u, respectively. When it comes to a steady-state drifting controller, physical constraints such as the steering angle, but also for constraints that contribute to stability by means of constraining velocities, tire forces, or the sideslip angle.

$$\mathbb{P}_N(x_0, d, y_{ref}) \in \begin{cases} \min\limits_{N} & V_N(x_0, d, y_{ref,N}) \\ \text{s.t.} & x^+ = Ax + Bu + B_d d \\ & Gx + Hu \leq \psi \\ & x(N) \in_f (d, y_{ref}) \end{cases} \tag{5.3}$$

5.2. Vehicle state controller

For the sideslip stabilization, the vehicle state controller can be defined differential states (5.4) that describe the differential states of the set of differential equations 3.1, 3.2 are directly measured, or converted from the four wheel vehicle state signals in order to correspond with the single-track model.

$$\mathbf{x}_{vsc} = [V \quad \beta \quad r \quad \omega_F \quad \omega_R \quad \delta]^T \tag{5.4}$$

As can be indicated, the steering angle δ is also defined as a differential state, as the control input on the steering angle is described by required steering angle difference $\dot{\delta}$. This enables to constrain the gradient of the steering angle, which allows to mimic human steering behavior, as well as being able to capture physical steering constraints such as maximum applicable steering rate. The respective control inputs for the vehicle can therefore be described by equation 5.5.

$$\mathbf{u}_{vsc} = [\dot{\delta} \quad T_i]^T \tag{5.5}$$

An auto-generated solver [25] is applied, which creates an OCP of the vehicle description, enabling to compute the optimal control input that will lead to reaching a desired state $\mathbf{x}_{des}$. Additional to the differential states, the longitudinal acceleration a_x is also measured and injected into the solver as online data. Using the longitudinal acceleration allows to estimate the longitudinal load transfer, which estimates vertical load estimation as proposed 3.14. As mentioned, the single-track model will not capture load transfer exactly, however, using knowledge of the longitudinal load transfer positively contributes to the OCP.

5.3. Path-following controller

As briefly touched upon, converging the high sidelip vehicle state towards a desired trajectory takes place through dynamically determining desired references. This is established through compensating the desired path curvature in relation with the lateral error, through a proportional- integral- derivative gain (PID) controller that determines a compensating factor on the path curvature ΔK, which is defined by equation 5.6. The compensating factor is used to modify the desired path curvature is updated $\tilde{K}$, as described by equation 5.7 . With relatively small controller gains K_p K_i K_d, the desired path curvature is altered such that the vehicle state converges towards the desired trajectory.

$$\Delta K = K_p e_y + K_i \int_t^0 e_y + K_d \dot{e}_y \tag{5.6}$$

$$\tilde{K} = K - \Delta K \tag{5.7}$$

The altered path curvature functions as an input for a lookup table that contains a complete set of equilibria, which therefore picks the optimal equilibrium that functions as a reference for the controller. By means of interpolation intermediate values can be found, but however creating a large enough dataset is more computationally efficient.

6

Simulation validation

The proposed control system (5) has been evaluated both numerically through an extensive 17 degrees of freedom (DoF) simulation tool developed by BMW (6.1) as well as through an experimental setup using a serially produced sports sedan (7). Given that the test bench, the M3 competition (G80) is a vehicle of the subsidiary of BMW, M GmbH, there is no simulator available for the model. That is why the most sporty model in the same build row has been used for the numerical simulation of the controller, namely the BMW 340i (G20), where a corresponding powertrain layout has been applied to the test bench, i.e. rear wheel driven and a limited slip differential which allows to modify the locking rate. Tires of the same make were also used in the simulation and during the experiment, with differences mainly in the stiffness of the suspension and chassis. Since the G80 is even more designed for sporty driving than the G20, this will benefit the experiment, as less longitudinal and lateral load transfer takes place as compared to the simulator.

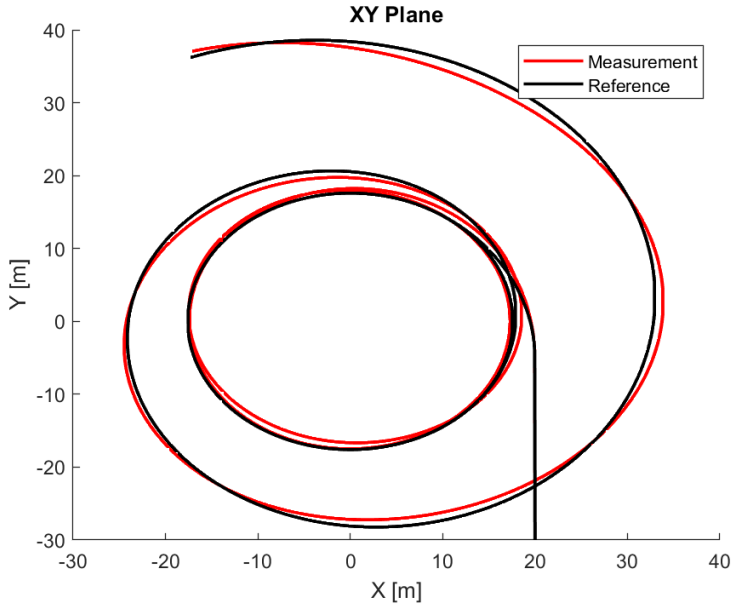

Figure 6.1: Vehicle position in XY plane, comparison between true and desired position

6.1. Combined sideslip stabilization and path-following

At first, a simulated response on an ideal world simulation for the combined path-following and sideslip stabilization is proposed, where a predefined path (6) is used as an input for the control system, as well as a desired sideslip angle β for the vehicle pose. The scenario consists of a straight drive, which

changes into a constant curvature for two laps, until the curvature spirals outwards. The travelled distance S_x is used to find the corresponding path curvature K_{ref}, which enables the control structure to determine the belonging drift equilibrium to the position in space. The lateral path deviation as obtained in figure 6.1 functions as an input for the PID control structure to compensate for the motion deviating from the desired path. As can be obtained from the vehicle states 6.1, a maximum lateral error of approximately 1 meter is obtained, where also notable deviation is seen in the sideslip angle tracking. Reason for this is the distribution of tuning weights for MPC solver, where the aim is to be in a high sideslip state, while, more importantly, remain within reasonable limits of a desired path. Th relation 3.16 shows that main focus for sustaining a desired path curvature should be on the vehicles yaw rate r and absolute velocity V, where focus on the tracking the exact sideslip angle is decreased such that a high sideslip state is still reached.

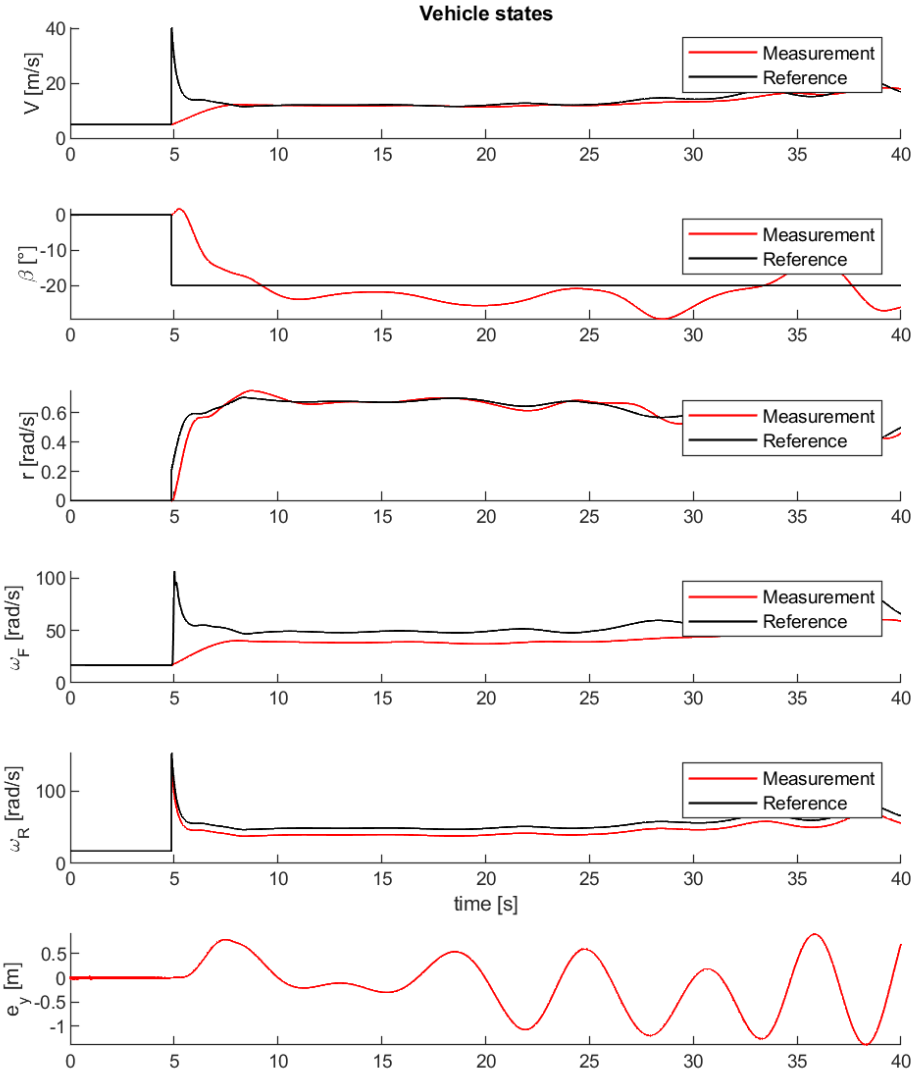

Figure 6.2: Vehicle states of a path following scenario while sustaining a stabilized drift movement

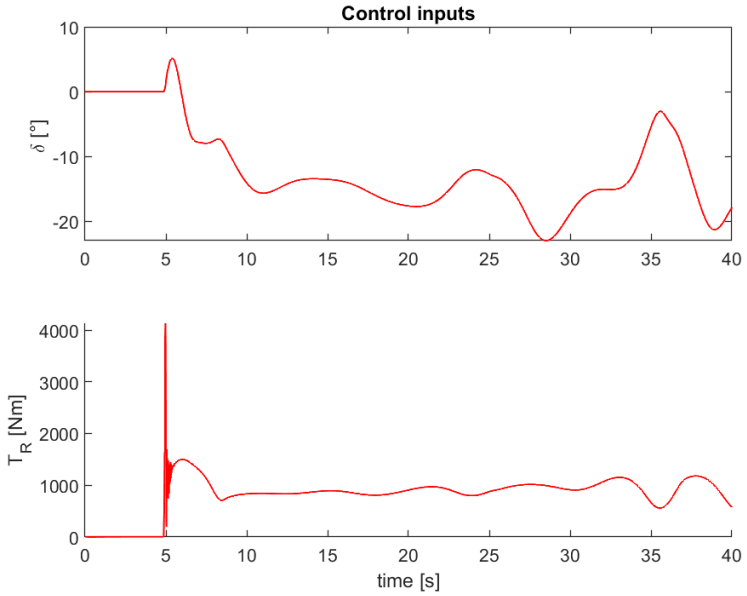

Figure 6.3: Control inputs of a path following scenario while sustaining a stabilized drift movement

6.2. Alternating drift scenario

At BMW, number of simulation tools is used to verify control systems and various dynamic properties with the purpose of indicating true driving response. A self-developed, widely applicable tool is the simulator called ISAR, which offers a very extensive description of a complete vehicle model based on a Simulink model, whereby a large scale of simulations can be performed based on laws of physics as well as obtained data regarding respective race tracks and environmental factors. Other than the vehicle description for the controller, ISAR is a two-track model, which incorporates all thinkable dynamics existing in a four-wheeled vehicle.

As the ACADO generator has the ability to generate an S-function for Simulink, a smooth integration of the proposed controller is implemented relatively easily. In case of the ISAR simulation, an alternating drifting scenario is applied on a high friction surface, which is initialized by a high yaw rate state within the limits of friction. As seen in figure , the simulated vehicle is able to track the initial left-hand drifting maneuver once initialized, while a nearly instant transition into a right-hand drift is achieved with corresponding tracking performance. In this case, we can obtain the response of the 30% LSD, as the left- and right wheelspeeds become similar, thus implying a locked state. In similar fashion, we obtain that the single-track model is able to capture a large amount of the vehicle dynamics for the drifting state, as the desired equilibrium is based upon that description.
As mentioned, the ISAR simulation tool capture much more dynamics as compared to the single-track model, where up to 17 DoFs are considered for describing vehicle dynamics. However, the dynamics are still considered to be an 'ideal' case, where both systematic- and measurement noise are ignored, as well as a constant friction coefficient exists for the complete simulation. Therefore, measurement noise and friction coefficient variation is included into the simulation, in order to prove robustness for a realistic case. Friction coefficient variation is based on surface measurements of the BMW proving grounds of Aschheim, which have shown that seemingly homogeneous surfaces tend to have friction coefficients variations of approximately 0.05. Amplitude and frequency of simulated measurement noise is based on obtained vehicle measurements from the test bench vehicle.

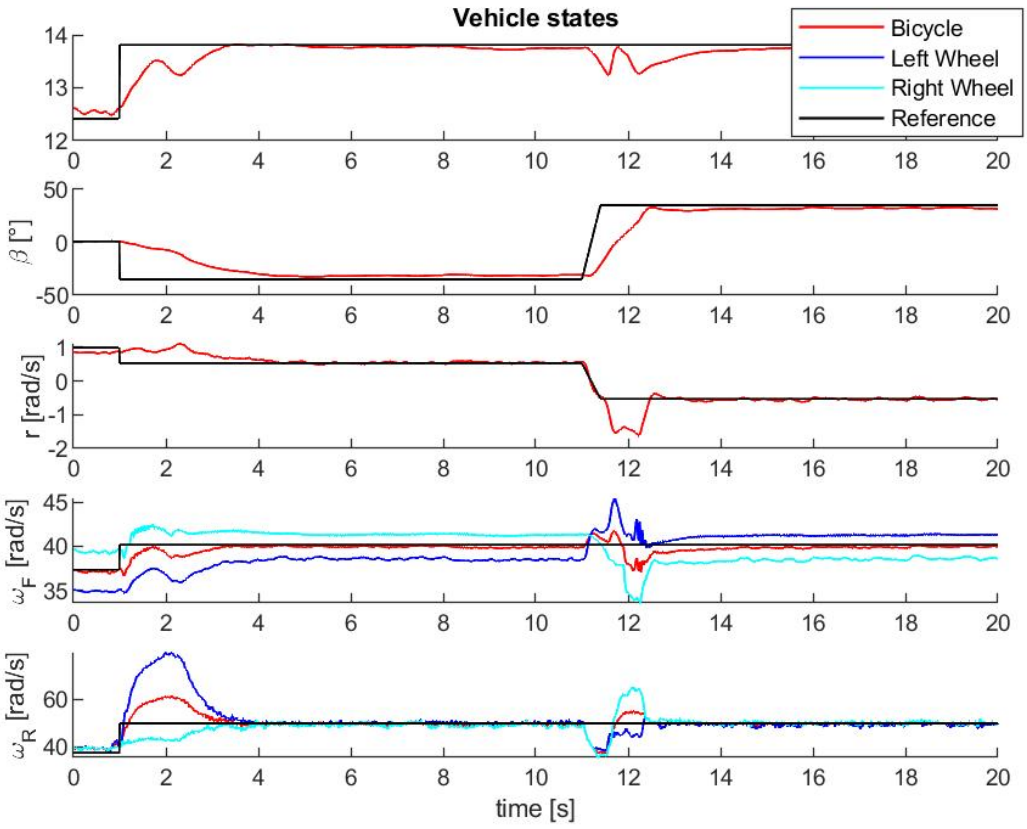

Figure 6.4: ISAR state response while sustaining an alternating drift scenario on a high friction surface

Due to the introduction of these noises, we obtain quite a noisy response from the desired control rear drive torque as seen in figure 6.2. Constant weighting for the complete simulation shows some erratic behavior in the linear driving range, yet the solver remained stable under these circumstances. There an optimization takes place on the steering angle rate $\dot{\delta}$, the desired steering angle remains more smooth, as the steering angle rate is constrained in the optimization.

Response of the the simulator shows that engine dynamics and systematic delays are seen, as the bicycle model calculation of the left- and right wheel drive torque is not of equal peak magnitude. This implies that rapid increase of desired drive torque is not tracked instantly, however since the drifting states are reached with optimal tracking, these model uncertainties can be covered with the proposed sideslip stabilization strategy.

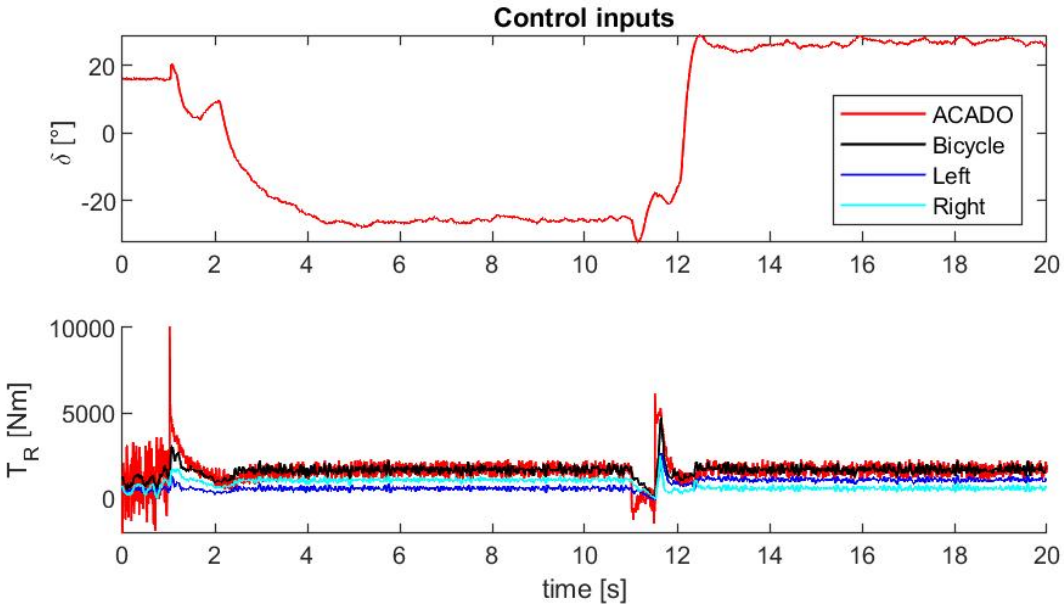

Figure 6.5: Control inputs for ISAR simulation while sustaining an alternating drift scenario on a high friction surface

6.3. Forward-looking approach to the reference

As in most automated driving applications, a scenario is proposed where actual 'looking ahead' is taking place for improving behavioral responses of the control strategy. Since many perception techniques are already applied in automated vehicles, the forward-looking factor can make a favorable contribution to improving, for example, an automatic evasive manoeuvre. As a comparison, we can see the results of a time-dependent reference setting, of which simulative results are shown in figures 6.6 and 6.7. These results show that looking ahead also has the ability to reach the desired drifting state, yet the response is more smooth, as at each time instant the solver can incorporate future desired state, thus choose its control inputs accordingly. We can see this mainly in the smoothness at which the sideslip angle is reached, but especially as we compare the yaw rate peak during the transitional drift. As we compare the static reference yaw rate (6.2) with the (6.6), we see that the magnitude of the yaw rate peak is lower as well as more evenly distributed. In practice, this means that the vehicle is more stable, where aggressive change in yaw rate may cause complete slip through. As indicated by the control inputs (6.7), the less aggressive response is consequence of smaller peak drive torques. As the updated control strategy has the ability to know the future state before reaching it, the desired transition takes place more towards the time instant the desired drifting state is initialized.

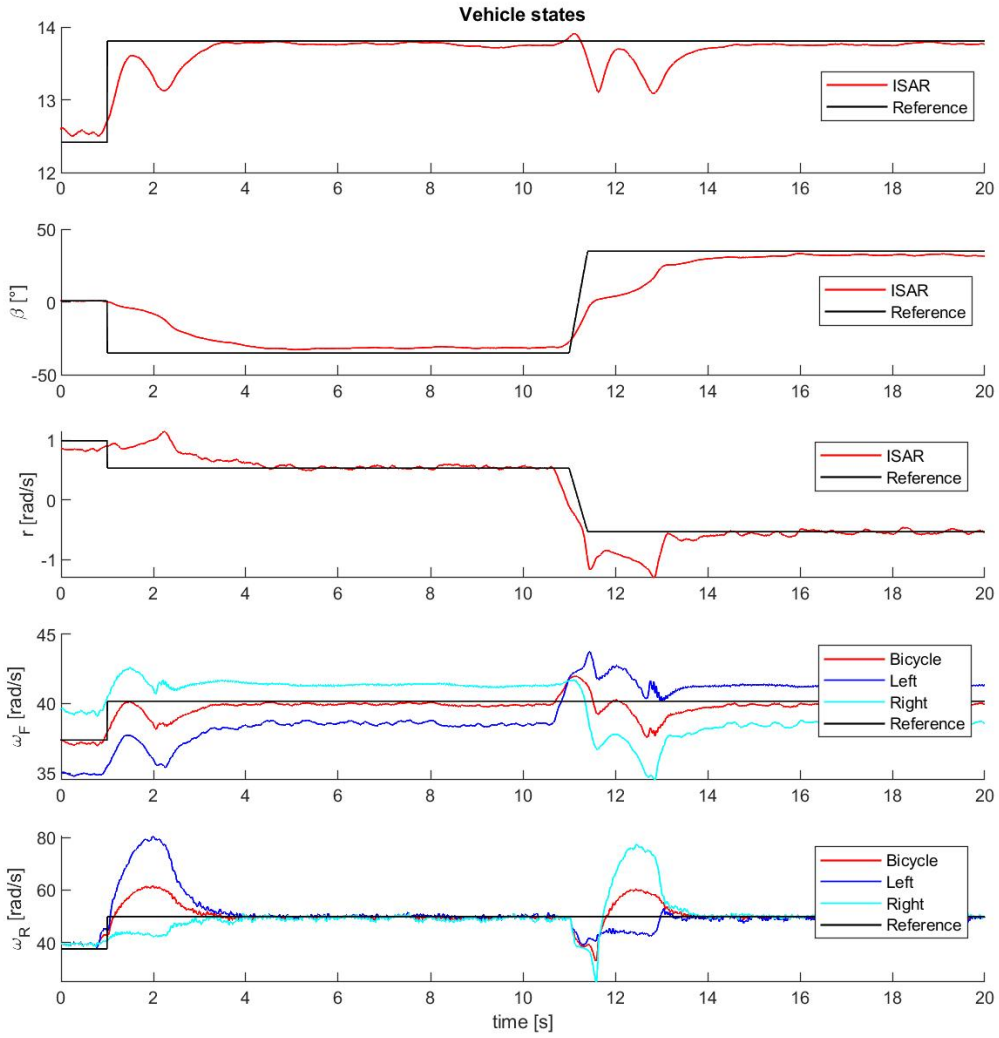

Figure 6.6: ISAR state response while sustaining an alternating drift scenario on a high friction surface, while future reference is considered

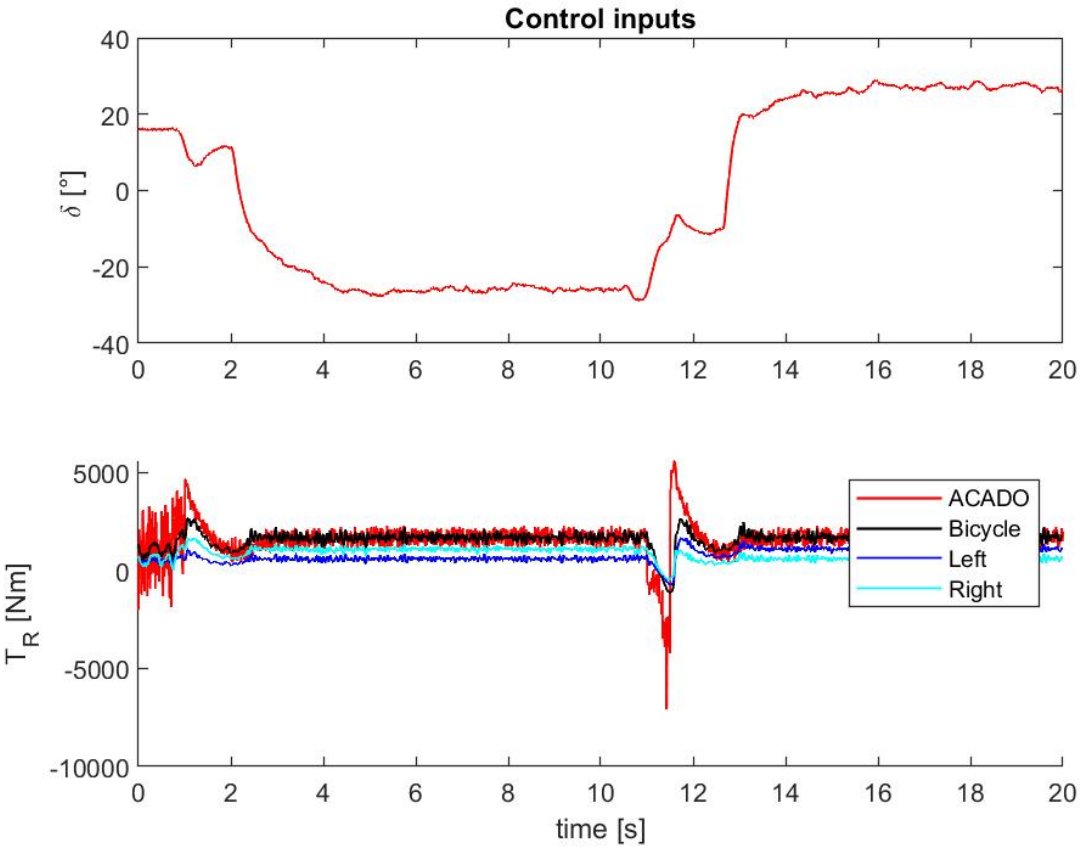

Figure 6.7: Control inputs for ISAR simulation while sustaining an alternating drift scenario on a high friction surface, while future reference is considered

7

Experimental validation

An experimental verification has been performed using a rear-wheel driven $BMW\ M3\ Competition\ (G80)$ [A.1], which is a high performance mid-size sports sedan which allows both daily driving as well as well performing on the racing track. This is established by an variety of engineered sport features such as a stiffened chassis as compared to the basic $BMW\ 3-series\ (G20)$ [A.3], and many modification that improve vehicle dynamics for performance purposes such as stiffened suspension, wider tires and optionally ceramic brakes and carbon fiber parts. The vehicle is serially equipped with an active differential, where an electric engine has the ability to actively apply pre-tension to the differential, to influence locking capabilities.

The implementation the proposed controller has been enabled through physically decoupling the driving assistance systems interface (FAS) of the testbench and replace control signals with the desired control signals from the proposed control system. The auto-generated real-time ACADO c-code has been implemented on a $DSpace\ Autobox\ DS1007$ platform, which enables an interface for desired Flexray- and CAN bus communication protocols in order to send- and receive information from from the vehicle and desired external devices such as DGPS or IMU. The controller is implemented using the measured- and estimated state signals at $10\ ms$ found on the Flexray BUS of the vehicle, as integrated control units of the vehicle the often apply Kalman filtering on the signals, having more numerically stable state signals as compared to measured states from a used IMU.

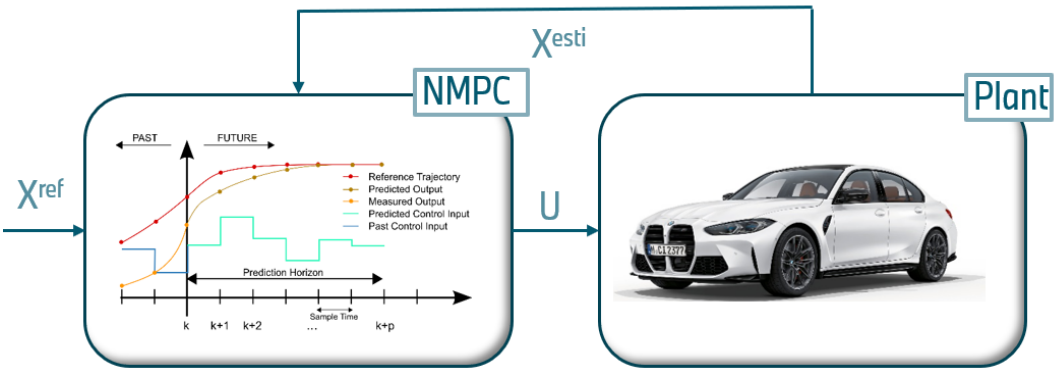

Figure 7.1: Proposed control system strategy for the experiment

7.1. Control system adjustments

As the generated NMPC code requires a significant amount of computational performance, the complexity and settings of the controller had to be reduced significantly, in order to run for the real-time application while remaining sufficient numerical stability. To start with, the path following properties have been neglected, which therefore the sideslip stabilization is experimentally verified as proposed

by the schematics (7.1). As the usage of signals that capture certain degree of measurement noise, the numerical stability of the solver is highly influenced by the choice of integrator. Where in case of the Flexray signals, at least the fourth order Runge-Kutta-Legendre method is desired as the integrator type for the solver. A timestep of $20\ ms$ enables sufficient time to solve the optimization for a prediction horizon of 25 steps. As a result of this decrease increase in timestep, the NMPC Tuning parameters have a different order of magnitude as compared to the ISAR Simulations, which was simulating using a timestep of maximum $10e-4s$. Due to the larger timestep used on the DSpace platform, larger differences in vehicle states are obtained for each timestep, which therefore decreases the weight towards a drifting equilibrium. However, as seen in the Table 7.1, distribution of the weights is somewhat corresponding. As the largest weight is always on the sideslip angle, in order to focus the controller on bringing the vehicle towards that state. Similarly, yaw rate desires a relatively large weight contribution, in order to generate sufficient yaw moment to reach the high sideslip state. While in order to ensure smooth steering, the weight on the steering rate is determined such that there is no erratic steering behavior is obtained, but still is quick enough to mimic a drifting maneuver. The weights on the wheelspeed and velocity work contributing to eachother when it comes to conventional driving. However, for the drifting maneuver, focus on the wheelspeed is of much higher importance due to the desired slip required at the rear wheels. Other parameters have been kept significantly low, as no reference drive torque nor steering angle where applied. Additionally, the simplified Magic Formula (3.7) is used to compute the front axle tire forces, as a drifting state assumes the front tires to have relatively lateral tire slip angles, thus having responses in the linear range of friction forces.

Table 7.1: Applied NMPC Tuning parameters used during the experiment

Parameter	ISAR	Experiment
W_V	1e-16	10e-4
W_β	10e4	350
W_r	10e3	250
$W_{\omega F}$	50	1.8
$W_{\omega R}$	50	1.8
W_δ	1e-16	10e-4
W_{TR}	1e-16	1e-16
$W_{\dot{\delta}}$	200	2

7.2. Production vehicle adjustments

As driving assistance systems such as automated lane keeping have the tendency to not be fully self-driving, applied steering torques and angles through the FAS interface are limited in magnitude for safety purposes. Where applied steering torque for the driving assistance systems is applied by means of the torque actuator in the electronic power-steering unit (EPS), a fallback safety feature ensures that the magnitudes of the respective units do not exceed certain margins. As these limits are implemented through standardized software for the serial vehicle, a custom software stage is uploaded to the EPS that maximizes the applicable steering angle and control torque.

A similar approach is used for the applied drive torque to the wheels, where integrated accelerometers on the rear axle constantly measure the state of the vehicle and process its magnitude in the digital motor electronics (DME) unit. Where in similar fashion to the EPS, a serially produced vehicle has safety limits on the relation between the applied drive torque and measured acceleration. Where in case the applied drive torque from the FAS interface exceeds $4m/s^2$, the vehicle runs into an emergency state. As a steady-state drifting motion commonly has centripetal accelerations beyond the integrated safety limit, the complete DME is replaced with an applicable DME, which as the name implies, enable to apply desired values such as extending safety limits. In case of the drifting control testbench, the complete functional safety system (FuSi) is switched off on the DME.

7.3. Parametric uncertainties and imperfections

7.3.1. Tire modelling

The proposed dynamical system described by the single track model (3) is considered very stiff as compared to the testbench, as well as for the simulator (6.1), where however the experimental test becomes more complex when it comes to parametric uncertainty, where most significant deviations are obtained when it comes to the road-tire surface. Where most significant influence is obtained by the state of the road surface, but also the tire- state, pressure and temperature have significant influence of the driving behavior. Even for road-tire interactions that seem of a relatively homogeneous nature, often friction coefficient deviations of approximately 5% are obtained through measurements. In an experimental setup for a dry surface test, the tire properties change rapidly after repeated testing, where the rubber compound of the tires visibly changes, where also tire properties can be indicated.

However the use of experimentally fitted tire measurement data can be compared to determined measurements of a manual drift. Experimentally fitted tire data is retrieved from a test bench setup, which verifies the respective loads under an extensive range of tire states. As a result, the MF parametrization can be obtained for a desired vertical load of which the data can be found in a tire property file for a respective tire. By using a tire that has underwent the tire fitting procedure, a relatively proper estimation can be done for the force-slip relation for that particular tire. Tuning parameters within the tire property files can be modified in order to correspond to tire behavior to a desired friction coefficient. By performing a manual drift towards an equilibrium state on the desired surface, state data is used

cover in for the respective equilibrium states as proposed in the equilibrium analysis. In this case, the MATLAB function $lsqnonlin$ is applied using the measured equilibrium state, in order to estimate the respective tire longitudinal and lateral tire forces F_{meas}^{eq}. In similar fashion, the data allows to approximate the respective tire slip coefficients, which can be used to modify the tire property files, such that the the the estimated tire forces from the measurement F_{meas}^{eq} correspond to the computed tire forces F_{MF}^{eq}. For a more dry, high friction surfaces, estimation for tuning parameters of the tire property files

is more convenient. As with in the larger range of friction coefficients, the peak friction force, as well as the saturated tire state is tuned according to the scale of the friction coefficient. In case of a very low friction surface, such as ice, snow or the constantly water skid pad of the BMW proving grounds of Aschheim, tire responses are not only changing in an evenly distributed scale. In this case, we often obtain tire responses, where the peak friction force is decreased more significant, up until the point where the tire forces only increase along with an increased slip. Estimating the amount of reduction on the peak friction force with the proposed approximation would require a trial and error to find the most accurate tire force approximation.

7.3.2. Actuator delay

Once both computed desired drive torque and steering angle are sent to the vehicle, delays and deviations occur due to the use a petrol engine vehicle and actuation delays towards desired control inputs. The actuation delay Actuation delay on the steering applied steering angle
The maximum deliverable drive torque of a petrol engine is not instantly available, which causes a mismatch on the desired and true applied drive torque. Especially at large increases of torque, the rate of change in drive torque is lacking the ability to track the MPC drive torque. As timing is key to performing a proper drift, drive torque and steering angle should be applied at the same time the predetermined MPC control input desires. Therefore a variation between references approximates the delay between drive torque and steering angle, namely through applying a step input to the rear wheelspeed, while a brief ramp is applied to all other references. This enables the vehicle to build up a desired torque, before starting to steer towards a drifting state.

7.4. Standard production vehicle limits

A reasonably large amount of test were executed in not the best period of the year to perform automated drifting tests, namely during winter time. As a consequence of the season, temperatures around and below zero degrees caused changing of regular changing of proving grounds, which implied that the above parameter estimation had to be performed in case a new proving ground is used.

Figure 7.2: Experimental vehicle while sustaining a high sideslip state

The NMPC control approach in combination with the testbench has showed that fully automated drifts are non-reproducible, as a full lap drift only occurred a single time. Whereas the best measured and recorded drift existed for about half a circle with a path radius of 25 meters, as seen by the vehicle in high sideslip state in figure 7.2. Corresponding vehicle state measurements are shown in figure 7.3, which shows the initial velocity of the circular driving reference might be relatively high, which is caused by having the velocity of the desired drifting close to the initializing driving velocity to ensure smooth transition between driving and drifting.

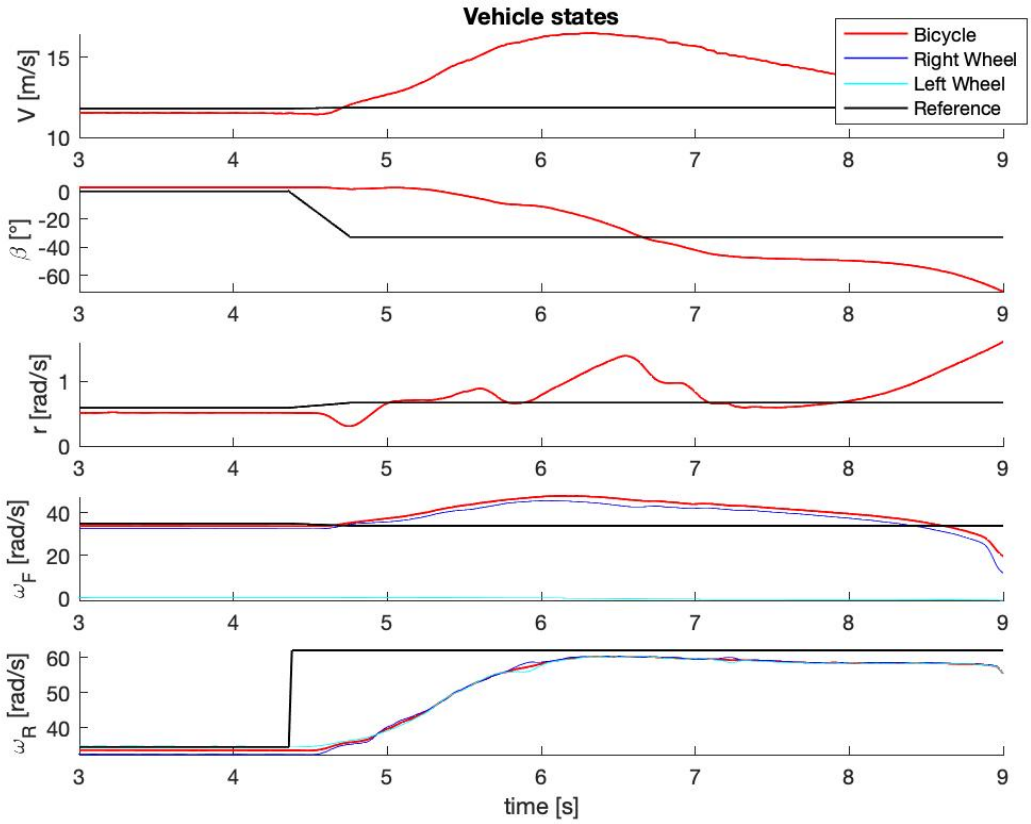

Figure 7.3: Measured vehicle states during full automation

Signal analysis shows a deviation between the desired and measured steering angle (7.4) for nearly all cases, where the front axle aligns with the direction of travel rather than compensate for the vehicle state. Two thinkable assumptions to consider that may cause this issue can be found in the steering conversion within the vehicle. At first, a lack of applicable torque from the standard EPS that could not be able to apply sufficient amount of torque to overcome the self-aligning moment occurring at the front tires. A statement that can be supported considering the used EPS motor only produces about $30\ Nm$

and is designed to function for several relatively low torque desiring ADAS systems such as automatic lane change.

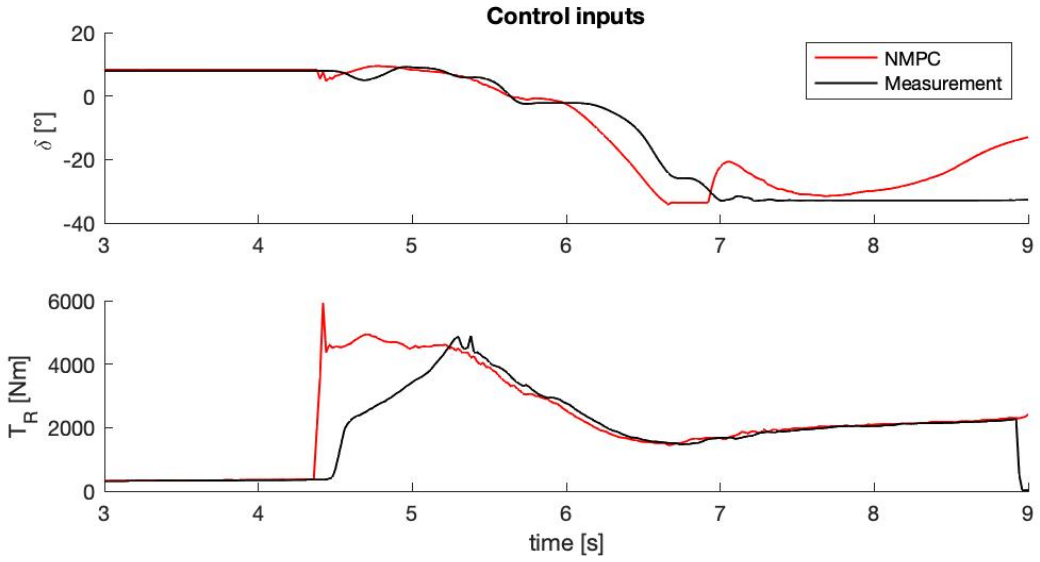

Figure 7.4: Desired MPC control inputs and the measured control inputs during automated drifting deployment

A second assumption is the conversion in the integrated control systems of the vehicle, where an input path curvature signal should be converted to a desired steering angle. However, it could be the case that these control systems assume conventional driving, thus computation of the right steering angle is not happening correctly while the vehicle is in a high sideslip state.

As a consequence of the incorrect conversion, the steering angle cannot be decreased as desired by the NMPC. As a result, the true steering angle remains on its limit, which causes a spin through of the vehicle, as the front axle is not performing the desired compensation for the deviations in absolute velocity and sideslip angle. In case the steering angle is applied as proposed by the controller, we would see a decrease in yaw rate and sideslip angle, which would aim for stabilizing the drifting state around the desired equilibrium.

A comparison between the desired MPC drive torque and the true measured drive torque shows the deviating response in case of instant increase of torque (7.4), as explained and seen before in ISAR simulations. We obtain from the plot, that a peak rear drive torque is applied, in order to overcome the peak longitudinal- and lateral tire forces in order to reach full tire saturation.

7.5. Semi-automated experimental validation

As we can now assume issues on the steering conversion or the EPS is not being capable of applying a reasonable amount of torque to the front axle in order to bring the steering angle into the desired state, we can assume that only hardware modifications can solve the non-corresponding steering angle conversion. However, a semi-automatic drifting maneuver shows the response of the vehicle and the desired control inputs from the solver.

Therefore, a proposed experiment runs the NMPC solver through the experimental setup, where in this case only the desired drive torque is forwarded to the vehicle, while steering is performed by a human driver. By performing the experiment in this setting, we can obtain a result with respect to the applied drive torque, as well as a comparison between the measured and desired steering input of the NMPC. This approach has shown that the applied drive torque shows corresponding behavior to a manually initiated drift, under the condition that the tire response is estimated within reasonable limits.

Measurements show that the vehicle can be brought into the desired drifting state as seen in figure 7.5, where the experiment is performed on both a dry high friction surface and a watered skid pad, with high and low friction coefficients, respectively. The high sideslip state is stabilized for multiple rounds,

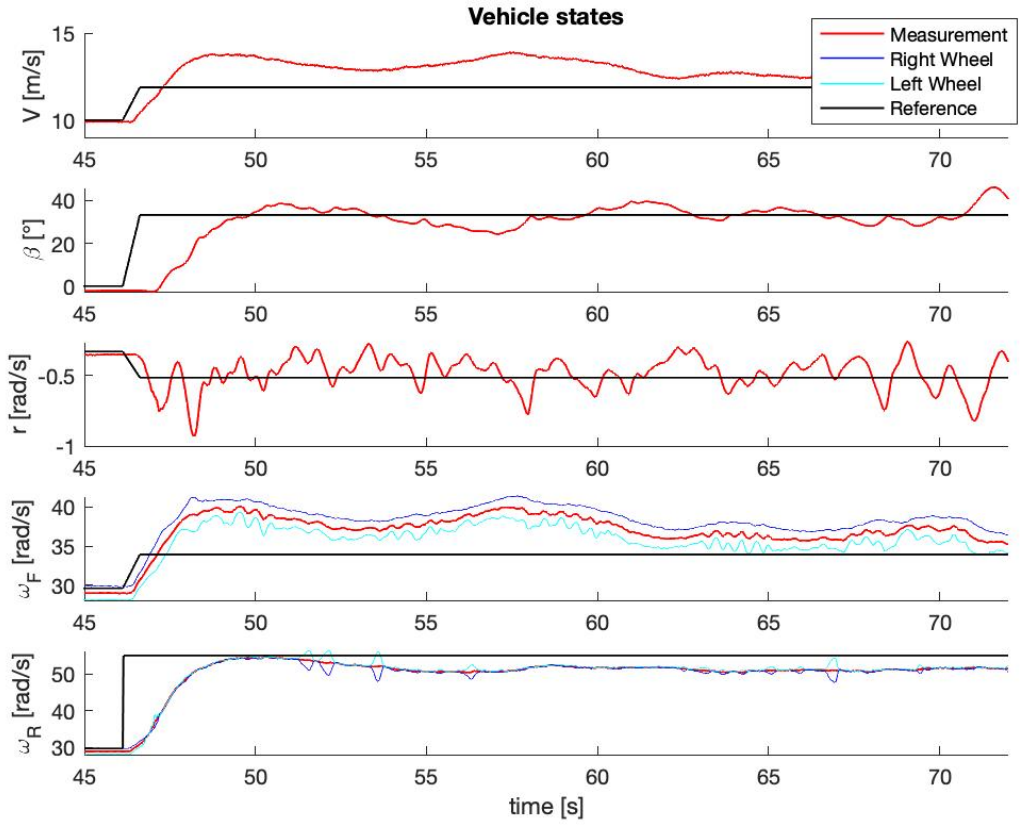

Figure 7.5: Measured vehicle states during a manual steering scenario, torque commands forwarded from the NMPC solver

where theoretically the drifting state could be continued for a significant time. From these results we can obtain that the applied drive torque is sufficient and solved optimally for bringing the vehicle into the drifting state, and remaining its steady-state drifting position.

In correspondence to the fully automated setting, the tracking performance of the velocity and front wheelspeed is less accurate as compared to the sideslip angle, yaw rate and rear wheelspeed. Reason for this is the applied tuning weights on for the controller, as the main focus is bringing the vehicle into high sideslip state, which is established with high yaw rate and rear wheelspeed tracking. While the front axle aligns with the direction of travel, the front wheelspeed, and the the absolute velocity are related with eachother.

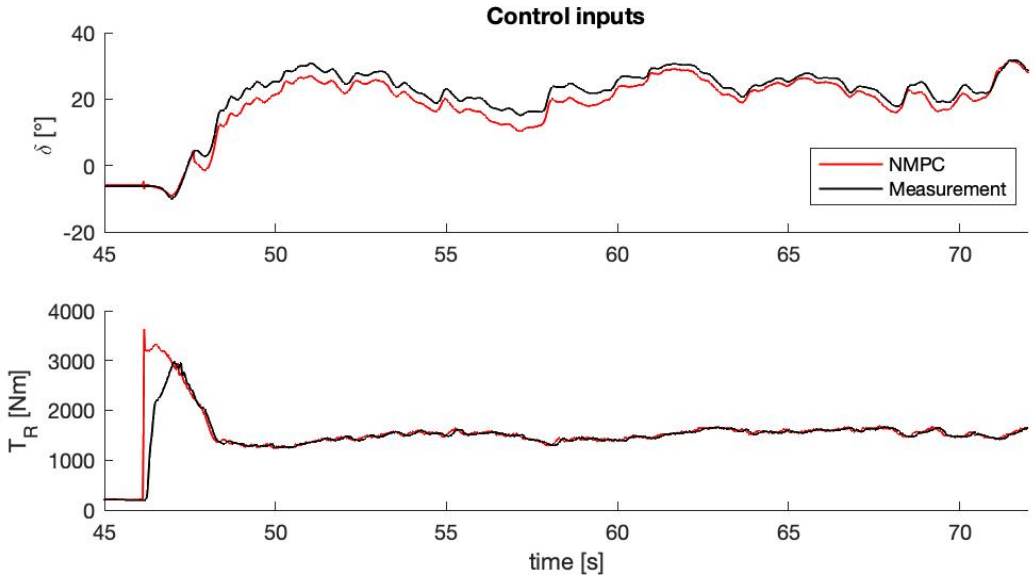

Figure 7.6: Desired MPC control inputs and the measured control inputs during semi-automated controller deployment

Due to the steering conversion issue in the fully automated setting, we can see the comparison between the desired MPC steering angle and the manually performed drift (7.6) has more significant added value. From the comparison, we can obtain that the steering angle from the human driver is corresponding in its response with the desired steering angle computed by the NMPC solver. Only magnitude varies with maximum peaks of approximately $5°$, which shows us that in case steering conversion within the vehicle happened accordingly, sustaining a stabilized drift for at least a couple of rounds would be very much possible.

In case of the applied drive torque (7.6), we obtain corresponding response with both experimental torque application.

Conclusion

Drifting can be described as intentionally bringing a vehicle to a state of high sideslip and the rear wheels are saturated due to high proportions of longitudinal- and lateral slip, while the front wheels align with the direction of travel. As the tire behavior for high quantities of slip reaches a nonlinear behavior, drifting can be described as vehicle motion beyond the limits. As the vehicle states beyond the tire friction limits extends the possible motion primitives, future automated safety systems are likely to be deployed with applications that enable safe control while in high sidelip state. This can be in the form of an integrated vehicle system, with the aim of promoting the safety of the driver or the environment, but also as an eye-catcher with regard to attracting customers for high performance vehicles with automated or auxiliary drifting capabilities.

The key component to successful automated drifting lies with the reference drifting state that finds its origin in an equilibrium analysis. Equilibrium locations of of a set of differential equations that describe the dynamical system of a drifting vehicle, show that the drifting state of a vehicle equals an unstable equilibrium, that can be stabilized using control inputs. As experimentally verified, equilibrium locations of a single-track model show great correspondence with an experimental setup, which therefore proves that equilibrium locations can be used as references for the proposed control strategy.

In this research, a control strategy is proposed that uses a nonlinear model predictive controller to stabilize the vehicle into a high sideslip state, while dynamic referencing is used to to adjust references such that path curvature becomes variable. As solely reading the path curvature would not ensure conversion towards a desired path, an additional PID controller is applied to adjust the path curvature by means of the lateral path deviation.
Simulation performance of the proposed control strategy can be indicated by the ability of the controller to track a desired reference drifting state, while converging towards a desired path. Experimental verification has shown that the use of a standard production vehicle without significant hardware and-or software modifications is not able to convert desired control inputs into the applied control inputs, due to unsuccessful processing of the desired steering angle. Degradation of the EPS, or a power output that is generally too low to overcome the induced self-aligning moment on the front axle is the first assumption made that causes the steering issue, which could be solved with a more powerful and robust electric motor. A second assumption is based on the software that lies on the integrated braking (IB) controller, which converts the desired steering angle from the NMPC controller into the applied steering angle. As the FAS interface to the vehicle is designed for relatively small driving tasks and interventions, an assumption of being in a normal driving state. This can be noticed from the instant where desired and measured steering angle start to deviate significantly, namely once the vehicle has entered the high sideslip state. However, a semi-automatic verification of the controller has proven that the determined NMPC sideslip stabilization control inputs are very likely to stabilize the drifting motion, as the proposed steering input is corresponding in behavior of a manual driver. Therefore, the controller can be assumed to be layed out for automated drifting, however, modifications to the vehicle are desired to decrease the control input error between controller and vehicle.

The approached control strategy shows that in case parametric knowledge is known, or at least approximated within certain limits, the model based NMPC is able to bring the vehicle into a desired high-slip state. However, this implies that if the control approach would be proposed for safety purposes, knowledge of that particular situation should be estimated before being used in the controller. In a simulation environment, this is relatively easy to be deployed, however a real road situation could become quite critical. The latency that would exist due to filtering, estimation and data transfer could be too significant to account for a critical evasive maneuver, not to mention the computational performance the NMPC desires. In similar fashion, real knowledge of model parameters could be highly differing between variations of wheels, considering μ-split situations, where one wheel is on high friction tarmac, where the other is on ice. Allowing adjustment to a multi-purpose controller would imply a significant amount of logic that would enable use of such system in a large spectrum of vehicle conditions.

References

[1] Mujahid Abdulrahim. *On the Dynamics of Automobile Drifting*. Tech. rep. 2006. DOI: 10.4271/2006-01-1019.

[2] Manuel Acosta, Stratis Kanarachos, and Michael E. Fitzpatrick. "On full MAGV lateral dynamics exploitation: Autonomous drift control". In: *Proceedings - 2018 IEEE 15th International Workshop on Advanced Motion Control, AMC 2018*. Institute of Electrical and Electronics Engineers Inc., June 2018, pp. 529–534. ISBN: 9781538619469. DOI: 10.1109/AMC.2019.8371149.

[3] Craig Earl Beal and J. Christian Gerdes. "Model predictive control for vehicle stabilization at the limits of handling". In: *IEEE Transactions on Control Systems Technology* 21.4 (2013), pp. 1258–1269. ISSN: 10636536. DOI: 10.1109/TCST.2012.2200826.

[4] BimmerToday. *BMW M4 G82: Drift-Maschine mit 1000 PS für die Driftbrothers*. 2021. URL: https://www.bimmertoday.de/2021/06/17/bmw-m4-g82-drift-maschine-mit-1000-ps-fur-die-driftbrothers/ (visited on 06/17/2021).

[5] BMW AG. *BMW GROUP SAFETY ASSESSMENT REPORT SAE LEVEL 3 AUTOMATED DRIVING SYSTEM*. Tech. rep. URL: https://www.bmwusa.com/content/dam/bmwusa/innovation-campaign/autonomous/BMW-Safety-Assessment-Report.pdf.

[6] BMW AG. "BMW M Bike Limited Carbon Edition". In: (2017). URL: https://www.press.bmwgroup.com/deutschland/article/detail/T0274368DE/bmw-m-bike-limited-carbon-edition?language=de.

[7] Szilárd Czibere et al. "Model predictive controller design for vehicle motion control at handling limits in multiple equilibria on varying road surfaces". In: *Energies* 14.20 (Oct. 2021). ISSN: 19961073. DOI: 10.3390/en14206667.

[8] Marco Gadola and Daniel Chindamo. *The Mechanical Limited-Slip Differential Revisited: High-Performance and Racing Car Applications*. Tech. rep. 2. 2018, pp. 1478–1495. URL: http://www.ripublication.com.

[9] Jonathan Y Goh, T Goel, and J Christian Gerdes. *A Controller for Automated Drifting Along Complex Trajectories*. Tech. rep.

[10] Jonathan Y. Goh and J. Christian Gerdes. "Simultaneous stabilization and tracking of basic automobile drifting trajectories". In: *IEEE Intelligent Vehicles Symposium, Proceedings*. Vol. 2016-August. Institute of Electrical and Electronics Engineers Inc., Aug. 2016, pp. 597–602. ISBN: 9781509018215. DOI: 10.1109/IVS.2016.7535448.

[11] Jonathan Y. Goh, Tushar Goel, and J. Christian Gerdes. "Toward Automated Vehicle Control beyond the Stability Limits: Drifting along a General Path". In: *Journal of Dynamic Systems, Measurement and Control, Transactions of the ASME* 142.2 (Feb. 2020). ISSN: 15289028. DOI: 10.1115/1.4045320.

[12] João P.C. Gonçalves and Jorge A.C. Ambrósio. "Road vehicle modeling requirements for optimization of ride and handling". In: *Multibody System Dynamics*. Vol. 13. 1. Feb. 2005, pp. 3–23. DOI: 10.1007/s11044-005-2528-5.

[13] Thomas Gustafsson. "Computing The Ideal Racing Line Using Optimal Control". PhD thesis. Institutionen för systemteknik Department of Electrical Engineering Examensarbete, 2008.

[14] Rami Y Hindiyeh and J Christian Gerdes. "A Controller Framework for Autonomous Drifting: Design, Stability, and Experimental Validation". In: ().

[15] Rami Y. Hindiyeh and J. Christian Gerdes. "A controller framework for autonomous drifting: Design, stability, and experimental validation". In: *Journal of Dynamic Systems, Measurement and Control, Transactions of the ASME* 136.5 (2014). ISSN: 15289028. DOI: 10.1115/1.4027471.

[16] Chengfeng Huang and Dejun Yin. “Steady State Drifting Controller for Rear-Wheel Independent Driving Electric Vehicels”. In: *Journal of Physics: Conference Series*. Vol. 1550. 4. Institute of Physics Publishing, June 2020. DOI: 10.1088/1742-6596/1550/4/042023.

[17] ISO - International Organization for Standardization. *Passenger cars — Test track for a severe lane-change manoeuvre — Part 2: Obstacle avoidance*. Tech. rep. ISO - International Organization for Standardization, 2011.

[18] Corvin Kück. *MPC Design For Autonomous Drifting*. Tech. rep. KTH Royal Institute of Technology, 2017.

[19] via Wikimedia Commons Martin Behrendt. *MPC Scheme*. URL: https://commons.wikimedia.org/wiki/File:MPC_scheme_basic.svg.

[20] Sina Milani, Hormoz Marzbani, and Reza N. Jazar. “Vehicle drifting dynamics: discovery of new equilibria”. In: *Vehicle System Dynamics* (2021). ISSN: 17445159. DOI: 10.1080/00423114.2021.1887499.

[21] William Norris. *Modern steam road wagons*. Longmans, Green, and Co., 1906, pp. 63–67.

[22] Hans B. Pacejka. *Tyre and Vehicle Dynamics*. Tech. rep. Delft University of Technology, 2006.

[23] Hans B. Pacejka, Egbert Bakker, and Lars Nyborg. “Tyre Modelling for Use in Vehicle Dynamics Studies”. In: (1987).

[24] Mincheol Park and Yeonsik Kang. “Experimental Verification of a Drift Controller for Autonomous Vehicle Tracking: a Circular Trajectory Using LQR Method”. In: *International Journal of Control, Automation and Systems* 19.1 (Jan. 2021), pp. 404–416. ISSN: 20054092. DOI: 10.1007/s12555-019-0757-2.

[25] R. Quirynen et al. “Autogenerating microsecond solvers for nonlinear MPC: A tutorial using ACADO integrators”. In: *Optimal Control Applications and Methods* 36.5 (Sept. 2015), pp. 685–704. ISSN: 10991514. DOI: 10.1002/oca.2152.

[26] Georg Rill and Abel Castro. *Road Vehicle Dynamics: Fundamentals and Modeling with MATLAB®*. May 2020. ISBN: 9780429244476. DOI: 10.1201/9780429244476.

[27] Fatimaezzahra Saber et al. *Vehicle Dynamics and Steering Angle Estimation Using a Virtual Sensor*. Tech. rep. URL: https://hal.archives-ouvertes.fr/hal-01260766.

[28] Stefanie Reiffert and Christine Lehner. *TUM ist Vizeweltmeister im autonomen Rennfahren*. 2021. URL: https://www.tum.de/die-tum/aktuelles/pressemitteilungen/details/37130.

[29] *The DARPA Grand Challenge: Ten Years Later*. 2014. URL: https://www.darpa.mil/news-events/2014-03-13.

[30] E Velenis and P Tsiotras. *Minimum Time vs Maximum Exit Velocity Path Optimization During Cornering*. Tech. rep.

[31] Efstathios Velenis. *FWD Vehicle Drifting Control: The Handbrake-Cornering Technique*. 2011. ISBN: 9781612847993. DOI: 10.0/Linux-x86{_}64.

[32] Efstathios Velenis, Emilio Frazzoli, and Panagiotis Tsiotras. “On steady-state cornering equilibria for wheeled vehicles with drift”. In: *Proceedings of the IEEE Conference on Decision and Control*. 2009, pp. 3545–3550. ISBN: 9781424438716. DOI: 10.1109/CDC.2009.5399782.

[33] Efstathios Velenis, Panagiotis Tsiotras, and Jianbo Lu. “Optimality properties and driver input parameterization for trail-braking cornering”. In: *European Journal of Control* 14.4 (2008), pp. 308–320. ISSN: 09473580. DOI: 10.3166/ejc.14.308-320.

[34] Efstathios Velenis et al. “Steady-state drifting stabilization of RWD vehicles”. In: *Control Engineering Practice* 19.11 (Nov. 2011), pp. 1363–1376. ISSN: 09670661. DOI: 10.1016/j.conengprac.2011.07.010.

[35] B Verlaan. *An optimization based approach to autonomous drifting A scaled implementation feasibility study*. Tech. rep.

[36] Rami Yusef Hindiyeh. “DYNAMICS AND CONTROL OF DRIFTING IN AUTOMOBILES”. PhD thesis. Stanford: Stanford University, 2013. URL: http://purl.stanford.edu/vz162hz7668.

[37] Vivian Zhang, Sarah M Thornton, and J Christian Gerdes. *Tire Modeling to Enable Model Predictive Control of Automated Vehicles From Standstill to the Limits of Handling*. Tech. rep.

A

Model and controller parameters

A.1. Experimental vehicle parameters

Table A.1: BMW M3 Competition Parameters

Variable	Definition	Value	Unit
m	Vehicle mass	1800	kg
g	Gravity Coefficient	9.81	m/s^2
I_z	Yaw Inertia	2800	kg/m^2
a	Front axle distance to CoG	1.503	m
b	Rear axle distance to CoG	2.852	m
T_{max}	Maximum Wheel Torque	650	Nm
δ_{max}	Maximum Steering Angle	33.6	deg

A.2. Simulation vehicle parameters

Table A.2: BMW M340iX Parameters

Variable	Definition	Value	Unit
m	Vehicle mass	1939	kg
g	Gravity coefficient	9.81	m/s^2
I_z	Yaw inertia	3225.22	kg/m^2
a	Front axle distance to CoG	1.437	m
b	Rear axle distance to CoG	2.8501	m
T_{max}	Maximum drive torque	500	Nm
δ_{max}	Maximum steering angle	34	deg

A.3. Tire parameters

Table A.3: Magic Formula parameters based single-wheel load for simulation vehicle

Tire	Dimensions	i	B_i	C_i	D_i	E_i	S_i
Michelin Pilot Supersport*	275 35R19	x	9.20	1.96	1.55	-0.04	0
		y	11.35	1.88	1.29	0.69	17.37
Pirelli Pzero ALP	285 30R20	x	15.84	1.66	1.25	-0.11	0
		y	9.37	2.10	1.36	0.59	19.39

A.4. NMPC Tuning Parameters

Table A.4: Applied tuning parameters for ISAR Simulator

Parameter	ISAR	Experiment
W_V	1e-16	10e-4
W_β	10e4	350
W_r	10e3	250
$W_{\omega F}$	50	1.8
$W_{\omega R}$	50	1.8
W_δ	1e-16	10e-4
W_{TR}	0	0
$W_{\dot{\delta}}$	0	0

A.5. NMPC Tuning Parameters: Terminal control

Table A.5: Applied tuning parameters for ISAR Simulator

Parameter	ISAR	Experiment
WN_V	0	0
WN_β	0	0
WN_r	0	0
$WN_{\omega F}$	0	0
$WN_{\omega R}$	0	0
WN_δ	0	0

A.6. Path following PID path following

Table A.6: Applied tuning parameters for ISAR Simulator

K_p	K_i	K_d
10e-2	50e-7	10e-4

B

Controller structures

B.1. Combined path-following sideslip stabilisation

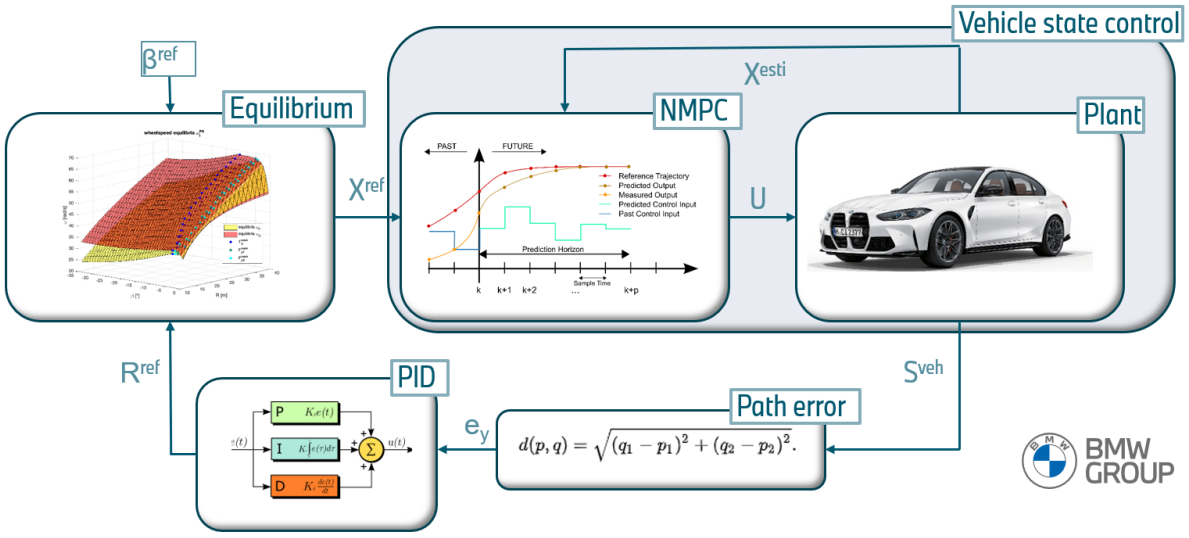

Figure B.1: Proposed control system strategy

C

Informative

C.1. ISAR Information schedule

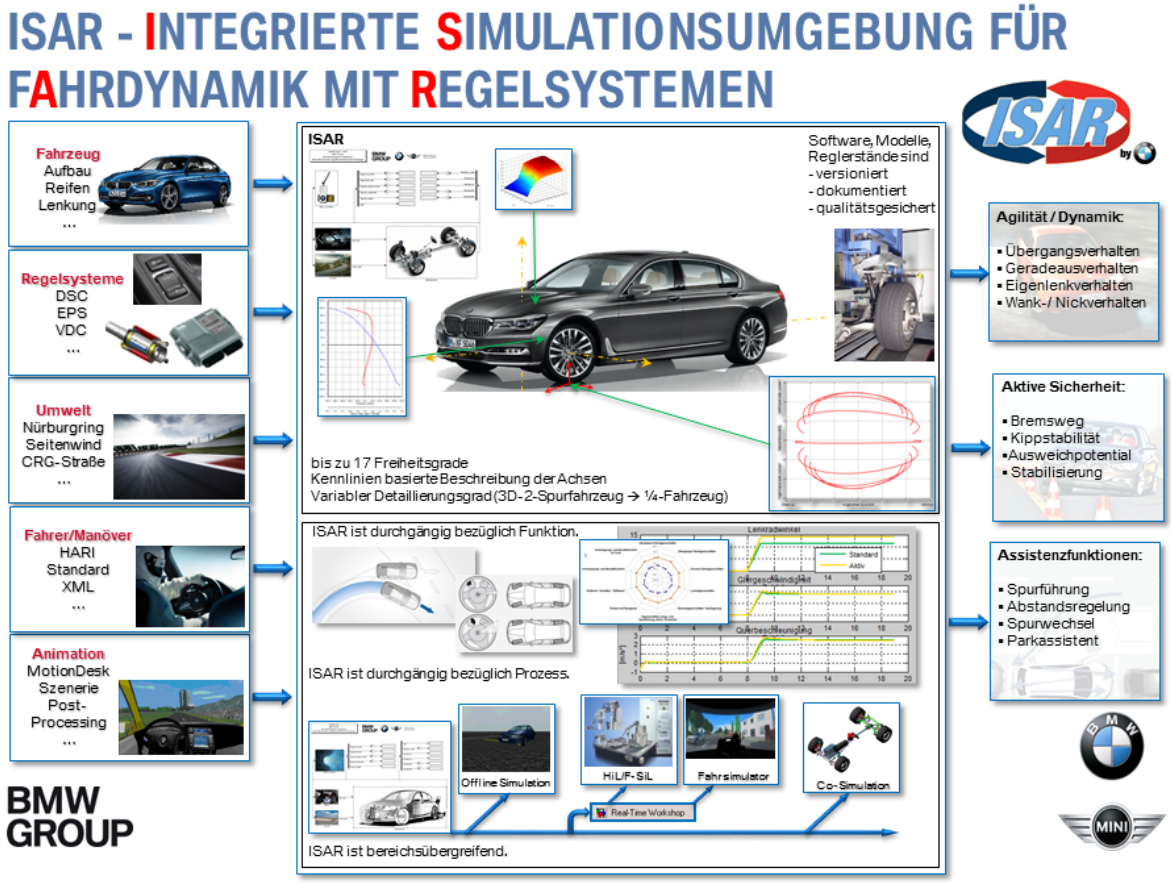

Figure C.1: Schematic overview of capabilities of the ISAR simulator

Experimental verification of an NMPC approach for automated drifting

Stan Meijer

***Abstract*—This paper proposes a Nonlinear Model Predictive Control (NMPC) application for automated drifting, with experimental verification on a standard production vehicle, without hardware modifications. The controller stabilizes the vehicle on a high sideslip angle, which implies an equilibrium condition beyond tyre friction limits. The proposed control strategy shows feasible results that succesfully brings the vehicle towards a high sideslip state, for a variety of drifting scenarios. Simulations show that the control structure is able to sustain an automated drift along a desired path, with maximal lateral path deviation of 1 meter. An experimental implementation on a production vehicle testbench without hardware modifications has shown feasible control of bringing the vehicle into a high sideslip state, for both low- and high μ situations.**

I. Introduction

The angled drifting pose of the vehicle as seen in Fig. 1 can be described by an angle commonly known as the vehicle sideslip angle β, which describes the angle between the longitudinal axis of the vehicle and the direction of the absolute velocity vector V, measured at the vehicles centre of gravity CoG. The sideslip angle is computed through the mathematical relation expressed in equation 1, where V_y and V_x denote the lateral- and longitudinal velocity components of the vehicle velocity, respectively. The front wheels are counter-steering, where the wheel center aligns with the direction of travel.

$$\beta = \arctan \frac{V_y}{V_x} \tag{1}$$

Assuming no steering at the rear axle, rear wheels align with the vehicle from a top view perspective, which implies that during conventional driving only minor rear lateral tyres slip angles α_r are obtained. Similarly, while drifting, the lateral tyre slip angles are significantly large and can be found in the same order of magnitude as the vehicle sideslip angle. As the front tyres usually align with the direction of travel, front lateral tyre slip angles α_f are commonly minor. The lateral tyre slip angles are in fact mathematically similar to the vehicle sideslip angle, as the angle describes the angle between the longitudinal- and lateral velocity components tyre frame velocity components [1]. As for the longitudinal slip component κ of the tires, the same relation holds when it comes to distribution of slip magnitudes. As for a RWD vehicle, front wheels are aligned with the direction of the drift in rolling motion, as no drive torque is applied to the front axle. Large quantities of longitudinal slip can be found at the rear axle, resulting in a large absolute slip.

The sport of drifting shows that driving at large angles of sideslip does not necessarily imply terminal loss of control.

Fig. 1. BMW M3 Competition Testbench, performing experimental automated drift

Drifting challenges skilled drivers to travel along a track while sustaining a large sideslip angle by exploiting coupled nonlinearities in the tyre force response [2]. While sustaining a drift, the rear tyres are considered saturated [3].

Research on drifting performance in low friction surfaces [4], [5], [6] show that for several high dynamic cases, the objective of a maximum exit velocities and cornering time are optimal in a drifting state. Thus, higher velocities can be reached compared to vehicles turning conventionally.

In general, controlling the vehicle in a stable drift requires a significant amount of skill, where most average drivers would not be able to perform such maneuver without practice. However, a driver always has the possibility to find itself in a high sideslip state due to poor weather and road surface conditions. As near-future vehicles are most likely to be automated, control beyond the tyre friction limit is highly profitable for passenger safety, in case of high dynamical evasive maneuvers [7].

Proposed sliding-mode control for both steady-state drifting [3], [8], as well as a path-following sliding-mode control [9], [10], [11] show real-time experimental drifting control. However, the experimental platform had powertrain properties that you would not see on common road vehicles, i.e. fully locked differential. This research therefore distincts itself as a production vehicle without hardware modifications is used for experiments, proving feasibility for powertrain layouts in production vehicles for automated drifting. This contributes to the study of drifting for evasive maneuvers in a real traffic situation, given a production vehicle can be in this condition.

Conducting experiments with a full-sized vehicle for this research on drifting also differs from current state-of-art on non-linear model predictive control NMPC for path following drift approaches proposed [12], [13]. This research proves feasibility of a real-time NMPC drifting approach, therefore contributing to the state-of-art.

II. Vehicle Dynamics

A. Single-track model

The single-track model is characterized by simplifying the vehicle kinematics and dynamics of a four-wheel vehicle model by lumping the tyres on the left- and right side together in the center-line of the vehicle. This decreases complexity through reduction of parameters, as well as degrees of freedom. Since the Ackermann steering geometry will in practice have slight deviation [14], the lumped steering angle δ of the single-track model is considered a good approximation for many applications. In similar fashion, force- and moment leverage points are decreased from four to two lumped wheels by vector addition of left and right quantities. Rotational velocities as of the wheels are averaged between the left- and right wheels, whereas vertical loads are added, indicating that lateral load transfer between left- and right is not captured using the single-track model. The dynamic single-track model is graphically shown in Fig. II-A, where you can find the centered single-track model fitted over the actual vehicle. The system of equations 2, where time derivatives of the states sideslip angle β, the yaw rate r, and the absolute vehicle velocity V represent the single-track model dynamics. The absolute velocity describes the true velocity the vehicle in space, combining both the lateral- and longitudinal velocities with respect to the vehicle frame. The sideslip angle is the angle between the vehicle x-axis and the absolute velocity, which is therefore the main indication for a vehicle being in drift at large sideslip angles. The yaw rate describes the rotation around the z-axis of the vehicle. In many vehicle motion algorithms [15], [16], the single-track model is usually not expressed in with the time derivative of the sideslip angle $\dot{\beta}$, but as information of the sideslip angle characterizes the state of a drift, it is rather convenient to directly have that value at hand, for both reading of state, as well as defining a reference for NMPC. Using the absolute velocity V, a path following property is established, as path curvature κ_{path} can be expressed as a function of absolute velocity divided by the yaw rate r.

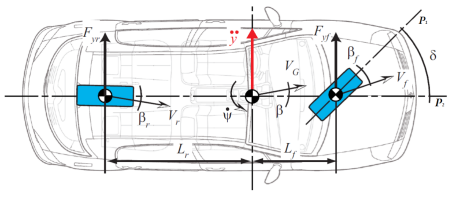

Fig. 2. A schematic representation of the single-track model [17]

$$
\begin{aligned}
\dot{V} =& \frac{1}{m}[F_{xF}\cos(\delta-\beta) - F_{yF}\sin(\delta-\beta) \\
&+ F_{xR}\cos\beta + F_{yR}\sin\beta] \\
\dot{\beta} =& \frac{1}{mV}[F_{yF}\cos(\delta-\beta) - F_{xF}\sin(\delta-\beta) \\
&- F_{xR}\sin\beta + F_{yR}\cos\beta] - r \\
\dot{r} =& \frac{a[F_{xF}\sin\delta + F_{yF}\cos\delta] - bF_{yR}}{I_z}
\end{aligned} \tag{2}
$$

B. Tire-Road interaction

To enable a control strategy to drift automatically, the interaction between the vehicle and the road surface is of most significant importance on the drifting motion. As can be intuitively derived from the single-track model layout in Fig. II-A, the transition between conventional driving and drifting requires a relatively large rear lateral force to establish a state of drift, while similarly being able to maintain an optimal lateral force to remain in a steady-state drift. This implies that the knowledge of the tyres should be as accurate as possible, capturing most characteristics with the least complexity. Once the drive torque exits the differential of the left and right, the torque is transmitted to the wheel, which is considered a rigid body with certain mass. As a result of the applied torque, the longitudinal component of the contact patch exerts a force in opposite longitudinal direction of travel. The dynamics of the rotating wheel are described by 3, where the time derivative of the rotational velocity of the wheel $\dot{\omega}$ is determined by the sum of moments around the wheel center, divided by the rotational inertia of the wheel $I_{\omega j}$.

$$
\dot{\omega_j} = \frac{T_j - F_{xj}r_j}{I_{\omega j}} \quad j = F, R \tag{3}
$$

The amount movement between two surfaces describes the phenomenon of slip, where in case of wheels, the amount of sliding between contact patch between tyres and road surface. Practical tyre slip quantities [18] are determined, for both longitudinal slip κ_i and a lateral slip angle α_i, which are mathematically described by equation 4. These practical tyre slips preserve the view purely in lateral or longitudinal direction where in correspondence to the high sideslip angle, significant decomposition of directions occur at the rear tyre slip during a drifting maneuver.

$$
\kappa_i = \frac{\omega_i r_i - V_{ix}}{\omega_i r_i} \quad \alpha_i = \tan^{-1}\frac{V_{iy}}{V_{ix}} \quad i = F, R \tag{4}
$$

The absolute slip occurring at the rear tyres can be mathematically described by means of the theoretical coefficients of slip, where lateral- and longitudinal theoretical slip quantities (5) result in a combined slip definition (6) [19]. Opposed to the practical slip quantities, theoretical slip quantities take into account the effect on the directional slip component of perpendicular direction. Thus both decomposed theoretical quantities are reduced with respect to the practical slip quantities, as the slip in other directions then increase their true velocity at the contact patch. I.e. a practical lateral slip angle is determined by the longitudinal and lateral velocity component, however longitudinal slip due to wheel spinning increases the true longitudinal velocity vector at the contact patch, decreasing the true slip angle.

$$
S_{xj} = \frac{V_{xj} - \omega_j r_j}{\omega_j r_j} \quad S_{yj} = \frac{V_{yj}}{\omega_j r_j} \quad j = F, R \tag{5}
$$

$$
S_j = \sqrt{S_{yj}^2 + S_{xj}^2} \quad j = F, R \tag{6}
$$

In case of this research, a combination of the standardized magic formula 5.2 as shown in Eq.7 and a simplified

representation as shown in Eq.8. Preliminary results on both computational capacity and the controller tracking show that the simplified MF can be applied at the front wheels, while the standard formula is desired to capture more knowledge on the rear tire characteristics. As front wheels are considered within the tyre friction limits during a drift, the simplified model can capture those characteristics. Where rear tyres are considered beyond the friction limit, knowledge of tyre characteristics at that point should be captured as good as possible. Both equations are described with similar parameters, where B and C are stiffness- and shape- factors, respectively. Magic formula parameters D and E describe the slip at peak force at rated load F_z. The amount of parameters allow to fit the magic formula to almost any type of measured tyre, where the standardized magic formula is able to capture properties throughout the complete slip range quite precise. Where the simplified model lacks force estimation in the larger slip ranges, thus being a good solution for control applications within the linear range of tyres. Tyre characteristics can be desribed by an increase in tyre forces until the peak friction point is reached. Once slip becomes larger than this point, a decrease of exerted forces on the contact patch is seen.

$$\mu_{ij} = D_{ij}\sin(C_{ij}\arctan B_{ij}S_j - E_{ij}(B_{ij}S_j - \arctan(B_{ij}S_j))i = x,y \qquad j = F,R \tag{7}$$

$$\mu_{ij} = D_{ij}\sin(C_{ij}\arctan B_{ij}S_j) \quad i = x,y \quad j = F,R \tag{8}$$

$$F_{ij} = -\frac{S_{ij}}{S_j}F_{zj}\mu_{ij} \quad i = x,y \quad j = F,R \tag{9}$$

C. Differential

Preliminary simulations of an NMPC approach show feasible results with varying degrees of locked differentials. As seen in the experiment proposed [20], a fully locked differential shows feasible drifting control. This is mainly due to the corresponding wheelspeed that occur between left and right, thus also for the single-track estimation of the rear wheelspeed, the relation holds. In case of the fully locked differential the wheel torques differ amongst sides, but a resultant drive torque can still be used as a control input for an NMPC approach. In similar fashion, LSDs also lock, such that the drive torques between left and right are not larger than a respective ratio. Once a LSD locks, the wheelspeed difference also equals zero, thus the single-track relation holds. Successful controller simulations as well as experimental measurements using a driver input shows that a 30% locked differential is feasible in case a single-track vehicle modelling as confirmed in section .

D. Load Transfer

Several proposed drifting control strategies [8], [10], [13] assume a static normal loads on all wheels, assuming there is no longitudinal load transfer taking place between the front- and rear axle of a vehicle. This assumption holds mainly for conventional driving in curves, where the load transfer mainly exist in lateral direction, due to the centripetal acceleration a_c causing a load increase on the outer wheels of the vehicle, which can be neglected due to the single-track model approach.

Based on preliminary results of the NMPC design, incorporating suspension dynamics requires a significant amount of computational capacity, with real-time infeasible solutions. Therefore, vertical loads are expressed in a quasi-static way, where differences in force can be estimated through the relation described in equation 10, resulting in the load estimation in equation 11.

$$\Delta_{F_z} = a_x\frac{mh}{L} \tag{10}$$

$$\begin{aligned} F_{zF} &= F_{zF0} - \Delta_{F_z} \\ F_{zR} &= F_{zR0} + \Delta_{F_z} \end{aligned} \tag{11}$$

III. Equilibrium analysis

As proposed mathematical analysis of vehicle states focused on drifting, shows that determining steady state equilibria as well as a phase portrait analysis can tell us a lot about desired steady state drift locations poses [3], [21], [22]. This chapter proposes a strategy of obtaining the locations of these equilibrium points (III-A), where also a comparison with experimentally obtained data is performed(III-B).

A. Steady-state equilibrium locations

The model described in section (II) and its set of nonlinear differential equations 2-3 capture most important dynamics of the vehicle states considering the single-track model. Steady state implies that the time derivatives of the system of equations is equal to zero, meaning that the state does not change with time, i.e. $\dot{V} = \dot{\beta} = \dot{r} = 0$. Based on this condition, the set differential equations can therefore be rewritten and solved using a nonlinear least-squares (MATLAB: $lsqnonlin$), which allows the incorporation constraints on respective states. An initial guess often allows the solver to converge to a desired state, e.g. a high sideslip drifting equilibrium, but the use of constraints on desired velocities, wheelspeeds and/or wheelslip make finding equilibria significantly faster. However, as can be mathematically derived, the proposed model contains more variables than equations, which means that certain equilibrium values therefore have to be chosen by a value that could describe a drifting motion. Therefore, the system of equations is solved using a set of desired sidelip angles β^{eq} in combination with a set of experimentally confirmed feasible path radii R^{eq} for drifting motion. This implies that all other system states are considered free variables, that the least squares problem solves for. As a result, the optimization variables are described by $\mathbf{x}_{eq}$ (12), which allows to compute all respective tyre force components.

$$\mathbf{x}^{eq} = [V^{eq} \quad \beta^{eq} \quad r^{eq} \quad \omega_F^{eq} \quad \omega_R^{eq} \quad \delta^{eq} \quad T_i^{eq}]^T \tag{12}$$

Results of the equilibrium points are considered non-unique, as a drifting equilibrium is controlled through a balancing

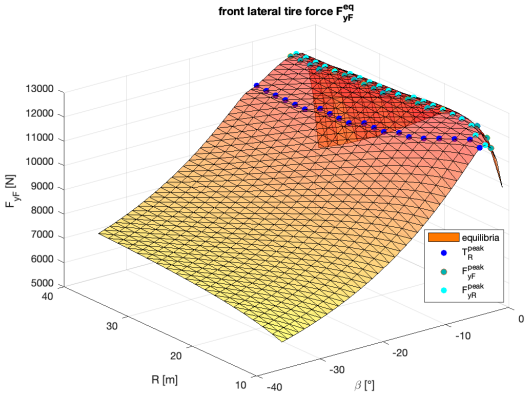

Fig. 3. Equilibrium front lateral tyre forces F_{yF}^{eq}

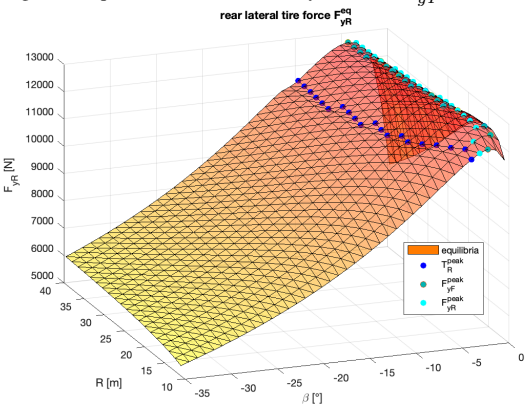

Fig. 4. Equilibrium rear lateral tyre forces F_{yR}^{eq}

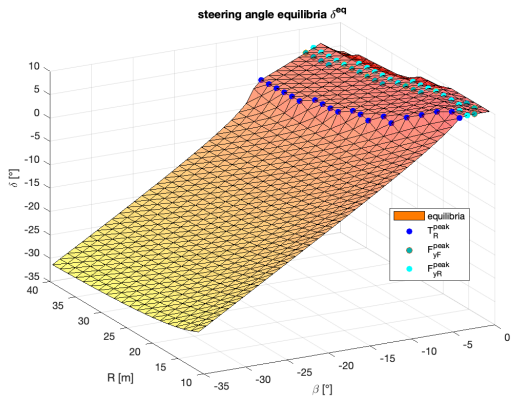

Fig. 5. Equilibrium steering angle δ^{eq}

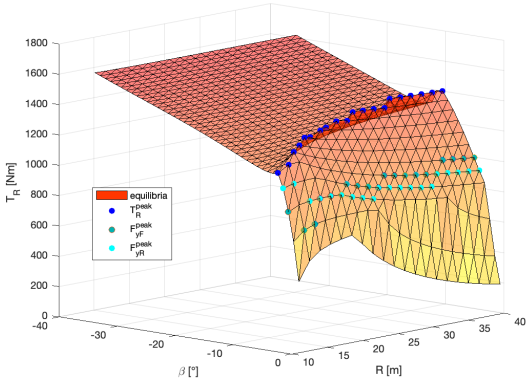

Fig. 6. Equilibrium rear axle drive torque T_R^{eq}

relation between the front- and rear force magnitudes. This implies that variations in rear drive torques, and its resultant slip coefficient may vary, as the front axle is subject to different poses, thus varying forces. The equilibrium analysis shows that the velocity of vehicle state equilibria as shown in Fig. 9 increases as the desired path radius at constant sideslip angle, whereas a constant radius causes a decrease in sideslip angle as a result of the force balance required between the front and rear axle. As a result, the yaw rate of the vehicle increases with the path radius through the relation as described by equation 13.

$$K = \frac{r}{V} = \frac{1}{R}, \quad R = \frac{V}{r} \tag{13}$$

In correspondence to the magic formula definition (II-B) figures 3,4 show that that the lateral tyre forces are at its highest at relatively small sideslip angles, thus small tyre slip angles. This implies that towards these peaks, the vehicle is considered conventional driving in the linear range of tyres, which can also be indicated by the near corresponding wheelspeeds (8) and positive steering angles (5). At a further increasing sideslip angle, clear indications show that the front- and rear wheelspeeds start to deviate in magnitude, indicating that the vehicle state is entering a drifting state where the steering angle approaches zero, while the rear longitudinal force has not reached its peak force (6). This means that the applied rear torque results in a reasonable amount of slip such that the rear tyres become saturated in lateral direction with a reasonable sidelip state. However, since the peak friction force in longitudinal direction is not reached, we consider the the state towards this point a transient state, i.e. there is a slight drift, however tyres are not fully saturated nor counter steer is taking place. All equilibria plots have the locations of the peak drive torques •, rear lateral peak forces • and the front lateral peak forces marked •, in order to support information.Once the the peak longitudinal slip is reached, thus the amount of wheelspeed becomes significantly larger than the rear axle longitudinal velocity, we consider the tyres saturated in both lateral- and longitudinal direction, where a direct change in steering angle is obtained (5) in order to balance the front and rear forces. Larger sideslip are considered fully drifting equilibria, where we see proportional behavior in the steering angle, and further deviation in the wheelspeeds (8) which are are a result of larger required rear slip, and decreasing front wheelspeed due to decreasing yaw rate.

B. *Experimental verification*

An experimental verification has been conducted in order to determine the correspondence between practical and theoretical equilibria, which can be deployed as a confirmation of the identified model parameters. Fig. 10 shows a comparison of theoretical equilibria with measured vehicle states, of which the latter are measured by means of the vehicle state estimation signals, which are found on the CAN bus of most production vehicles. The measured sideslip angle functions as

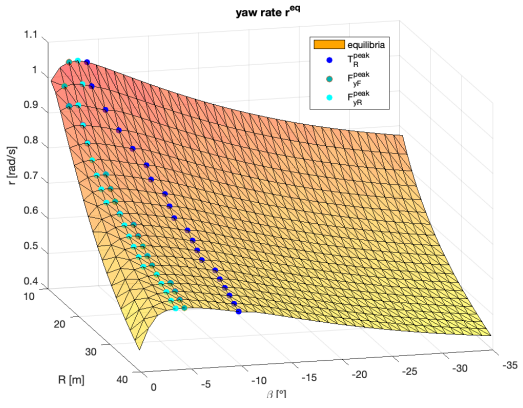

Fig. 7. Equilibrium yaw rate r^{eq}

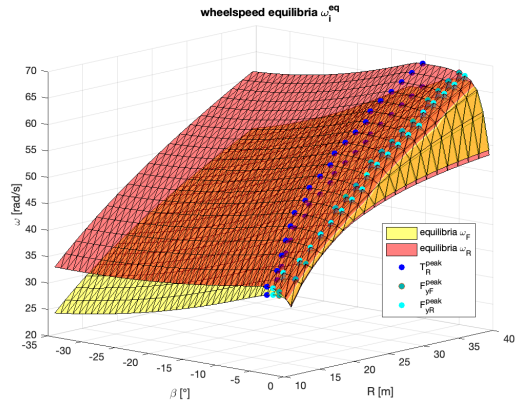

Fig. 8. Equilibrium wheelspeeds ω_F^{eq},ω_R^{eq}

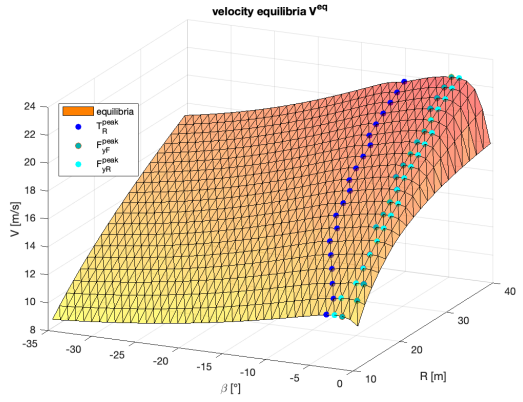

Fig. 9. Equilibrium absolute velocity V^{eq}

a fixed parameter for the $lsqnonlin$ function optimizing for the equilibrium vehicle state equilibria. The measured vehicle state functions as an initial guess for the equilibrium analysis, in order to bring the equilibria as close as possible. The results show that remaining an actual equilibrium point as a manual driver is relatively hard, due to many disturbances on the vehicle such as road surface, and uncaptured dynamics. True road surfaces are considered non-homogeneous where a $5-10\%$ variation in the friction coefficient is measured for the respective proving ground, which a driver needs to compensate through changing the steering angle or throttle commands causing the steering angle and applied drive torque never really being constant. The slightly tilted position of the vehicle due to the conical shape of the surface also remains uncaptured in the bicycle model definition, causing variations in the vertical axle loads. In addition, it should be taken into account that the driver both has to stabilize the desired drifting state, while stabilizing on a desired path. This implies that the experimental data is not considered to be in an equilibrium for all time instants, however, the comparison does show reasonable similarities in the order of magnitude.

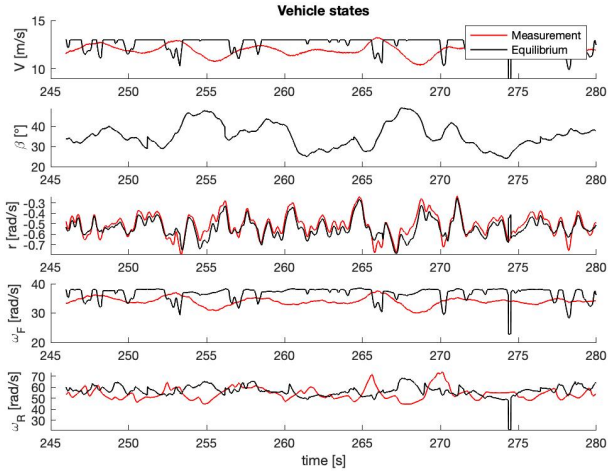

Fig. 10. Experimental/Theoretical drifting state comparison

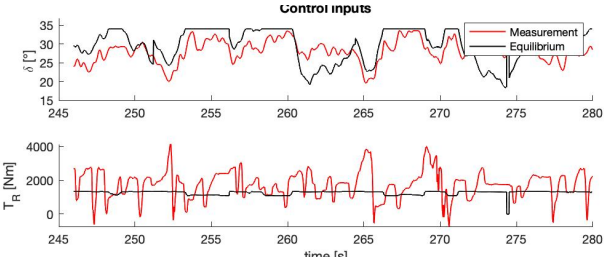

Fig. 11. Experimental/Theoretical drifting control inputs comparison

The comparison between experimental and theoretical drifting states has shown that around an actual drift equilibria, many variations of drifting equilibria exist. Where physical constraints such as steering angle limits δ_{max} does not significantly influence the high sideslip state, as small deviations in the front lateral slip angle α_F would still converge to an equilibrium drifting state. In similar fashion, slight variations in the drive torque, thus wheelspeed show that equilibria exist for multiple wheelspeeds. As indicated by Fig. 11, the optimization algorithm converges to the maximum allowable value of steering angle δ, while the experimental data shows smaller steering angles with intervention needed reach a desired path.

IV. Controller Structure

The proposed control system that has the ability to both stabilize the vehicle into a high sideslip state, while maintaining a desired state in space is summarized in the schematics in Fig. 12. However, for the length of this report, this paper

focuses solely on the NMPC sideslip stabilization, i.e. vehicle state control. Where a nonlinear model predictive controller (NMPC) functions as the foundation of the proposed control system, which is able to compute required control inputs to reach any feasible reference state of the vehicle. This implies that the NMPC solver can be deployed to both optimize for control inputs in the high sideslip state, but also for conventional driving thus enabling an initializing drive towards a drifting motion. Hence the definition of vehicle state control as described in Fig. 12. Dynamic referencing allows to influence the direction of the vehicle, where the offline computed equilibria as proposed in chapter III can be selected dynamically by means of using positional data of the vehicle S^{veh} to alter the path curvature such that the lateral error e_y of a desired path is decreased. The combination dynamic referencing and the vehicle state controller enables to bring a vehicle in both into a desired high sideslip state, while converging towards a desired trajectory.

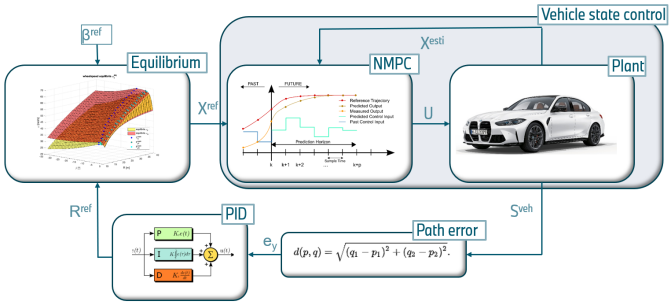

Fig. 12. Proposed control system strategy [23]

In general, the minimization of a cost function (Equation 15) determines the optimal control input that minimizes the error of the vehicle states with respect to a desired reference state x_{ref}. Depending on the purpose of the drifting controller, a potential reference for a steady-state drifting controller could for example be the steady-state sideslip angle or yaw rate of the vehicle, as determined by the equilibrium analysis. Similarly, a drifting pose can be expressed without explicitly referencing on the sideslip angle, as a revision on the mathematical expression of the sideslip angle (1) shows us that a drifting state can also be expressed by longitudinal- and lateral velocity components, as proposed [13].

$$V_N(x_0, y_{ref}, \boldsymbol{u}_N) = \frac{1}{2}\sum_{k=0}^{N-1}\left(\ell(x(k) - x_{ref}, u(k) - u_{ref})\right) + V_f(x(N) - x_{ref}) \tag{14}$$

The cost function describes the model dynamics $x(k) = \phi(k; x_0, \boldsymbol{u}_k)$, while $\ell(x(k), u(k))$ and $V_f(x(N))$ are the stage cost and terminal cost, respectively. The stage cost and terminal cost are considered quadratic cost functions, with tunable positive-definite weight matrices Q, R and M, for the states x and input u alike (see Equation 15), while V_f is the terminal cost which is used to guarantee the steady-state is reached.

$$\ell(x(k), u(k)) = x(k)^T Q x(k) + u(k)^T R u(k) + 2x(k)^T M u(k)$$
$$V_f(x(N)) = \frac{1}{2} x(N)^T P x(N) \tag{15}$$

The MPC optimization problem can be summarised as follows (16), where a minimisation of the cost function is subject to the system dynamics and constraints. The inequality constraints are represented in form where the matrices G and H contain information on the application of constraints, for both the states x as input u, respectively. When it comes to a steady-state drifting controller, you can think of physical constraints such as the steering angle, but also for constraints that contribute to stability by means of constraining velocities, tyre forces, or the sideslip angle.

$$\mathbb{P}_N(x_0, d, y_{ref}) \in \begin{cases} \min\limits_{\boldsymbol{u}_N} & V_N(x_0, d, y_{ref}, \boldsymbol{u}_N) \\ \text{s.t.} & x^+ = Ax + Bu + B_d d \\ & Gx + Hu \leq \psi \\ & x(N) \in \mathbb{X}_f(d, y_{ref}) \end{cases} \tag{16}$$

A. Vehicle state controller

For the sideslip stabilization, the vehicle state controller can be defined differential states (17) that describe the differential states of the set of differential equations 2, 3 are directly measured, or converted from the four wheel vehicle state signals in order to correspond with the single-track model.

$$\mathbf{x}_{vsc} = [V \quad \beta \quad r \quad \omega_F \quad \omega_R \quad \delta]^T \tag{17}$$

As can be indicated, the steering angle δ is also defined as a differential state, as the control input on the steering angle is described by required steering angle difference $\dot{\delta}$. This enables to constrain the gradient of the steering angle, which allows to mimic human steering behavior, as well as being able to capture physical steering constraints such as maximum applicable steering rate. The respective control inputs for the vehicle can therefore be described by equation 18.

$$\mathbf{u}_{vsc} = [\dot{\delta} \quad T_i]^T \tag{18}$$

An auto-generated solver [24] is applied, which creates an OCP of the vehicle description, enabling to compute the optimal control input that will lead to reaching a desired state $\mathbf{x}_{des}$. Additional to the differential states, the longitudinal acceleration a_x is also measured and injected into the solver as online data. Using the longitudinal acceleration allows to estimate the longitudinal load transfer, which estimates vertical load estimation as proposed 10. As mentioned, the single-track model will not capture load transfer exactly, however, using knowledge of the longitudinal load transfer positively contributes to the OCP.

V. Results and Discussion

A. Simulation validation

The proposed control system (IV) has been evaluated through an extensive 17 degrees of freedom (DoF) simulation tool developed by BMW B as well as through an experimental setup, where in both cases produced RWD sports sedans are used that have an 30% LSD.

1) Alternating drift scenario: An internally developed simulation tool named ISAR, offers an extensive description of a complete vehicle model based on a Simulink model, whereby a large scale of simulations can be performed based on laws of physics as well as experimentally obtained data regarding vehicle dynamics, respective race tracks and environmental factors. Differing from vehicle description for the controller, ISAR is a two-track model, which captures a very accurate description of the vehicle dynamics. As a worst case scenario, alternating drifting is simulated on a high friction surface, which is initialized by a high yaw rate state within the limits of friction, i.e. conventionally turning. As seen in Fig. 13, the simulated vehicle is able to track the initial left-hand drifting maneuver once the drifting reference is initialized, while a nearly instant transition into a right-hand drift is achieved with corresponding tracking performance. In this case, we can obtain the response of the 30% LSD, as the left- and right wheelspeeds become similar, thus implying a locked state. In similar fashion, we obtain that the single-track model is able to capture a large amount of the vehicle dynamics for the drifting state, as the desired equilibrium is based upon that description. As mentioned, the ISAR simulation tool capture much more dynamics as compared to the single-track model, where up to 17 DoFs are considered for describing vehicle dynamics. However, the dynamics are still considered to be an 'ideal' case, where both systematic- and measurement noise are ignored, as well as a constant friction coefficient exists for the complete simulation. Therefore, measurement noise and friction coefficient variation is included into the simulation, in order to prove robustness for a realistic case. Friction coefficient variation is based on surface measurements of the BMW proving grounds of Aschheim, which have shown that seemingly homogeneous surfaces tend to have friction coefficients variations of approximately 0.05. Amplitude and frequency of simulated measurement noise is based on obtained vehicle measurements from the test bench vehicle. Due to the introduction of these noises, we obtain a noisy response from the desired control rear drive torque as seen in Fig. 14. Constant weighting for the complete simulation shows some erratic behavior in the linear driving range, yet the solver remained stable under these circumstances. There an optimization takes place on the steering angle rate $\dot{\delta}$, the desired steering angle remains more smooth, as the steering angle rate is constrained in the optimization. Response of the the simulator shows that engine dynamics and systematic delays, as the single-track model calculation of the left- and right wheel drive torque is not of equal peak magnitude. This implies that rapid increase of desired drive torque is not tracked instantly, however since the drifting states are reached, as the solver computes the equilibrium drive torque. Please see the appendix for the applied controller settings.

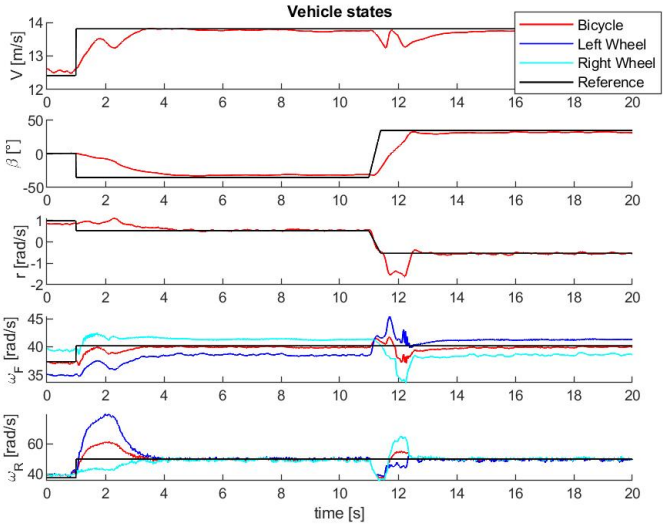

Fig. 13. ISAR state response while sustaining an alternating drift scenario on a high friction surface

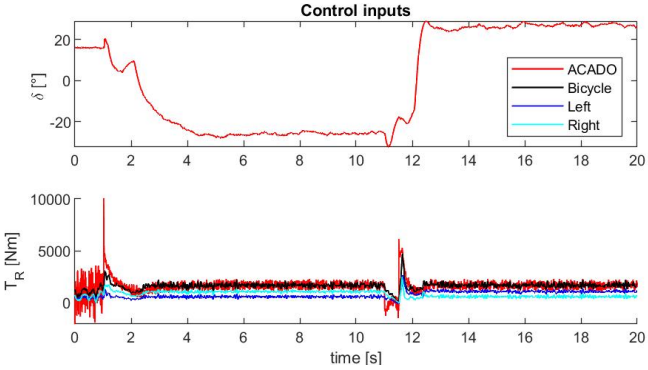

Fig. 14. Control inputs for ISAR simulation while sustaining an alternating drift scenario on a high friction surface

B. Experimental validation

An experimental verification has been proposed using an RWD BMW $M3$ $Competition$ $(G80)$, which is a more powerful vehicle compared to the simulation vehicle, with higher stiffness coefficients found in chassis, suspension and tyre properties. The vehicle is serially equipped with an active differential, where an electric engine has the ability to actively apply pre-tension to the differential, to influence locking capabilities at an earlier stage indicated by the vehicle-control system.

The implementation of the proposed controller has been enabled through physically decoupling the driving assistance systems interface (FAS) of the testbench and replace control signals with the desired control signals from the proposed control system, which allow to apply a path curvature and drive torque to the vehicle BUS. The auto-generated real-time ACADO c-code has been implemented on a $DSpace$ $Autobox$ $DS1007$ platform, which enables an interface for desired Flexray- and CAN bus communication protocols in order to

send- and receive information from from the vehicle and desired external devices such as DGPS or IMU. Measured- and estimated state signals at 10 ms are found on the Flexray BUS of the vehicle. As the integrated control units of the vehicle have all single-track states available, through measurements and estimation, the vehicle CAN signals are used as states for the control system.

1) Control system adjustments: As the generated NMPC code requires a significant amount of computational performance, the complexity and settings of the controller had to be reduced significantly in order to run for the real-time application while remaining sufficient numerical stability. To start with, the path following properties have been neglected, which therefore the sideslip stabilization is experimentally verified as proposed by the the vehicle state controller (12). As the usage of signals that capture certain degree of measurement noise, the numerical stability of the solver is highly influenced by the choice of integrator. Where in case of the Flexray signals, at least the fourth order Runge-Kutta-Legendre method is desired as the integrator type for the solver. A timestep of 20 ms enables sufficient time to solve the optimization for a prediction horizon of 25 steps. Additionally, the simplified magic formula (8) is used to compute the front axle tyre forces, as this can be assumed in the linear force range.

2) Production vehicle adjustments: As ADAS functions such as automated lane keeping have the tendency to not be fully self-driving, applied steering torques and angles through the FAS interface are limited in magnitude for safety purposes. Where applied steering torque for the driving assistance systems is applied by means of the torque actuator in the electronic power-steering unit (EPS), a fallback safety feature ensures that the magnitudes of the respective units do not exceed certain margins. As these limits are implemented through standardized software for the serial vehicle, a custom software stage is uploaded to the EPS that maximizes the applicable steering angle and control torque. A similar approach is used for the applied drive torque to the wheels, where integrated accelerometers on the rear axle constantly measure the state of the vehicle and process its magnitude in the digital motor electronics (DME) unit. Where in similar fashion to the EPS, a serially produced vehicle has safety limits on the relation between the applied drive torque and measured acceleration. Where in case the applied drive torque from the FAS interface exceeds $4m/s^2$, the vehicle runs into an emergency state. As a steady state drifting motion commonly has centripetal accelerations beyond the integrated safety limit, the complete DME is replaced with an applicable DME, which as the name implies, enable to apply desired values such as extending safety limits. In case of the drifting control testbench, the complete functional safety system (FuSi) is switched off on the DME.

3) Parametric uncertainties and imperfections: Tire modelling The proposed dynamical system described by the single track model as described II is considered stiff as compared to the testbench as well as for the simulator, where the experimental test becomes more complex when it comes to parametric uncertainty, most significantly considering road-tyre surface. A constantly changing state of the road surface, but also the tyre- state, pressure and temperature have significant influence of the driving behavior. Even for road-tyre interactions that seem of a relatively homogeneous nature, friction coefficient deviations of approximately 5% are obtained through measurements. In an experimental setup for a dry surface test, the tyre properties change rapidly after repeated testing, where the physical compound of the tyres visibly change, thus also the force properties.

Experimentally fitted tyre data is retrieved from a test bench setup, which verifies the respective loads under an extensive range of tyre states. As a result, the MF parametrization can be obtained for a desired vertical load of which the data can be found in a tyre property file for a respective tyre. By using a tyre that has underwent the tyre fitting procedure, a relatively proper estimation can be done for the force-slip relation for that particular tyre. By performing a manual drift on the desired surface, an estimation of the respective equilibrium states can be computed as proposed in the equilibrium analysis. In this case, respective longitudinal- and lateral tyre forces F_{meas}^{eq} can be estimated. In similar fashion, the data allows to approximate the respective tyre slip coefficients, which can be used to modify the tyre property files, such that the the the estimated tyre forces from the measurement F_{meas}^{eq} correspond to the computed tyre forces F_{MF}^{eq}.

In case of a very low friction surface, such as ice, snow or the constantly water skid pad of the BMW proving grounds of Aschheim, tyre responses are not only changing in an evenly distributed scale. In this case, we often obtain tyre responses, where the peak friction force is decreased more significant, up until the point where the tyre forces only increase along with an increased slip. Estimating the amount of reduction on the peak friction force with the proposed approximation is relatively unreliable, as the measurements are constantly affected by changing conditions.

Actuator delay As seen in the simulations, a maximum deliverable drive torque of a petrol engine is not instantly available, which causes a mismatch on the desired and true applied drive torque as visible in Fig. 16. Therefore a variation between references approximates the delay between drive torque and steering angle, namely through applying a step input to the rear wheelspeed, while a brief ramp is applied to all other references. This enables the vehicle to build up a desired torque, before starting to steer towards a drifting state, in order to reduce control input mismatch.

4) Standard production vehicle limits: Due to constantly changing weather conditions during wintertime, the above parameter estimation had to be performed each time when the drifting surface changed significantly. The NMPC control approach in combination with the testbench has showed that fully automated drifts are non-reproducible, as a full lap drift only occurred a single time. Whereas the best measured drift existed for about half a circle with a path radius of 25 meters, as seen by the vehicle in high sideslip state in Fig. 1. Corresponding vehicle state measurements are shown in Fig.15, which shows the initial velocity of the circular driving reference is relatively high, which is caused by having the velocity of the desired drifting close to the initializing driving

velocity in order to perform a smooth transition between driving and drifting.

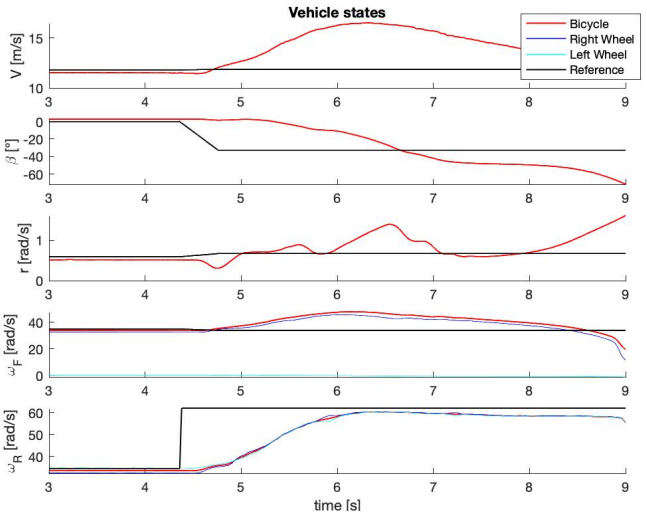

Fig. 15. Measured vehicle states during full automation

Signal analysis shows a deviation between the desired and measured steering angle (16) for all performed tests reaching high sideslip, where the front axle aligns with the direction of travel rather than compensate for the vehicle state. Two possible assumptions to consider that may cause this issue can be found in the steering conversion within the vehicle. At first, we can think of a lack of applicable torque from the standard EPS that should be able to apply sufficient amount of torque to overcome the self-aligning moment occurring at the front tyres. Considering the used EPS motor only produces about 30 Nm and is designed to function for several relatively low torque desiring ADAS systems such as automatic lane change, the assumption is possible.

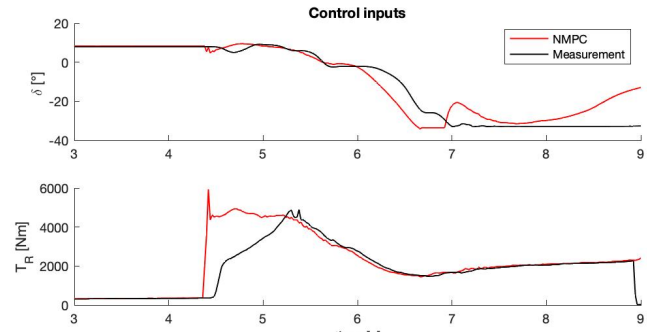

Fig. 16. Desired MPC control inputs and the measured control inputs during automated drifting deployment

A second assumption is the conversion in the integrated control systems of the vehicle, as the FAS interface to the vehicle takes path curvature as a control input. This implies that the proposed steering angle is converted to a path curvature on the internal vehicle control system, which are not possible to modify. It could be the case that these control systems assume conventional driving, thus computation of the right steering angle is not happening correctly while the vehicle is in a high sideslip state. As a consequence of the incorrect conversion, the steering angle cannot be decreased as desired by the NMPC. As a result, the true steering angle remains on its limit, which causes a spin through of the vehicle, as the front axle is not performing the desired compensation for the deviations in absolute velocity and sideslip angle. In case the steering angle is applied as proposed by the controller, we would see a decrease in yaw rate and sideslip angle, which would aim for stabilizing the drifting state around the desired equilibrium. A comparison between the desired MPC drive torque and the true measured drive torque shows the deviating response in case of instant increase of torque (16), as explained and seen before in ISAR simulations. We obtain from the plot, that a peak rear drive torque is applied, in order to overcome the peak longitudinal- and lateral tyre forces in order to reach full tyre saturation.

C. Semi-automated experimental validation

According to the findings on the steering conversion between controller and vehicle, we can assume that only hardware modifications or internal software can solve the non-corresponding steering angle conversion. However, a semi-automatic drifting maneuver can tell us the response of the vehicle and the desired control inputs from the solver. Therefore, a proposed experiment runs the NMPC solver through the experimental setup, where in this case only the desired drive torque is forwarded to the vehicle, while steering is performed by a human driver. By performing the experiment in this setting, we can obtain a result with respect to the applied drive torque, as well as a comparison between the true and desired steering input of the NMPC. This approach has shown that the applied drive torque shows corresponding behavior to a manually initiated drift, under the condition that the tyre response is estimated within reasonable limits.

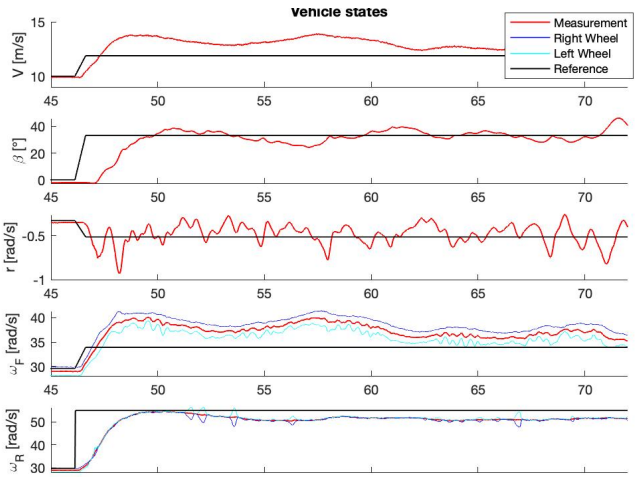

Fig. 17. Measured vehicle states during a manual steering scenario, torque commands forwarded from the NMPC solver

Measurements show that the vehicle can be brought into the desired drifting state as seen in figure 17, where the experiment is performed on both a dry high friction surface and a watered skid pad, with high and low friction coefficients, respectively. This proves that the proposed control system is suitable for

a variety of tyre-road interactions, under the condition that the behaviour of the tyres is well defined in the controller. The high sideslip state is stabilized for multiple rounds, where theoretically the drifting state could be continued for a significant time. From these results we can obtain that the applied drive torque is sufficient and solved optimally for bringing the vehicle into the drifting state, and remaining its steady-state drifting position. In correspondence to the fully automated setting, we see that the tracking performance of the velocity and front wheelspeed is less accurate as compared to the sideslip angle, yaw rate and rear wheelspeed. Reason for this is the applied tuning weights on for the controller, as the main focus is bringing the vehicle into high sideslip state, which is established with high yaw rate and rear wheelspeed tracking. While the front axle aligns with the direction of travel, the front wheelspeed and the the absolute velocity are proportional under constant path curvature.

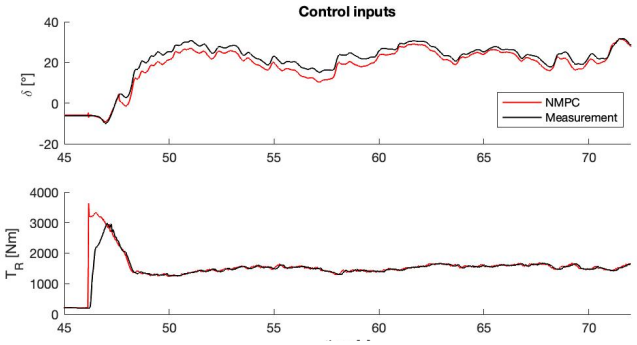

Fig. 18. Desired MPC control inputs and the measured control inputs during semi-automated controller deployment

Due to the steering conversion issue in the fully automated setting, we can see the comparison between the desired MPC steering angle and the manually performed drift (18) has more significant added value. From the comparison, we can obtain that the steering angle from the human driver is corresponding in its response with the desired steering angle computed by the NMPC solver. Only magnitude varies with maximum peaks of approximately 5, which shows us that in case steering conversion within the vehicle happened accordingly, sustaining a stabilized drift for at least a couple of rounds would be very much possible. In case of the applied drive torque (18), we obtain corresponding response with both experimental torque application.

Conclusion and Future Work

Experimentally verified equilibrium locations of a single-track model show great correspondence between setup and theory, which therefore proves that equilibrium locations can be used as references for a drifting control strategy. Simulation performance of the proposed controller shows accurate tracking in an alternating drift maneuver under difficult drifting circumstances .

Experimental verification has shown that the use of a standard production vehicle without significant hardware and-or software modifications is not able to convert desired control inputs into the applied control inputs after the point where the high sideslip state is reached, due to the low-level controls of the standard production vehicle.

Degradation of the EPS, or a power output that is generally too low to overcome the induced self-aligning moment on the front axle is the first assumption made that causes the steering issue, which could be solved with a more powerful and robust steering motor. A second assumption is based on the software that lies on the integrated braking (IB) controller, which converts the desired steering angle from the NMPC controller into the applied steering angle. Further research on the hardware- and software components will determine the source of failure at low-level control, and potential modifications can be proposed.

A semi-automatic verification, where manual steering is applied in parallel to drive torque proposed by the controller, shows that the NMPC is able to output proper control inputs for the vehicle. Results show that the controller is likely to stabilize the drifting motion, as the proposed steering input of the NMPC is corresponding in behavior of a manual driver. Therefore, the controller can be assumed to be deployable for automated drifting, however, modifications to future vehicles are desired to decrease the control input error between controller and vehicle.

The proposed control strategy shows that in case parametric knowledge within certain limits, the model based NMPC is able to bring the vehicle into a desired high-slip state for a variety of tyre-road characteristics. Further experiments on snow or gravel should be conducted to prove controller stability for most road conditions. However, this implies that if the control approach would be proposed for safety purposes, knowledge of that particular situation should be instantly available in real-time. This desires a highly sensitive as well as frequently updated state estimator of the vehicle dynamics. Future research on NMPC drifting control should therefore aim on increasing controller performance, by means of computational effort and -capacity. An improved modelling approach that captures unmeasured disturbances could be thought of, as well as using a platform with increased computational power. As true road-conditions might vary among the tyre contact patches, a state estimation at each wheel is therefore desired in order to generate a most optimal control input.

References

[1] E. Velenis, D. Katzourakis, E. Frazzoli, P. Tsiotras, and R. Happee, "Steady-state drifting stabilization of RWD vehicles," *Control Engineering Practice*, vol. 19, no. 11, pp. 1363–1376, 11 2011.

[2] M. Abdulrahim, "On the Dynamics of Automobile Drifting," Tech. Rep., 2006.

[3] R. Yusef Hindiyeh, "DYNAMICS AND CONTROL OF DRIFTING IN AUTOMOBILES," Ph.D. dissertation, Stanford University, Stanford, 2013. [Online]. Available: http://purl.stanford.edu/vz162hz7668

[4] E. Velenis, P. Tsiotras, and J. Lu, "Optimality properties and driver input parameterization for trail-braking cornering," *European Journal of Control*, vol. 14, no. 4, pp. 308–320, 2008.

[5] E. Velenis and P. Tsiotras, "Minimum Time vs Maximum Exit Velocity Path Optimization During Cornering," Tech. Rep.

[6] T. Gustafsson, "Computing The Ideal Racing Line Using Optimal Control," Ph.D. dissertation, Institutionen för systemteknik Department of Electrical Engineering Examensarbete, 2008.

[7] ISO - International Organization for Standardization, "Passenger cars — Test track for a severe lane-change manoeuvre — Part 2: Obstacle avoidance," ISO - International Organization for Standardization, Tech. Rep., 2011.

[8] R. Y. Hindiyeh and J. Christian Gerdes, "A Controller Framework for Autonomous Drifting: Design, Stability, and Experimental Validation."

[9] J. Y. Goh, T. Goel, and J. C. Gerdes, "A Controller for Automated Drifting Along Complex Trajectories," Tech. Rep.

[10] J. Y. Goh and J. C. Gerdes, "Simultaneous stabilization and tracking of basic automobile drifting trajectories," in *IEEE Intelligent Vehicles Symposium, Proceedings*, vol. 2016-August. Institute of Electrical and Electronics Engineers Inc., 8 2016, pp. 597–602.

[11] J. Y. Goh, T. Goel, and J. Christian Gerdes, "Toward Automated Vehicle Control beyond the Stability Limits: Drifting along a General Path," *Journal of Dynamic Systems, Measurement and Control, Transactions of the ASME*, vol. 142, no. 2, 2 2020.

[12] M. Acosta, S. Kanarachos, and M. E. Fitzpatrick, "On full MAGV lateral dynamics exploitation: Autonomous drift control," in *Proceedings - 2018 IEEE 15th International Workshop on Advanced Motion Control, AMC 2018*. Institute of Electrical and Electronics Engineers Inc., 6 2018, pp. 529–534.

[13] B. Verlaan, "An optimization based approach to autonomous drifting A scaled implementation feasibility study," Tech. Rep.

[14] W. Norris, *Modern steam road wagons*. Longmans, Green, and Co., 1906.

[15] J. Subosits and J. C. Gerdes, "Impacts of Model Fidelity on Trajectory Optimization for Autonomous Vehicles in Extreme Maneuvers," *IEEE Transactions on Intelligent Vehicles*, 2021.

[16] V. Zhang, S. M. Thornton, and J. C. Gerdes, "Tire Modeling to Enable Model Predictive Control of Automated Vehicles From Standstill to the Limits of Handling," Tech. Rep.

[17] F. Saber, M. Ouahi, A. Saka, and F. Ezzahra Saber, "Vehicle Dynamics and Steering Angle Estimation Using a Virtual Sensor," Tech. Rep. [Online]. Available: https://hal.archives-ouvertes.fr/hal-01260766

[18] H. B. Pacejka, E. Bakker, and L. Nyborg, "Tyre Modelling for Use in Vehicle Dynamics Studies," 1987.

[19] E. Velenis, E. Frazzoli, and P. Tsiotras, "On steady-state cornering equilibria for wheeled vehicles with drift," in *Proceedings of the IEEE Conference on Decision and Control*, 2009, pp. 3545–3550.

[20] R. Y. Hindiyeh and J. C. Gerdes, "A controller framework for autonomous drifting: Design, stability, and experimental validation," *Journal of Dynamic Systems, Measurement and Control, Transactions of the ASME*, vol. 136, no. 5, 2014.

[21] S. Milani, H. Marzbani, and R. N. Jazar, "Vehicle drifting dynamics: discovery of new equilibria," *Vehicle System Dynamics*, 2021.

[22] E. Velenis, E. Frazzoli, and P. Tsiotras, "Steady-state cornering equilibria and stabilisation for a vehicle during extreme operating conditions," *International Journal of Vehicle Autonomous Systems*, vol. 8, no. 2-4, pp. 217–241, 2010.

[23] S. Meijer, "Automated Control Beyond the Limits of Friction - A nonlinear model predictive control approach with production vehicle experimental verification," Ph.D. dissertation, TU Delft.

[24] R. Quirynen, M. Vukov, M. Zanon, and M. Diehl, "Autogenerating microsecond solvers for nonlinear MPC: A tutorial using ACADO integrators," *Optimal Control Applications and Methods*, vol. 36, no. 5, pp. 685–704, 9 2015.

APPENDIX

TABLE I
BMW M3 COMPETITION EXPERIMENTAL VEHICLE PARAMETERS

Variable	Definition	Value	Unit
m	Vehicle mass	1800	kg
g	Gravity Coefficient	9.81	m/s^2
I_z	Yaw Inertia	2800	kg/m^2
a	Front axle distance to CoG	1.503	m
b	Rear axle distance to CoG	2.852	m
T_{max}	Maximum Wheel Torque	650	Nm
δ_{max}	Maximum Steering Angle	33.6	deg

TABLE II
BMW M340IX SIMULATION VEHICLE PARAMETERS

Variable	Definition	Value	Unit
m	Vehicle mass	1939	kg
g	Gravity coefficient	9.81	m/s^2
I_z	Yaw inertia	3225.22	kg/m^2
a	Front axle distance to CoG	1.437	m
b	Rear axle distance to CoG	2.8501	m
T_{max}	Maximum drive torque	500	Nm
δ_{max}	Maximum steering angle	34	deg

TABLE III
MAGIC FORMULA PARAMETERS BASED SINGLE-WHEEL LOAD FOR EXPERIMENTAL VEHICLE
TIRE 1: MICHELIN PILOT SUPERSPORT*
TIRE 2: PIRELLI PZERO ALP

Tire	Dimensions	i	B_i	C_i	D_i	E_i	S_i
1	275 35R19	x	9.20	1.96	1.55	-0.04	0
		y	11.35	1.88	1.29	0.69	17.37
2	285 30R20	x	15.84	1.66	1.25	-0.11	0
		y	9.37	2.10	1.36	0.59	19.39

APPENDIX A
NMPC TUNING PARAMETERS

TABLE IV
APPLIED TUNING PARAMETERS FOR ISAR SIMULATOR

Parameter	ISAR	Experiment
W_V	1e-16	10e-4
W_β	10e4	350
W_r	10e3	250
$W_{\omega F}$	50	1.8
$W_{\omega R}$	50	1.8
W_δ	1e-16	10e-4
W_{TR}	0	0
$W_{\dot{\delta}}$	0	0

TABLE V
PATH FOLLOWING PID PATH FOLLOWING

K_p	K_i	K_d
10e-2	50e-7	10e-4

APPENDIX B
ISAR INFORMATION SCHEDULE

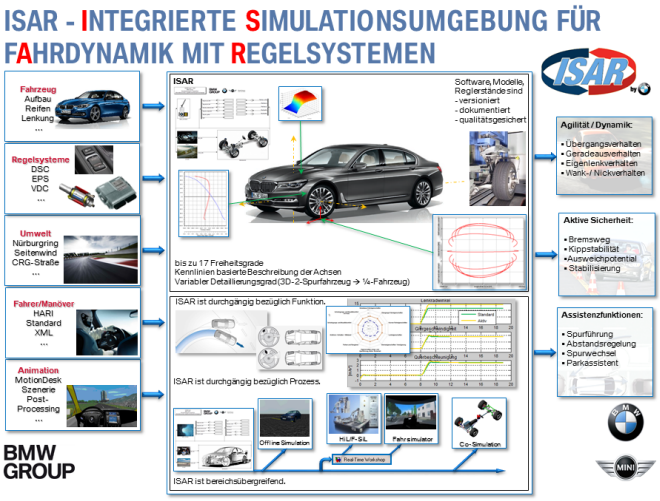

Fig. 19. Schematic overview of capabilities of the ISAR simulator